Fibroblast Activation Protein in Atherosclerosis and Atherothrombosis

Dissertation

zur

Erlangung der naturwissenschaftlichen Doktorwürde

(Dr. sc. nat.)

vorgelegt der

Mathematisch-naturwissenschaftlichen Fakultät

der

Universität Zürich

von

Chad Eric Brokopp

aus

den Vereinigten Staaten von Amerika

Promotionskomitee

Prof. Dr. Simon P. Hoerstrup (Vorsitz)

PD Dr. Christian Matter

Prof. Dr. François Verrey

Prof. Dr. Elena Aikawa

Zürich, 2011

From 2007 until 2011 Chad Brokopp was a member of the PhD Program in **Integrative Molecular Medicine** (imMed) at the **Zurich Center for Integrative Human Physiology** (ZIHP).

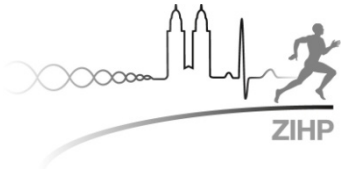

TABLE OF CONTENTS

SUMMARY

Heart attacks and strokes currently kill more people every year than cancer and HIV combined. These cardiovascular diseases are caused by atherosclerosis - the formation of so-called “plaques” in blood vessels. Interestingly, an enzyme called “Fibroblast Activation Protein (FAP)” contributes to arthritis and inflammatory liver disease; both of which are governed by similar inflammatory mechanisms as atherosclerosis. However the role of FAP in atherosclerosis had never been investigated. The studies presented in this thesis find that FAP is “switched-on” by inflammation in potentially life-threatening atherosclerotic plaques. We also found evidence that FAP contributes to plaque destabilization; the main cause of heart attack and stroke. When plaques rupture open, blood clots form, which block the vital flow of oxygen in a dangerous process known as “atherothrombosis.” Our research found that FAP contributes to atherothrombosis in patients who suffered a heart attack. These findings may motivate both the development of anti-FAP drugs, and also diagnostic measurements of FAP for heart attack and stroke prevention.

ZUSAMMENFASSUNG

Koronare Herzerkrankung und Schlaganfall töten heutzutage mehr Menschen als Krebserkrankunegn und HIV zusammen. Diese Herzkreislauferkrankungen werden verursacht durch Atherosklerose, welche der Entwicklung sogenannter „Plaques“ in den Blutgefässen entspricht. Interessant erscheint dabei, dass ein Enzym - „Fibroblast Activation Protein“ (FAP) - eine wichtige Rolle bei Arthritis und chronischen Lebererkrankungen spielt, wobei in beiden Erkrankungen ähnliche Entzündungsmechanismen wie bei der Arteriosklerose nachgewiesen wurden. Dennoch wurde die Rolle von „FAP“ im Bereich der Arteriosklerose bisher nicht untersucht. Die vorliegenden Studien zeigen, dass FAP durch die Entzündung von potenziell bedrohlichen Plaques „aktiviert“ wird. Dabei wurden Hinweise gefunden, dass FAP zu Komplikationen in den Plaque führt, welche ihrerseits als Hauptquellen von Herzinfarkt und Schlaganfall gelten. Wenn diese Plaques aufbrechen, entstehen „Blutgerinnsel“, welche den Durchfluss des lebenswichtigen Sauerstoffs hemmen. Dieser gefährliche Prozess wird „Atherothrombose“ genannt. Unsere Ergebnisse zeigen, dass FAP zur Entwicklung von Atherothrombose bei HerzinfarktpatientInnen beiträgt. Diese Entdeckungen konnten die Entwicklung von „Anti-FAP-Medikamenten“ und diagnostischen Messungen des FAP zur Prävention von Herzkreislauferkrankungen stimulieren.

CHAPTER 1

INTRODUCTION

Partially Based on:

A Role of Fibroblast Activation Protein in Cardiovascular Disease.

Brokopp CE, Weber B, Emmert M, Baumgartner L, Matter CM, Hoerstrup SP.

Manuscript in Preparation

1.1 ATHEROSCLEROSIS

1.1.1 HISTORY AND SOCIOECONOMIC IMPACT OF ATHEROSCLEROSIS

A Brief History of Atherosclerosis – an ancient disease

Atherosclerosis is characterized as the formation of arterial plaques consisting largely of fat, cholesterol, and cellular wastes which reduce blood flow (**Figure 1**). Recently, atherosclerosis has been linked to risk factors associated with the modern western lifestyle including: high-fat and high-glucose diets, lack of exercise, and cigarette smoking. However, paleopathological investigations of ancient Egyptian mummies reveal that atherosclerosis was present as early as 1980 BC. [15,] Egyptians of the highest social status, who consumed exclusive diets rich in animal products and saturated fats, were often mummified. In contrast, the Egyptian peasantry consumed strictly vegetarian diets. Coronary plaques identified in mummies of the Egyptian aristocracy suggest that atherosclerosis is an ancient disease, induced by diet, and that the modern day atherosclerosis epidemic may simply be history repeating itself. [16]

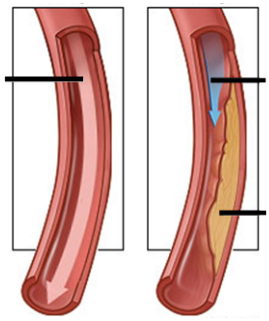

Figure 1. Atherosclerosis reduces arterial blood flow. Adapted from Healthwise, Inc.

"The Atherosclerosis Epidemic"

In modern western civilization, the occurrence of clinical atherosclerosis-related events (including heart attack and stroke) increased sharply around 1920 (**Figure 2**). While this sudden increase temporally associates with industrialization, its cause remains debated. However, many clinicians and scientists concur with two leading explanations.

The first argument suggests that environmental changes such as increased cigarette smoking and higher consumption of animal fats consumed in the 1920's were central to the increase in atherosclerosis-related deaths.[17] This hypothesis is supported, for example, by findings in one study which investigated the ages of death in an extended Dutch family with genetic hypercholesterolemia. Half of these family members had a mutation in the gene for the low-density lipoprotein (LDL) receptor, and therefore experienced severe high blood cholesterol levels resulting in early death from coronary heart disease or stroke. Between 1830 and 1989, age-adjusted deaths in this family were drastically increased.[18] This increase was too rapid for genetic adaptation, therefore suggesting that environmental changes were responsible for the sudden observed increase.

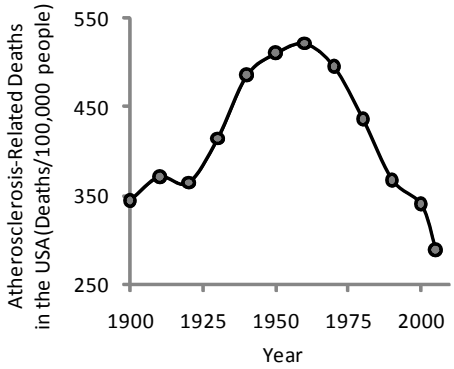

Figure 2. Atherosclerosis-Related Deaths in the USA in the 20th Century. Adapted from [1].

The second hypothesis explaining the sudden increase of atherosclerosis-related death suggests enhanced sensitization of physicians to coronary artery disease, and improved diagnostic capacities afforded by the electrocardiogram (ECG). Moreover, the use of leukocytosis measurements and red blood cell

sedimentation rates were also brought to routine clinical use for diagnosis of myocardial infarction.[17] Taken together, it is probable that both the improved diagnostic capabilities and the introduction of pro-atherogenic factors during the industrialization contributed to the sudden increase of reported atherosclerosis related deaths.

The Modern Decrease in Atherosclerosis Related Deaths

Mortality from atherosclerosis-related has recently been cut in half since reaching its peak in 1968 (**Figure 2**). Two primary factors are responsible for this decline. First, there has been a major reduction in the prevalence of classical cardiovascular risk factors (i.e. smoking and high cholesterol diets) due to more health-conscious lifestyles.[8] However it should be noted the hallmark risk factor, obesity, has increased strikingly in recent years, particularly in younger generations, which threaten to halt this favorable trend.[19]

The second cause for the recent reduction in cardiovascular-related deaths is the drastic improvement in treatments against coronary artery disease and stroke. Recent therapies including thrombolysis, coronary-artery bypass grafting, stents, angiotensin-converting-enzyme inhibitors, and statins have been instrumental towards preventing myocardial infarction and stroke (**Figure 3**).[8] In fact, a recent comparison between the relative contribution of reduced cardiovascular risk factors, vs. improved therapeutics in the observed reduction of cardiovascular-related deaths reveals that nearly half to this reduction is attributed to improved treatment, and half to a reduction of risk factors (**Figure 3**). However, it is interesting to note that improved treatment is now the most effective preventative measure against atherosclerosis-related deaths.

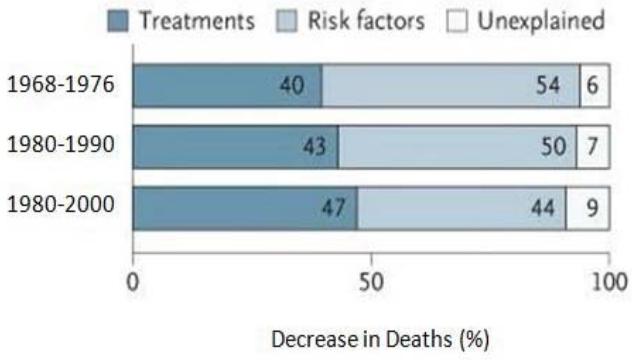

Figure 3. Percentage of the Decrease in Deaths from Coronary Heart Disease Attributed to Treatments and Risk-Factor Changes. Adapted from [8].

Atherosclerosis today – where do we stand?

Despite an improving trend, atherosclerosis remains the leading cause of death in the western world, killing more Americans and European Union members every year than human immunodeficiency virus (HIV) and cancer combined (**Figure 4**).[3, 20] According to the U.S. National Center for Health Statistics, approximately 6 years of life could be gained, per person by the complete elimination of atherosclerotic disease.[21] Therefore it appears indeed true that some people may "*only be as old as their arteries.*"

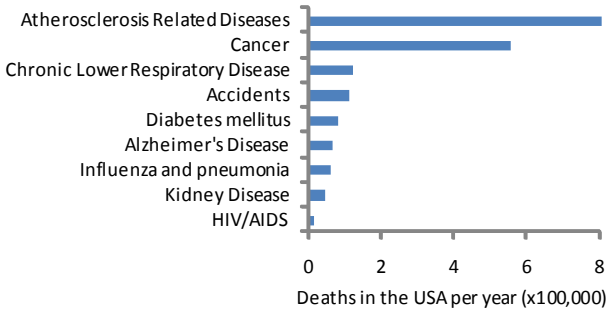

Figure 4. Atherosclerosis is the Leading Cause of Death in the United States (data taken in 2007).[3]

In 2010, the estimated mean direct cost of care for patients diagnosed with stroke or myocardial infarction in the United States was $579/month for 12 months before and $1,074/month for 12 months

after diagnosis.[22] Indeed, the economic burden of atherosclerosis is immense at an estimated cost of $156.4 billion in the United States in 2008 alone.[23]

1.1.2 THE HEALTHY ARTERY

An understanding of atherosclerosis requires knowledge of the anatomy, physiology, and cellular composition of the healthy human artery.

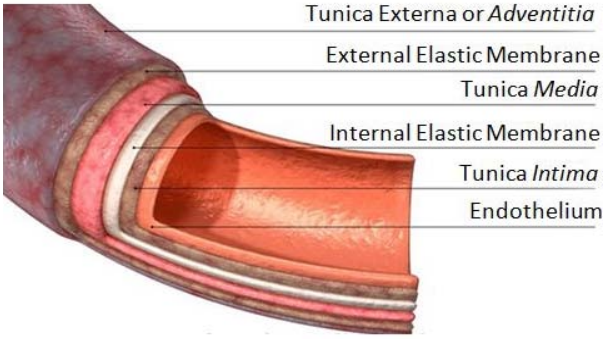

Figure 5. Six Layers of the healthy human artery. Adapted from Visuals Unlimited, Inc.

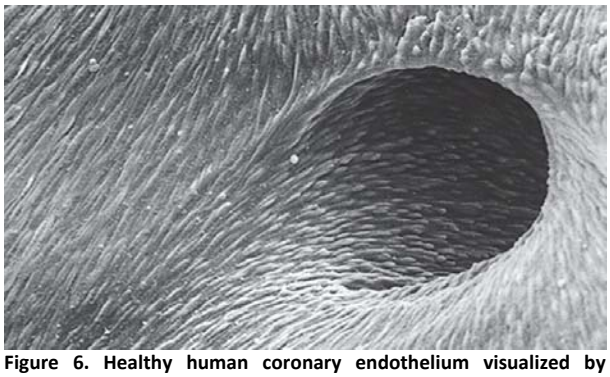

Figure 6. Healthy human coronary endothelium visualized by scanning electron microscopy. Endothelial cells are aligned in the direction of blood flow adapted from[9].

Endothelium

Healthy human arteries are most often described as a six-layered micro-anatomical structure (**Figure 5**). The inner most layer of the artery is called the endothelium. Under normal conditions, endothelial cells form a monolayer (**Figure 6**) which acts as an interface between circulating blood in the lumen and the rest of the arterial wall. The healthy endothelium has two known key functions. First, it provides a non-thrombogenic surface that prevents blood coagulation. Second, the endothelium acts as a "gate keeper" by selectively controlling the passage of circulating blood cells (i.e. monocytes and lymphocytes) and active molecules (i.e. nitric oxide and L-arginine) into and out of the arterial wall. The endothelium is tightly regulated by both cellular and systemic physiological mechanisms. However, these pathways and mechanisms often go awry during the formation of atherosclerosis, or so-called "atherogeneis."

Tunica Intima

The tunica intima (often referred to as simply "the intima") includes the endothelium, which covers a so-called "basement membrane." The basement membrane is an organized extracellular matrix (ECM) including collagen, laminin, fibronectin, and proteoglycans.[24] With aging, the intima thickens due to immigration of smooth muscle cells and their deposition of ECM. Beneath the basement membrane lays the internal elastic lamina; a fenestrated layer comprised of condensed elastin (**Figure 7**). The internal elastic membrane contributes to the elastic recoiling of the arterial wall following application of outward pressure during left ventricular systole.

Tunica Media

The tunica media (often referred to simply as "the media") is located beneath the internal elastic membrane, and is comprised of well-organized, concentric layers of smooth muscle cells. These muscle cells are surrounded by elastin-rich ECM. Similar to the internal elastic membrane of the intima, the media also provides regulated arterial compliance. Smooth muscle cells in healthy arteries are mostly quiescent, and experience low proliferation rates along with low-levels of cellular death. Moreover, ECM content does not significantly change in healthy human arteries over time. The external elastic membrane demarcates the outer boundary of the tunica intima and the beginning of the tunica externa (**Figure 7**).[25]

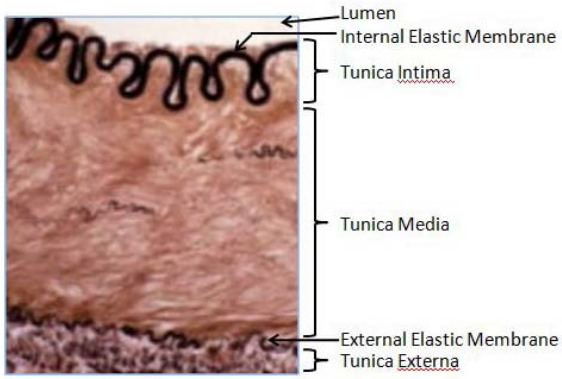

Figure 7. Histology of a muscular artery as visualized by aldehyde fuschin staining. Adapted from quizlet.com.

Tunica Externa

The tunica externa is most often referred to as the "adventitia," and has received little attention compared to the intima and media as to its role in vascular physiology. The adventitia is comprised mostly of disorganized collagen fibers, and a sparse distribution of adipocytes, mast cells, and fibroblasts. Recently, the adventitia has been shown to harbor mesenchymal progenitor and stem cells.[26] While it is plausible that these cell populations are involved in vascular homeostasis and regeneration following injury, their role in vascular physiology and atherogenesis remains largely conjectural.[10]

1.1.3 The Onset of Atherosclerosis

Low Density Lipoprotein Accumulation in the Intima

While atherosclerosis begins within the first decade of life, the initial triggers of atherosclerotic plaque formation, and their physiological mechanisms of action are not yet fully understood understood.[27] However, most scientists and clinicians concur with a growing body of scientific evidence which suggests that atherosclerosis is initiated by diets high in cholesterol and animal-derived fats. Ingested low-density lipoprotein (LDL) seems to play a particularly important role in the early onset of atherosclerosis. The notion of diet induced atherosclerosis is partially supported by electron microscopic evidence of experimental

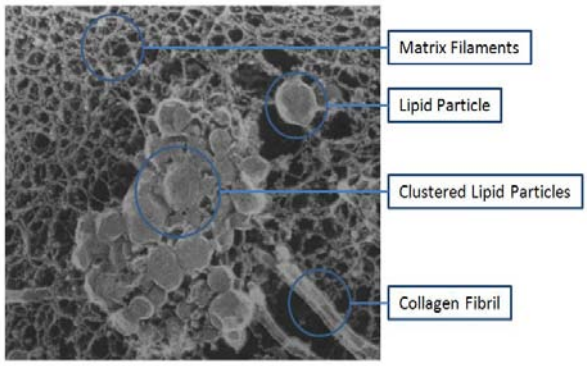

Figure 8. Lipid accumulation in the intima of rabbits injected with bolus dose of LDL. Adapted from[5].

animals infused with LDL. In this pioneering work, it was observed that lipid particles attach to the intimal ECM of rabbits and further associate into aggregates shortly after LDL injection (**Figure 8**). [5]

Additional studies using labeled LDL in rabbits also reveals an association between regions of LDL deposition and regions of plaque formation.[28] The mechanism by which LDL passes though the endothelium to reach the intimal ECM has been addressed in many studies, which conclude that the endothelium is in a natural state of disruption at sites prone to atherosclerosis formation.[29] Indeed, studies of fluid dynamics colocalize atherosclerosis-prone regions to sites of low endothelial shear stress and turbulent flow, whereas vascular regions exposed to laminar flow and high endothelial shear stress are less prone to lesion formation.[30, 31] These observations can partially be explained by further in-vivo data suggesting accelerated EC turnover in areas with disturbed flow and low shear stress.[32] Accelerated cell proliferation plausibly enhances LDL permeability through the endothelium, by temporarily leaving the intima exposed to the blood stream; thereby exposing circulating LDL to the intima.[33]

Oxidation of Low Density Lipoprotein

While blood serum LDL levels associate with atherosclerotic plaque burden, native LDL itself plays a minimal role in atherosclerosis onset.[34] Yet, LDL's chemically modified derivate, oxidized LDL (oxLDL) is a potent trigger of early plaque formation. LDL oxidation is catalyzed by its molecular binding to proteoglycans in the arterial intima. Moreover, in-vitro studies indicate that proteoglycan-bound LDL exhibits enhanced susceptibility to oxidation compared to unbound circulating LDL.[35]

Active contributors to the oxidative transformation of LDL include, but are not limited to:

- cigarette smoking (via enhanced F_2-iso-prostane levels) [36],
- bacterial infection (via lipopolysaccharide exposure) [37],
- yeast infection (via zymosan exposure) [37],
- exposure to chemical agents (i.e. turpentine)[37],
- excessive alcohol consumption (> two drinks/day),[38]
- lipoxygenases expressed by infiltrating leukocytes[39]

Moreover LDL can be transformed into pathological aggregates via sphinomyelinase[40] and also undergo glycation due to enhanced blood-sugar concentrations associated with diabetes.[41] Conversely, myriad antioxidants including grape-derived phenolic compounds[42] and vitamin E[43] are protective against LDL oxidation.

Leukocyte Infiltration

The second morphologically definable event during atherosclerosis onset is leukocyte recruitment into the intima. Under healthy conditions, circulating leukocytes do not firmly adhere to the arterial endothelium. Even in inflamed tissues, leukocyte adhesion to the endothelium typically occurs in the post capillary venules, rather than in the arteries.[44] However, hypercholesterolemia rapidly (<8 hr in rabbits) induces leukocyte adherence to the arterial endothelium, and directs diapedesis of leukocytes between endothelial cell

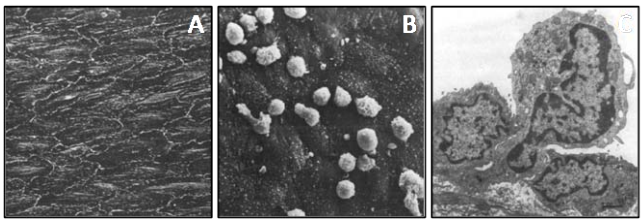

Figure 9. Hypercholesterolemia-induced leukocyte-endothelium binding and diapedesis. A. Scanning electron micrograph of an aortic endothelium from a non-human primate on a normal diet(control). B. Scanning electron micrograph of an aortic endothelium from a non-human primate on a high saturated fat/high-cholesterol diet (leukocyte are white). C. Leukocyte diapedesis through the endothelium. Adapted from [11].

junctions and into the intima (**Figure 9**).[45,46] Specifically, modified LDL has be shown to enhance leukocyte binding to the endothelium by upregulating expression of vascular cell adhesion molecule 1 (VCAM-1).[47] VCAM-1 selectively binds monocytes and lymphocytes to the endothelium thereby initiating their migration into the intima towards modified LDL (**Figure 10**). Moreover, oxLDL has been shown to induce monocyte chemotactic protein 1 (MCP-1), a potent chemo-attractant, and the binding of MCP-1 to its receptor chemokine (C-C motif) receptor 2 (CCR2) contributes to monocyte and lymphocyte migration into the arterial intima.[48]

Monocytes/Macrophages

Intimal monocytes quickly differentiate into macrophages, and lipid uptake by macrophages plays a central role in the pathophysiology of atherosclerosis. Macrophages express so-called "scavenger receptors" which bind oxidized or glycated lipoprotein particles and signal their internalization to generate foam cells.[4] Foam cells are a hallmark cell population characteristic of atherosclerotic lesions, which were named after their "foamy" appearance under the microscope as the result of intracellular lipid accumulation. Foam cells in turn express myriad pro-inflammatory cytokines and reactive oxygen species which provoke local inflammation. Foam cells may eventually become apoptotic to form the "necrotic core" characteristic of advanced atherosclerotic lesions (**Figure 10**).[4]

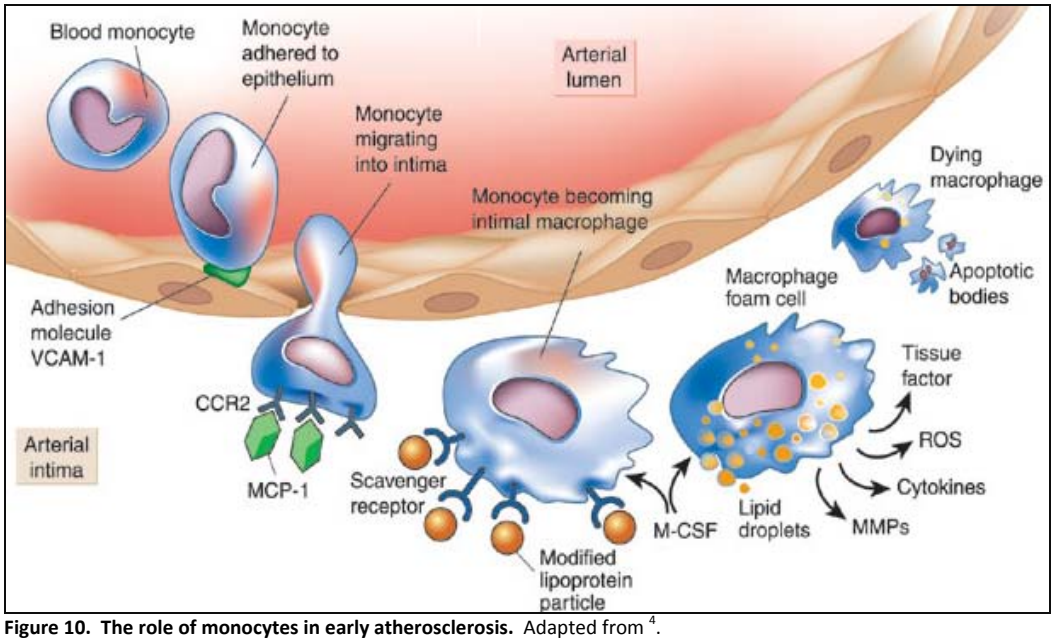

Figure 10. The role of monocytes in early atherosclerosis. Adapted from [4].

T-Lymphocytes

Similar to monocytes, T Lymphocytes (commonly referred to as T-Cells) also transmigrate through the arterial endothelium and into the intima, where they contribute to the formation of atherosclerosis (**Figure 11**). However, unlike monocytes which are attracted primarily by MCP-1, T-Cells are recruited towards gradients of inducible protein 10 (IP-10), monokine induced by interferon-γ (MIG), and interferon-inducible T-Cell α-chemoattractant (I-TAC). Each signaling molecule is derived from the local inflammatory response within the atherosclerotic plaque, and bind to T-Cells via chemokine receptor CXCR3.[2, 4]

Intimal T-cells encounter both endogenous antigens (i.e. oxidized LDL and glycated LDL) and also antigens of microbial origin (i.e. lipopolysaccharides) which initiate the release of cytokines, and/or promote the differentiation of the T cells in the predominantly "pro-inflammatory" T_H1 phenotype, or the "anti-inflammatory" T_H2 phenotype. Moreover, binding of T-Cell ligand CD40 to macrophage-expressed CD154 has been shown to induce macrophage expression of tissue factor, matrix metalloproteinases (MMPs), and pro-inflammatory cytokines; each contributing to the pathophysiology of atherosclerosis (Figure 11).[4]

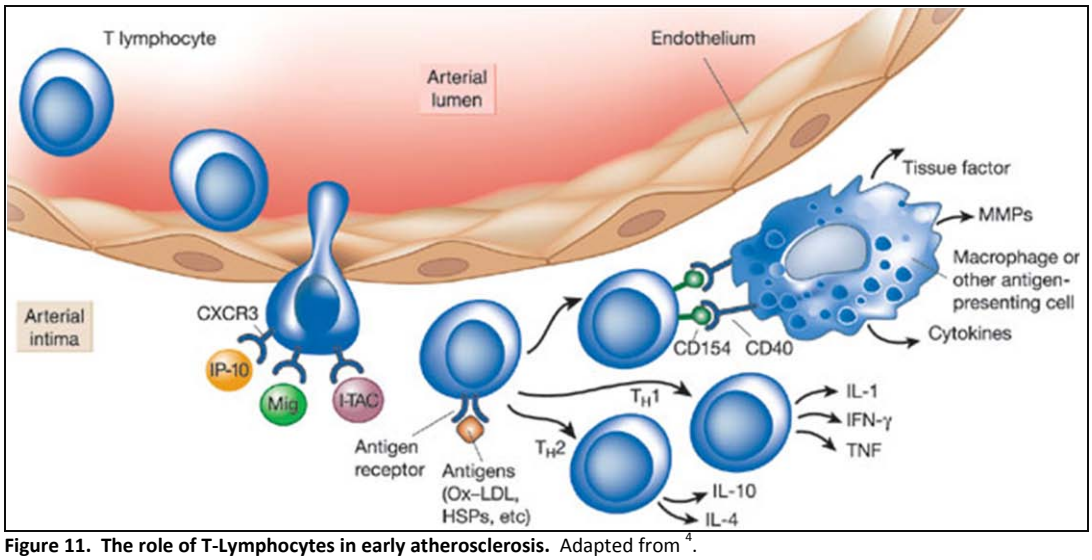

Figure 11. The role of T-Lymphocytes in early atherosclerosis. Adapted from [4].

Dendritic Cells

Dendritic cells (DC) are the most potent antigen-presenting cells and indeed play an important role in atherosclerosis. In the early atherogenesis, dendritic cells differentiate in the intima from monocytes, where they play an active role in both the adaptive and innate immune response. While DCs are found even in the subendothelial layer of apparently non-diseased arteries, it is known that comparatively increased amounts of subendothelial DCs are found in atherosclerosis prone regions of the vasculature. In atherosclerosis lesions, additional DCs invade via the inflamed endothelium and neovasculature of the vasa vasorum. As similar to other peripheral tissues, DCs are crucial to antigen capture, and presentation; a central process for T-Cell activation, and consequent release of pro-atherogenic cytokines. Dendritic cells themselves have also been shown to secrete high levels of pro-inflammatory TNF-α and interferon gamma upon activation within atherosclerotic plaques. [49, 50]

Mast Cells

A growing body of evidence also suggests that mast cells play an important, albeit lesser role compared to other leukocytes, in early atherosclerotic lesion formation.[51] In-vitro data suggests that mast cells transmigrate into the intima towards an eotaxin gradient where they undergo degranulation and release the hallmark pro-inflammatory cytokine tumor necrosis factor alpha (TNFα) and MMP activating proteases tryptase and chymase, which promote lesion formation and plaque destabilization.[52]

1.1.4 FORMATION OF ATHEROMATA

Type I – Initial Lesion

Atherosclerotic plaques are classified into five different histological classes ranging from an early Type I "fatty streak" to potentially life-threatening Type VI complicated lesions.[53, 54] Type I lesions have been observed in atherosclerosis prone regions as early as human infancy, and are characterized by the first microscopically and chemically detectable lipids in the intima. Moreover, the cellular reactions including intimal leukocyte infiltration, foam cell formation, and early SMC-associated intimal thickening are often detectable.[55]

Type II – Fatty Streak

Type II lesions are identified by so-called "fatty streaks", which are visible as yellow-colored streaks, in the intima.[56] The fatty streak in human arterial biopsies is of sufficient size such that it may be detected by the unaided eye. Cellular components of the fatty streak include lipid laden smooth muscle cells and macrophages (foam cells). Type II lesions also contain greater amounts of macrophages without lipid droplets compared to type I lesions.[57] T-lymphocytes and mast cells are typically found in the intima at much reduced numbers compared to macrophages. Both mechanical forces on the early lesion, and traditional risk factors including blood-cholesterol levels and blood pressure contribute to the transformation of Type II lesions into more advanced Type III lesions.[58]

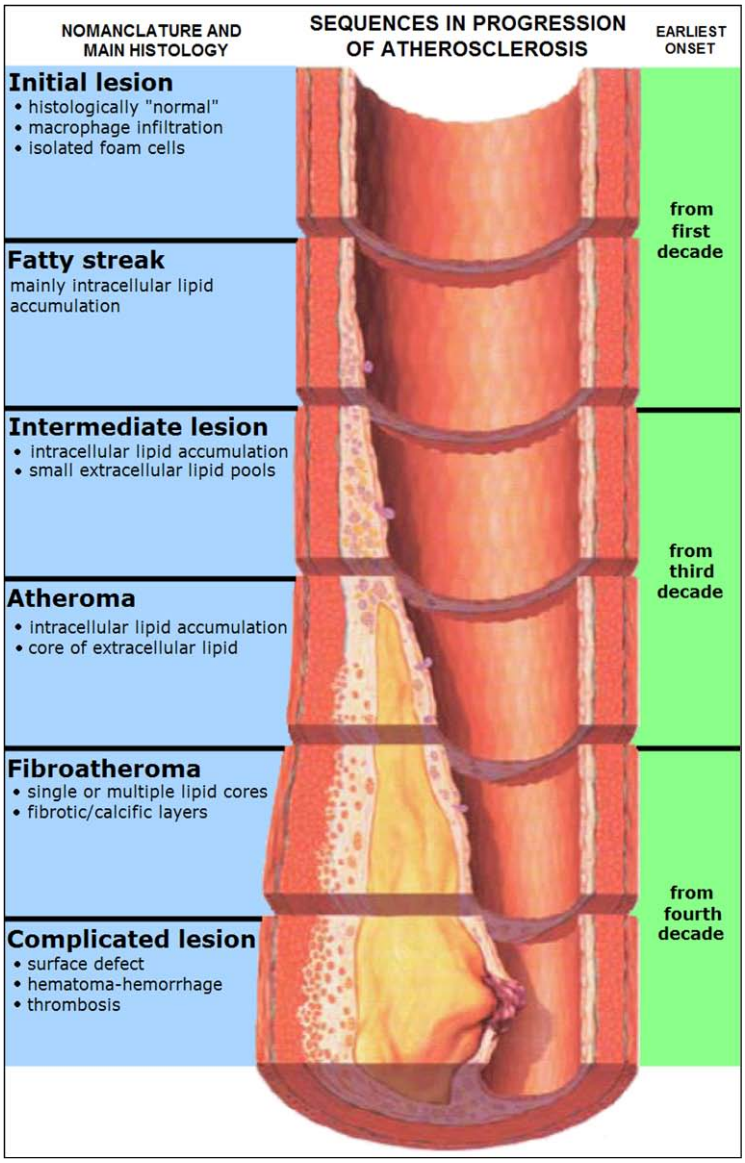

Figure 12. Pathogenesis of Atherosclerotic Plaques. Image released for free public use via the GNU Free Documentation License.

Type III – Intermediate Lesion

Type III intermediate lesions are also referred to as a pre-atheroma, and depict the morphological and chemical bridge between type II lesions and type IV atheroma.[59] While a type IV lesion is comprised

of a distinct lipid core and significant intimal disorganization, type III lesions show early signs of extracellular lipid pools. These pools typically form among the layers of smooth muscle cells in the thickened intima, immediately below a layer of macrophages and macrophage foam cells. Such lipid depositions replace resident intercellular matrix proteoglycans. However, at this stage a well-defined lipid core is not yet developed.[58]

Smooth Muscle Cell Migration

The initiation of atherosclerosis primarily involves LDL accumulation, endothelium function, and leukocyte migration. However the formation of atheromata involves smooth muscle cells. At birth, the arterial intima does not contain smooth muscle cells. However, during atheroma formation, smooth muscle cells are known to accumulate within the intima. Currently, there are two putative origins of intimal smooth muscle cells. The first purported origin is the underlying media. This theory is supported by evidence which indicates that smooth muscle cell chemoattractants including platelet-derived growth factor (PDGF) are secreted by activated plaque macrophages.[54, 60]

Progenitor-Derived Smooth Muscle Cells

The second purported origin of intimal smooth muscle cells is that of circulating smooth muscle progenitor cells. Circulating stem/progenitor cell populations have been shown to play a role in murine atherosclerosis formation by giving rise to neo-smooth muscles cells (**Figure 13**). Once migrated into the intima, these cells are believed to contribute to intimal thickening and vascular remodeling.[61] Endothelial cells which cover early lesions have a reduced lifespan due to pro-apoptotic stimuli by local inflammatory cytokines and low fluid sheer stress. When endothelial cells die, the sub-endothelial intima becomes temporarily exposed to the blood, thereby allowing an opportunity for progenitor cells to invade the intima (**Figure 13**).[10] These progenitor cells can then differentiate into so-called neo-SMCs. It has is also been observed that smooth muscle progenitor cells in the adventitia migrate to the intima via the vasa vasorum. While these mechanistic findings are primarily supported by animal studies, the identification of progenitor cells in human atherosclerotic plaque supports the notion of their role in atherogenesis.[61, 62] While the role of the progenitor cells in human atherogenesis remains largely conjectural it is generally accepted that progenitor cells are beneficial in vascular healing and impair atherosclerotic plaque formation.[63]

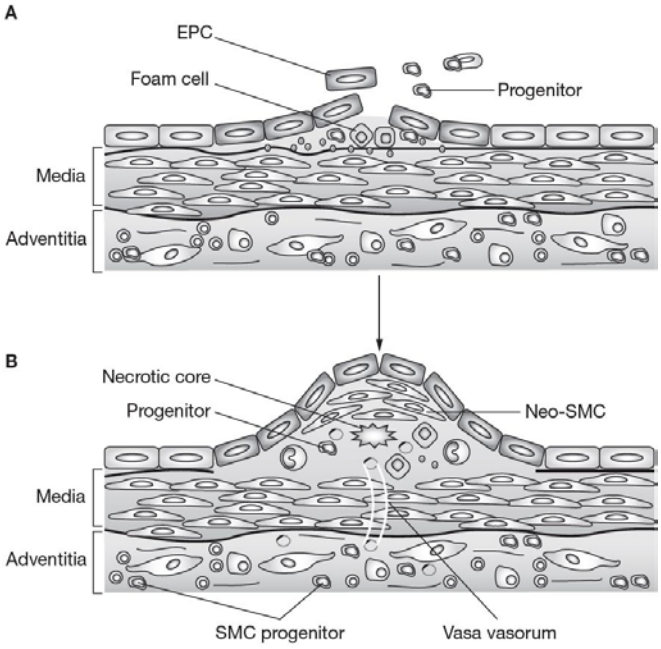

Figure 13. Schematic representation of the role of progenitor cells in the progression of atherosclerosis. (A) Endothelial cells covering and early lesion are derived from circulating endothelial progenitor cells. (B) Progenitor cell differentiate into Neo-SMCs above the necrotic core. Also smooth muscle progenitor cells (SMC progenitors) may migrate via the vaso vasorum in the plaque. Adapted from [10]

1.1.5 ADVANCED ATHEROSCLEROTIC PLAQUES

Type IV - Atheroma

Type IV atherosclerotic plaques are the earliest form of the so-called "advanced lesions", and show severe intimal disorganization caused by an extracellular lipid core. The lipid core appears to develop as smaller isolated extracellular lipid pools merge to form larger pools. Further growth of the lipid core is caused by continuous lipid transport from the blood. The intimal region between the lipid core and endothelium typically contains lipid-laden macrophages, smooth muscle cells, and to a lesser extent, lymphocytes and mast cells. Despite the classification of atheromata as advanced atherosclerotic plaques, fissures in the lesion surface and signs thrombosis are rarely observed.[59] Also the significant buildup of fibrous tissue is not yet present. However, the potential clinical significance of type IV lesions can be great, because the tissue region between the lipid core and blood stream is mechanically weak due to the lack of mature tissue formation. Therefore, Type IV lesions are particularly susceptible to the formation of fissures which often result in thrombosis and cardiovascular events.[53]

Type V – Fibroatheroma

Type V fibroatheromata are distinguished from type IV atheromata by the appearance of fibrous tissue. Fibrous tissue formation mimics that of reparative connective tissue, and forms around the lipid core. The fibrous tissue which forms between the lipid core and the endothelium is referred to as the "fibrous cap". The thickness of the fibrous cap is a key indicator of atherosclerotic plaque stability. It is frequently observed that new fibrous tissue accounts for a greater thickness of the lesion, than does the underlying lipid pool. The newly formed fibrous tissue consists of substantial increases in collagen and smooth muscle cells and occasionally, thrombi which have been incorporated into the fibrous cap and are re-organized.[64] Fibroatheroma are often multi-layered, containing several isolated lipid cores, separated by layers of fibrous tissue. Moreover, significant calcification is often observed in type V lesions. Importantly, as with type IV lesions, type V lesions may develop fissures, hematoma, and/or superficial thrombi (type VI lesion), and for this reason too they are clinically relevant. [53]

Type VI – Complicated Lesion

Atherosclerotic plaque-derived morbidity and mortality are believed to be most attributed to type IV atheromata, and type V fibroatheromata due to lesion rupture and thrombus formation. Lesions which show signs of surface defects or thrombus formation are labeled type VI, or complicated lesions. Surface defects may vary, but can typically be visualized under a microscope. The smallest defects may described as a partial loss of the endothelium to more severe deep fissures which expose the bloodstream to the plaque core.[65] These surface defects often result in thrombosis, which leads to cardiovascular events.

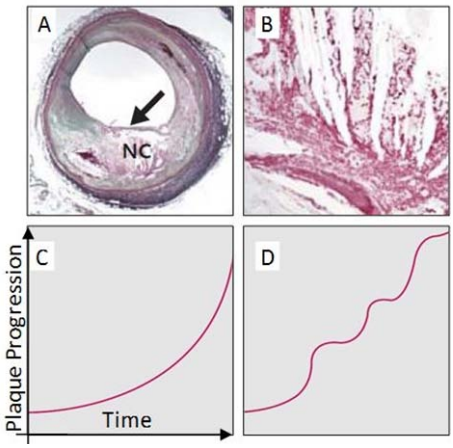

Figure 14. Intraplaque hemorrhaging contributes to a "step-wise" progression of atheroma formation. A Type V human coronary plaque (A) with a necrotic core (NC) fibrous cap (arrow) shows intraplaque hemorrhaging as visualized by an erythrocyte membrane component glycophorin A within the plaque (B). The traditional model of steady plaque progression (C) is compared to a current hypothesis of "step-wise" atheroma formation (D) due to reoccurring intraplaque hemorrhaging. Adapted from [1, 2]

The surface defects which cause thrombotic deposits are often recurrent. These thrombi, in turn, are known to be incorporated into the lesion, which may contribute to narrowing of the arterial lumen. However some thrombi enlarge to occlude the entire arterial lumen within hours or days, and are thereby life-threatening.[53]

Intraplaque Hemorrhage - Role of the Vasa Vasorum

The arterial microcirculation is characterized by a network of newly formed vessels called the vasa vasorum. The vasa vasorum in healthy large arteries form a network of microvessels that originate primarily in the adventitial layer; where they play a beneficial role supplying oxygen and nutrients to the outer layers of the arterial wall.[66] Conversely, the vasa vasorum observed within advanced atherosclerotic plaque is believed to be pathogenic and accelerate atherogenesis. Indeed, vasa vasorum density is increased four-fold in Type VI-complicated lesions vs. type IV and V atheromata and also associates with the occurrence of stroke.[67, 68]

Recent studies indicate the vasa vasorum provokes plaque progression when neo-vessels within the plaque rupture open in a process known as intraplaque hemorrhaging. Intraplaque hemorrhaging is believed to contribute to plaque progression on many levels including: deposition of free cholesterol, macrophage infiltration, and enlargement of the necrotic core. Moreover, erythrocyte membranes which are deposited into the plaque are potently atherogenic (**Figure 14 A,B**).[1]

While it is traditionally believed that atheroma development progresses in a linear fashion with age, a more current hypothesis suggests rather that short bursts of atheroma are responsible for disease progression (**Figure 14 C,D**). According to this hypothesis intraplaque hemorrhaging contributes to brief and rapid acceleration of disease progression, by introducing atherogenic stimuli into the plaque.

1.1.6 VULNERABLE ATHEROSCLEROTIC PLAQUES AND ATHEROTHROMBOSIS

Arterial Stenosis

Atherosclerosis is most often present for decades of life as an unnoticed disease. Atherosclerotic plaques typically remodel the artery outwards, away from the lumen, resulting in a minimal effect on blood-flow, and are therefore asymptomatic.[69] As atherosclerotic plaques enlarge further, they often undergo so-called inward remodeling, defined by encroachment on the arterial lumen and a restriction of arterial blood flow.[2] Lesions which produce an approximate 60% reduction of luminal cross-area, may cause insufficient flow under conditions of increased demand such as exercise. Specifically, in the coronary arteries, which vascularize the heart, limited blood flow during increased demand may result in chest pain called angina pectoris.

In most cases, patients never experience angina pectoris before suffering a myocardial infarction.[2] Indeed, many clinical studies indicate that myocardial infarction is often the not the result of arterial stenosis. Indeed only around 15% of myocardial infarctions are caused by plaques with stenosis of greater than 60% luminal occlusion. These findings suggest that many myocardial infarctions are caused by atherothrombotic complications arising from previously asymptomatic plaques.[65, 70]

Atherothrombosis

Most scientists and physicians agree that physical disruption of atherosclerotic plaques is the primary cause of acute thrombosis. Coronary thrombi derive from two known modes of plaque disruption; fibrous cap rupture and superficial intimal erosion. While plaque rupture accounts for roughly 66% of

all myocardial infarctions, superficial erosion accounts for approximately 25%.[65, 71] The magnitude of the thrombotic process triggered upon plaque disruption is regulated by elements which determine both plaque and blood thrombogenicity including: local shear rate, tissue factor (TF), apoptotic microparticles, circulating cell populations, and others.[14] An understanding of the data presented in this thesis requires a basic knowledge of blood coagulation pathways.

Blood is known to coagulate according to two processes: platelet aggregation and fibrin polymerization. Some scientists believe that platelet activation is the main trigger of atherothrombosis. Typically, platelets circulate in an inactivated state, and interact only very briefly with the arterial wall. However, at the site of plaque disruption, platelets are recruited, adhere, and become activated to form microaggregates (**Figure 15**). For information regarding the molecular mechanisms of platelet recruitment and activation, the reader is referred to the following review articles.[72, 73]

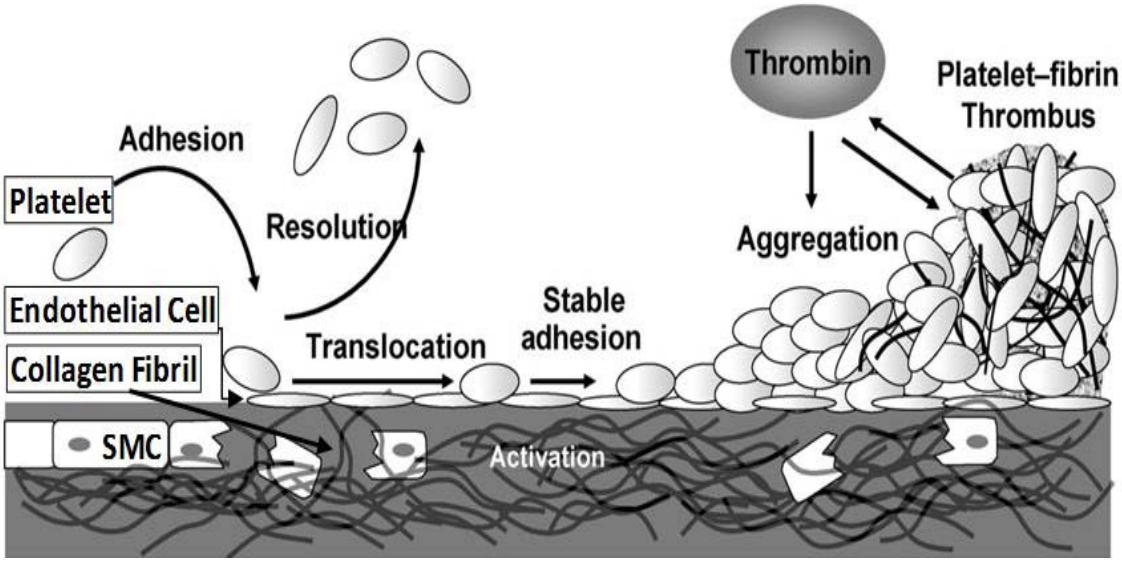

Figure 15. The Role of Platelet Activation in Atherothrombosis. Most platelets briefly contact the endothelium and then recirculate. However, platelets may also contact the intimal collagen and prothrombotic smooth muscle cells (SMC) at the site of plaque disruption, thereby promoting their activation. Activated platelets stably adhere to the vessel wall, directing further platelet aggregation; a process further promoted by thrombin. Thrombin catalyzes the crosslinking of fibrinogen into fibrin, and the resulting thrombus is comprised of both polymerized fibrin and aggregated platelets. Adapted from [12].

The contribution of fibrin to thrombus formation is governed by two opposing mechanisms; fibrinolysis and fibrin polymerization (**Figure 16**). Advanced atherosclerotic plaques are known to release factors which inhibit fibrinolysis (such as plaminogen activator inhibitor-1), and other factors which accelerate blood coagulation (i.e. Tissue Factor). Myriad review publications are available for more complete information regarding blood coagulation pathways.[74]

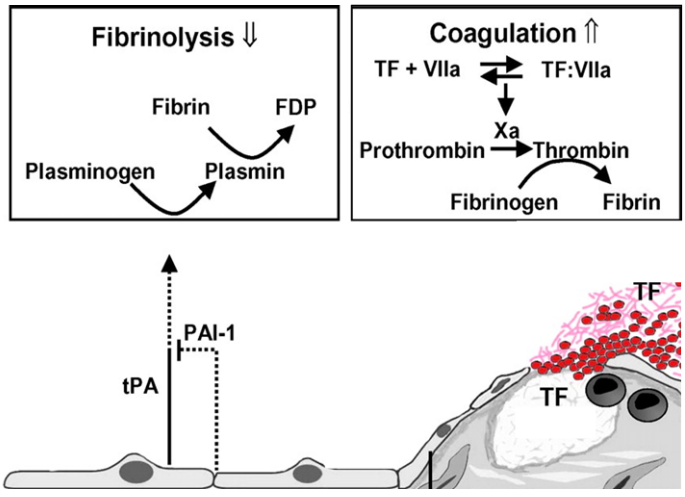

Figure 16. Blood Coagulation Pathways in Atherothrombosis. The healthy endothelium produces tissue plasminogen activator (tPA), an enzyme which catalyzes the conversion of plasminogen to plasmin, therefore promoting clot lysis (fibrinolysis; fibrin is converted to fibrin degradation products (FDP) by plasmin). Plaminogen activator inhibitor-1 (PAI-1) expression is enhanced in atherosclerotic plaques and neutralizes (tPA) activity, thereby limiting fibrinolysis. Coagulation is characterized by the polymerization of fibrinogen into fibrin. In this process, tissue factor (TF) is known to be released by disrupted plaques and combine with factor VIIa to activate factor Xa; an enzyme that catalyzes the conversion of prothrombin to thrombin. In turn, thrombin catalyzes the conversion of fibrinogen to fibrin, thereby promoting thrombus formation. Adapted from [14]

Role of Inflammation in Plaque Rupture and Atherothrombosis

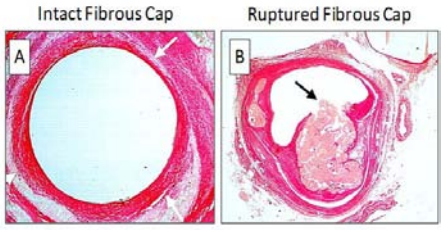

Figure 17. Fibrous Cap Rupture. A representative atherosclerotic plaque with a fibrous cap (A; white arrows) overlying lipid-rich areas, and a plaque with a fibrous cap rupture (b; black arrow) are

The fibrous cap is a layer of fibrotic connective tissue, which separates the arterial lumen from the prothrombogenic necrotic core. Rupture of the fibrous cap is a critical trigger of atherothrombosis that directs cardiovascular events. A critical event in plaque rupture is the degradation of the fibrous cap, which exposes the underlying thrombogenic core to the bloodstream, thereby provoking thrombosis and subsequent vessel occlusion (**Figure 17**). Coronary fibrous caps with a thickness of less than 65 microns have been shown to associate with plaque rupture and sudden cardiac death.[75] While the mechanical strength of the fibrous cap is provided primarily by type I collagen, collagenases including matrix metalloproteinases and cysteine proteases have been associated with plaque instability and the occurrence of acute thrombotic events.[76-78]

Macrophages often accumulate in the fibrous cap and shoulder regions of rupture-prone coronary plaque. Indeed activated macrophages produce matrix degrading proteases known to degrade collagen and destabilize the plaque. Moreover, plaque macrophages express tissue factor in response to CD154 (a T-Cell-surface inflammatory cytokine) which initiates thrombosis (**Figure 16**). Therefore, inflammation contributes to plaque rupture by degrading collagen in the fibrous cap, and also enhancing the thrombogenicity of the plaque's interior; thereby accelerating thrombus formation upon plaque disruption.[79]

Thrombosis due to Superficial Erosion

While the pathophysiology of fibrous cap rupture has received much attention, atherothrombosis derived from superficial erosion has been less aggressively pursued. This may perhaps in part be attributed to studies of the coronary vasculature which reveal that asymptomatic platelet deposition is commonplace in advanced lesions, and indeed most plaque disruptions do not give rise to clinically apparent coronary events. However, atherothrombosis derived from intimal erosion remains a serious clinical concern, accounting for approximately 25% of all acute myocardial infarction-related deaths.[71] It has been hypothesized that apoptotic endothelial cells could indeed contribute to thrombosis in areas of superficial erosion. Also, inflammation induced extracellular collagenases and elastinases may degrade the structural components of the basement membrane, which tether the endothelium. In turn, removal of endothelial cells from the basement membrane exposes platelets and coagulation factors to the basement membrane, thereby promoting their activation.[12, 71, 80]

1.1.7 CLINICAL IDENTIFICATION OF VULNERABLE ATHEROSCLEROTIC PLAQUES

Circulating Biomarkers

While established cardiovascular risk factors including smoking, diabetes mellitus, and hypertension are used in cardiovascular risk assessment, they do not fully explain patient vulnerability to cardiovascular events.[81] Therefore, many scientists and clinicians have pursued additional biomarkers to add value in clinical decision making, including: C-reactive Protein (CRP), homocystiene, and soluble CD40 ligand. [13, 81] Moreover, it is logical that several biomarkers could be measured simultaneously in relationship to each other to improve risk stratification in patients. Most of the currently investigated

circulating biomarkers are indeed linked by a shared involvement in pro-atherogenic inflammatory processes (**Figure 18**). While many biomarkers spill over from the plaque and into the bloodstream at all stages of atherosclerosis, those which are released immediately prior to myocardial infarction or stroke may hold the highest clinical potential. Here, only the two most thoroughly investigated biomarkers (C-Reactive Protein and IL-6) will be addressed to exemplify their common link to inflammation. For further review of circulating atherosclerosis biomarkers, the reader is referred to a review article by Koenig et al.[13]

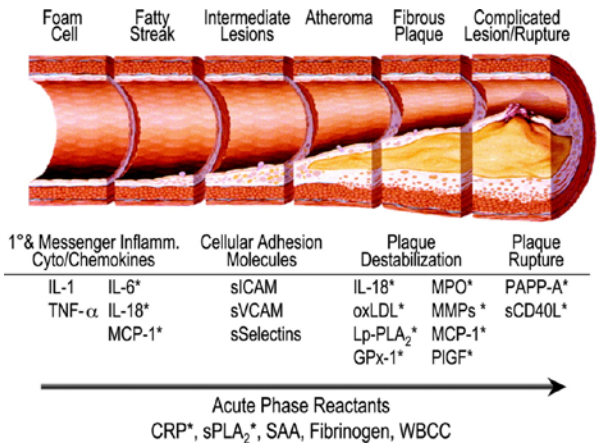

Figure 18. Circulating Biomarkers of Atherosclerosis. Investigated biomarkers for each stage of plaque progression are shown. IL-1 = interleukin 1, TNF-α = tumor necrosis factor, MCP-1 = monocyte chemoattractant protein-1, sICAM = soluble intercellular adhesion molecule-1, sVCAM = soluble vascular cell adhesion molecule,oxLDL = oxidized low density lipoprotein, Lp-PLA_2 = lipoprotein associated phospholipase A_2, GPx-1 = glutathione peroxidase, MPO = myeloperoxidase, MMPs = matrix metalloproteinases, PlGF = placental growth factor, PAPP-A = pregnancy-associated plasma protein-A, sCD40L = soluble CD40 ligand, CRP = C-reactive protein, $sPLA_2$, secretory type II phospholipase A_2, SAA = serum amyloid A, WBCC = white blood cell count. Adapted from [13].

C-Reactive Protein (CRP) is perhaps the best studied pro-inflammatory biomarker with over 25 prospective studies conducted to date. While CRP is generally believed to address the acute inflammatory response in the body, recent evidence also indicates its expression by smooth muscle cells and macrophages in atherosclerotic plaques.[82] An additional study also shows that high CRP levels strongly correlate with vulnerable atherosclerotic plaque burden.[83]

Interleukin-6 (IL-6) is a cytokine expressed in activated monocytes/macrophages and endothelial cells. IL-6 expression is typically localized to the shoulder region of unstable human plaques, where it contributes to enhanced free radical oxygen production and endothelial dysfunction.[84, 85] IL-6 amplifies plaque inflammation, and is also a potent pro-coagulant cytokine involved in atherothrombosis. Indeed, several studies have demonstrated a predictive value of circulating IL-6 levels for future cardiovascular events. Perhaps the most relevant data are derived from the Fragmin and Fast Revascularization During Instability in Coronary Artery Disease II (FRISC II) studies, which demonstrate that patients with high IL-6 level might benefit the most from an early invasive strategy, such as a coronary bypass or stenting.[86]

Indeed, multiple biomarkers have been shown to predict plaque destabilization and rupture and subsequent clinical complications. However, these cytokines measure the substantial relative risk of cardiovascular events on the order of 2-3 fold, and therefore may not yet be sufficient in clinical decision-making with regards to early interventions.[13] This is exemplified by exhaustive clinical CRP studies which, taken together, have yet to define CRPs incremental value in clinical decision making towards cardiovascular events. Therefore, additional biomarkers which predict the clinical complications of atherosclerosis are still needed. If discovered, these biomarkers must demonstrate specificity, sensitivity, predictive value, practical implementation, and cost-effectiveness to ultimately be of significant clinical use.[87]

Molecular Imaging

60% of myocardial infarctions are caused by vulnerable plaques which go undetected by current clinical imaging methods (i.e. magnetic resonance imaging and intravascular ultrasound). While currently employed imaging methods provide anatomical and morphological information, they cannot detect the biological signals which predict plaque rupture.[88] Specifically, inflammatory cytokines,

proteolytic enzymes, and oxidative species which provoke atherothrombosis remain difficult to identify *in vivo*. The rationale behind molecular imaging derives from the recognition that molecular and cellular processes govern vulnerable plaque disruption. Once brought into the clinic, molecular imaging could have many capabilities including more precise visualization of rupture-prone atherosclerotic lesions, and provide imaging endpoints for clinical trials of anti-atherosclerosis therapies. Moreover the combination of molecular imaging with circulating biomarker analyses may someday assist in clinical decision making.[89]

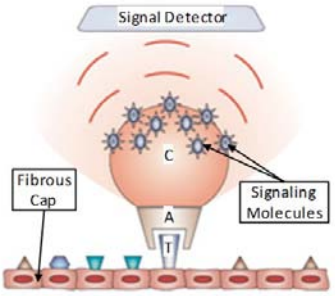

Figure 19. Molecular imaging of vulnerable atherosclerotic plaques. The vulnerable plaque target protein (T) is bound by an antibody (A). The antibody may be linked to a carrier particle (C) and a payload of signaling molecules (S). The emitted signals are recorded by a signal detector.

The fundamental molecular imaging approach consists of four parts; (i) a disease-specific target, (ii) a target binding agent, (iii) signalling molecules, and (iv) a signal detector (**Figure 19**).[89] In a more sophisticated approach some groups have employed enzyme-specific probes, that when cleaved by the enzyme of interest, emit a signal for detection.[90] Other groups have targeted specific transports with labelled substances which are taken up into the tissue, most notably fluorodeoxyglucose (^{18}F), commonly abbreviated ^{18}F-FDG.[91]

Molecular imaging, unlike anatomic imaging, focuses on plaque biology and may therefore identify rupture-prone atherosclerotic plaques. Once rupture-prone plaques are identified, decisive measures can be employed, systemically or locally, to prevent myocardial infarction or stroke. For example a decision could be made to perform coronary artery bypass or to place a coronary stent. Conversely, a decision not to perform an intervention may avoid unnecessary complications and re-intervention. Therefore, improved molecular imaging strategies would certainly support these decisions. Taken together, molecular imaging should assess the lesion-specific risk, which could then be combined with traditional risk factors to personalize a therapeutic strategy.[92]

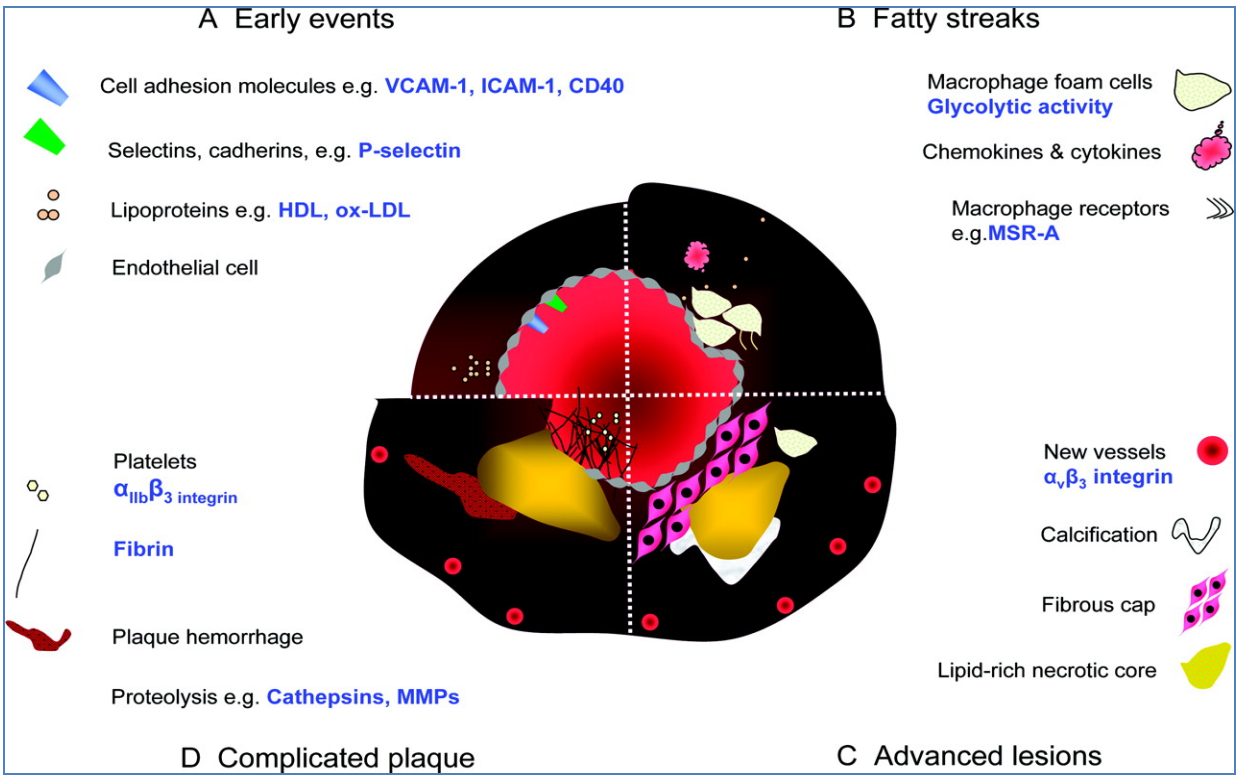

Figure 20. Targets for molecular imaging of atherosclerotic plaques at different stages of disease progression. Schematic arterial cross section demonstrating different phase of atherosclerotic lesion progress and the examples of appropriate molecular targets at each stage of plaque progression. Adapted from [6].

Selecting suitable molecular targets is central to molecular imaging strategies. While some molecular targets may be suitable for quantifying end-points of therapeutic interventions, different targets are perhaps more ideally suited for identifying potentially life threatening rupture-prone atherosclerotic lesions (**Figure 20**). For example, molecular targets of inflammation, arterial remodeling, and tissue metabolism are perhaps best suited for determining the efficacy of anti-atherosclerotic medications. However, to identify rupture-prone atheromata, molecular targets must be tightly associated with features of vulnerable plaque rupture. These factors include fibrous cap thickness, superficial intimal erosion, and sub-clinical thrombus formation.

1.1.8 REFERENCES

1. Kolodgie FD, Gold HK, Burke AP, Fowler DR, Kruth HS, Weber DK, Farb A, Guerrero LJ, Hayase M, Kutys R, Narula J, Finn AV, Virmani R. Intraplaque hemorrhage and progression of coronary atheroma. *New England Journal of Medicine*. 2003;349:2316-2325
2. Libby P. Vascular biology of atherosclerosis: Overview and state of the art. *The American Journal of Cardiology*. 2003;91:3-6
3. U.S. National center for health statistics, *health*. *United States, 2007*
4. Libby P. Inflammation in atherosclerosis. *Nature*. 2002;420:868-874
5. Nievelstein PFEM, Fogelman AM, Mottino G, Frank JS. Lipid accumulation in rabbit aortic intima 2 hours after bolus infusion of low density lipoprotein. *Arterioscler Thromb.* 1991;11:1795-1805
6. Choudhury RP, Fisher EA. Molecular imaging in atherosclerosis, thrombosis, and vascular inflammation. *Arteriosclerosis, Thrombosis, and Vascular Biology*. 2009;29:983-991
7. Pasterkamp G, Falk E, Woutman H, Borst C. Techniques characterizing the coronary atherosclerotic plaque: Influence on clinical decision making? *Journal of the American College of Cardiology*. 2000;36:13-21
8. Ford ES, Ajani UA, Croft JB, Critchley JA, Labarthe DR, Kottke TE, Giles WH, Capewell S. Explaining the decrease in u.S. Deaths from coronary disease, 1980–2000. *New England Journal of Medicine*. 2007;356:2388-2398
9. *Warrell DA*, C*ox TM*, F*irth JD*. ***Oxford textbook of medicine, fifth edition***. Oxford University Press; 2010.
10. Xu Q. The impact of progenitor cells in atherosclerosis. *Nat Clin Pract Cardiovasc Med*. 2006;3:94-101
11. Faggiotto A, Ross R, Harker L. Studies of hypercholesterolemia in the nonhuman primate. I. Changes that lead to fatty streak formation. *Arterioscler Thromb Vasc Biol*. 1984;4:323-340
12. Gawaz M. The evolving science of atherothrombotic disease. *European Heart Journal Supplements*. 2008;10:I4-I7
13. Koenig W, Khuseyinova N. Biomarkers of atherosclerotic plaque instability and rupture. *Arterioscler Thromb Vasc Biol*. 2007;27:15-26
14. Viles-Gonzalez JF, Fuster V, Badimon JJ. Atherothrombosis: A widespread disease with unpredictable and life-threatening consequences. *European Heart Journal*. 2004;25:1197-1207
15. Allam AH, Thompson RC, Wann LS, Miyamoto MI, Thomas GS. Computed tomographic assessment of atherosclerosis in ancient egyptian mummies. *JAMA: The Journal of the American Medical Association*. 2009;302:2091-2094
16. David AR, Kershaw A, Heagerty A. Atherosclerosis and diet in ancient egypt. *The Lancet*. 2010;375:718-719
17. Faergeman O. The atherosclerosis epidemic: Methodology, nosology, and clinical practice. *The American Journal of Cardiology*. 2001;88:4-7
18. Sijbrands EJG, Westendorp RGJ, Defesche JC, de Meier PHEM, Smelt AHM, Kastelein JJP, Kaprio J. / mortality over two centuries in large pedigree with familial hypercholesterolaemia: Family tree mortality study / commentary: Role of other genes and environment should not be overlooked in monogenic disease. *BMJ*. 2001;322:1019-1023
19. Franks PW, Hanson RL, Knowler WC, Sievers ML, Bennett PH, Looker HC. Childhood obesity, other cardiovascular risk factors, and premature death. *New England Journal of Medicine*. 2010;362:485-493
20. Mortality and global burden of disease, world health organization. 2004

21. Anderson rn. U.S. Decennial life tables for 1989–91: United states life tables eliminating certain causes of death. Vol. 1. Hyattsville, md: National center for health statistics; 1999.
22. Ohsfeldt RL, Gandhi SK, Fox KM, Bullano MF, Davidson M. Medical and cost burden of atherosclerosis among patients treated in routine clinical practice. *Journal of Medical Economics*. 2010;13:500-507
23. Kaul P, Douglas PS. Atherosclerosis imaging. *Circulation: Cardiovascular Imaging*. 2009;2:150-160
24. Wight TN. The extracellular matrix and atherosclerosis. *Current Opinion in Lipidology*. 1995;6:326-334
25. Schwartz S, Campbell G, Campbell J. Replication of smooth muscle cells in vascular disease. *Circ Res*. 1986;58:427-444
26. Crisan M, Yap S, Casteilla L, Chen C-W, Corselli M, Park TS, Andriolo G, Sun B, Zheng B, Zhang L, Norotte C, Teng P-N, Traas J, Schugar R, Deasy BM, Badylak S, Bqhring H-J, Giacobino J-P, Lazzari L, Huard J, Péault B. A perivascular origin for mesenchymal stem cells in multiple human organs. *Cell stem cell*. 2008;3:301-313
27. Torzewski M, Navarro B, Cheng F, Canisius A, Schmidt T, Bhakdi S, Urban R, Lackner KJ. Investigation of sudan iv staining areas in aortas of infants and children: Possible prelesional stages of atherogenesis. *Atherosclerosis*. 2009;206:159-167
28. Schwenke D, Carew T. Initiation of atherosclerotic lesions in cholesterol-fed rabbits. I. Focal increases in arterial ldl concentration precede development of fatty streak lesions. *Arterioscler Thromb Vasc Biol*. 1989;9:895-907
29. Björkerud S, Bondjers G. Endothelial integrity and viability in the aorta of the normal rabbit and rat as evaluated with dye exclusion tests and interference contrast microscopy. *Atherosclerosis*.15:285-300
30. Topper JN, Gimbrone Jr MA. Blood flow and vascular gene expression: Fluid shear stress as a modulator of endothelial phenotype. *Molecular Medicine Today*. 1999;5:40-46
31. Krams R, Wentzel JJ, Oomen JAF, Vinke R, Schuurbiers JCH, de Feyter PJ, Serruys PW, Slager CJ. Evaluation of endothelial shear stress and 3d geometry as factors determining the development of atherosclerosis and remodeling in human coronary arteries in vivo : Combining 3d reconstruction from angiography and ivus (angus) with computational fluid dynamics. *Arterioscler Thromb Vasc Biol*. 1997;17:2061-2065
32. Chien S. Effects of disturbed flow on endothelial cells. *Annals of Biomedical Engineering*. 2008;36
33. Chien S. Molecular and mechanical bases of focal lipid accumulation in arterial wall. *Progress in Biophysics and Molecular Biology*. 2003;83:131-151
34. Wilson PW, Garrison RJ, Castelli WP, Feinleib M, McNamara PM, Kannel WB. Prevalence of coronary heart disease in the framingham offspring study: Role of lipoprotein cholesterols. *The American Journal of Cardiology*. 1980;46:649-654
35. Witztum JL, Berliner JA. Oxidized phospholipids and isoprostanes in atherosclerosis. *Current Opinion in Lipidology*. 1998;9:7
36. Morrow JD, Frei B, Longmire AW, Gaziano JM, Lynch SM, Shyr Y, Strauss WE, Oates JA, Roberts LJ. Increase in circulating products of lipid peroxidation (f2-isoprostanes) in smokers — smoking as a cause of oxidative damage. *New England Journal of Medicine*. 1995;332:1198-1203
37. Memon RA, Staprans I, Noor M, Holleran WM, Uchida Y, Moser AH, Feingold KR, Grunfeld C. Infection and inflammation induce ldl oxidation in vivo. *Arterioscler Thromb Vasc Biol*. 2000;20:1536-1542
38. Navder KP, Baraona E, Leo MA, Lieber CS. Oxidation of ldl in baboons is increased by alcohol and attenuated by polyenylphosphatidylcholine. *Journal of Lipid Research*. 1999;40:983-987

39. George J, Afek A, Shaish A, Levkovitz H, Bloom N, Cyrus T, Zhao L, Funk CD, Sigal E, Harats D. 12/15-lipoxygenase gene disruption attenuates atherogenesis in ldl receptor-deficient mice. *Circulation*. 2001;104:1646-1650
40. Schissel SL, Jiang X-c, Tweedie-Hardman J, Jeong T-s, Camejo EH, Najib J, Rapp JH, Williams KJ, Tabas I. Secretory sphingomyelinase, a product of the acid sphingomyelinase gene, can hydrolyze atherogenic lipoproteins at neutral ph. *Journal of Biological Chemistry*. 1998;273:2738-2746
41. Lyons TJ. Glycation and oxidation: A role in the pathogenesis of atherosclerosis. *The American Journal of Cardiology*. 1993;71:B26-B31
42. Teissedre PL, Frankel EN, Waterhouse AL, Peleg H, German JB. Inhibition ofin vitrohuman ldl oxidation by phenolic antioxidants from grapes and wines. *Journal of the Science of Food and Agriculture*. 1996;70:55-61
43. Esterbauer H, Rotheneder M, Striegl G, Waeg G, Ashy A, Sattler W, Jürgens G. Vitamin e and other lipophilic antioxidants protect ldl against oxidation. *Lipid / Fett*. 1989;91:316-324
44. Kubes P, Kerfoot SM. Leukocyte recruitment in the microcirculation: The rolling paradigm revisited. *Physiology*. 2001;16:76-80
45. Scalia R, Appel JZ, III, Lefer AM. Leukocyte-endothelium interaction during the early stages of hypercholesterolemia in the rabbit : Role of p-selectin, icam-1, and vcam-1. *Arterioscler Thromb Vasc Biol*. 1998;18:1093-1100
46. Cybulsky M, Gimbrone M. Endothelial expression of a mononuclear leukocyte adhesion molecule during atherogenesis. *Science*. 1991;251:788-791
47. Collins T, Cybulsky MI. Nf-κb: Pivotal mediator or innocent bystander in atherogenesis? *The Journal of Clinical Investigation*. 2001;107:255-264
48. Li D, Mehta JL. Antisense to lox-1 inhibits oxidized ldl-mediated upregulation of monocyte chemoattractant protein-1 and monocyte adhesion to human coronary artery endothelial cells. *Circulation*. 2000;101:2889-2895
49. Bobryshev YV. Dendritic cells in atherosclerosis: Current status of the problem and clinical relevance. *European Heart Journal*. 2005;26:1700-1704
50. Tedgui A, Mallat Z. Cytokines in atherosclerosis: Pathogenic and regulatory pathways. *Physiological Reviews*. 2006;86:515-581
51. Sun J, Sukhova GK, Wolters PJ, Yang M, Kitamoto S, Libby P, MacFarlane LA, Clair JM-S, Shi G-P. Mast cells promote atherosclerosis by releasing proinflammatory cytokines. *Nat Med*. 2007;13:719-724
52. Wang Y, Shiota N, Leskinen MJ, Lindstedt KA, Kovanen PT. Mast cell chymase inhibits smooth muscle cell growth and collagen expression in vitro: Transforming growth factor-{beta}1-dependent and -independent effects. *Arteriosclerosis, Thrombosis, and Vascular Biology*. 2001;21:1928-1933
53. Stary HC, Chandler AB, Dinsmore RE, Fuster V, Glagov S, Insull W, Jr, Rosenfeld ME, Schwartz CJ, Wagner WD, Wissler RW. A definition of advanced types of atherosclerotic lesions and a histological classification of atherosclerosis : A report from the committee on vascular lesions of the council on arteriosclerosis, american heart association. *Circulation*. 1995;92:1355-1374
54. Stary HC, Chandler AB, Dinsmore RE, Fuster V, Glagov S, Insull W, Jr, Rosenfeld ME, Schwartz CJ, Wagner WD, Wissler RW. A definition of advanced types of atherosclerotic lesions and a histological classification of atherosclerosis : A report from the committee on vascular lesions of the council on arteriosclerosis, american heart association. *Arterioscler Thromb Vasc Biol*. 1995;15:1512-1531

55. Nakashima Y, Raines EW, Plump AS, Breslow JL, Ross R. Upregulation of vcam-1 and icam-1 at atherosclerosis-prone sites on the endothelium in the apoe-deficient mouse. *Arteriosclerosis, Thrombosis, and Vascular Biology*. 1998;18:842-851
56. Napoli C, D'Armiento FP, Mancini FP, Postiglione A, Witztum JL, Palumbo G, Palinski W. Fatty streak formation occurs in human fetal aortas and is greatly enhanced by maternal hypercholesterolemia. Intimal accumulation of low density lipoprotein and its oxidation precede monocyte recruitment into early atherosclerotic lesions. *The Journal of Clinical Investigation*. 1997;100:2680-2690
57. Stary HC. The sequence of cell and matrix changes in atherosclerotic lesions of coronary arteries in the first forty years of life. *European Heart Journal*. 1990;11:3-19
58. Stary HC, Chandler AB, Glagov S, Guyton JR, Insull W, Jr., Rosenfeld ME, Schaffer SA, Schwartz CJ, Wagner WD, Wissler RW. A definition of initial, fatty streak, and intermediate lesions of atherosclerosis. A report from the committee on vascular lesions of the council on arteriosclerosis, american heart association. *Circulation*. 1994;89:2462-2478
59. Virmani R, Kolodgie FD, Burke AP, Farb A, Schwartz SM. Lessons from sudden coronary death : A comprehensive morphological classification scheme for atherosclerotic lesions. *Arteriosclerosis, Thrombosis, and Vascular Biology*. 2000;20:1262-1275
60. Allen CL, Bayraktutan U. Differential mechanisms of angiotensin ii and pdgf-bb on migration and proliferation of coronary artery smooth muscle cells. *Journal of Molecular and Cellular Cardiology*. 2008;45:198-208
61. Sata M, Saiura A, Kunisato A, Tojo A, Okada S, Tokuhisa T, Hirai H, Makuuchi M, Hirata Y, Nagai R. Hematopoietic stem cells differentiate into vascular cells that participate in the pathogenesis of atherosclerosis. *Nat Med*. 2002;8:403-409
62. Zoll J, Fontaine V, Gourdy P, Barateau V, Vilar J, Leroyer A, Lopes-Kam I, Mallat Z, Arnal J-F, Henry P, Tobelem G, Tedgui A. Role of human smooth muscle cell progenitors in atherosclerotic plaque development and composition. *Cardiovascular Research*. 2008;77:471-480
63. Satoh K, Berk BC. Circulating smooth muscle progenitor cells: Novel players in plaque stability. *Cardiovascular Research*. 2008;77:445-447
64. Kolodgie FD, Burke AP, Farb A, Gold HK, Yuan J, Narula J, Finn AV, Virmani R. The thin-cap fibroatheroma: A type of vulnerable plaque: The major precursor lesion to acute coronary syndromes. *Current Opinion in Cardiology*. 2001;16
65. Falk E, Shah PK, Fuster V. Coronary plaque disruption. *Circulation*. 1995;92:657-671
66. Mulligan-Kehoe MJ. The vasa vasorum in diseased and nondiseased arteries. *American Journal of Physiology - Heart and Circulatory Physiology*. 2010;298:H295-H305
67. Kolodgie FD, Virmani R, Burke AP, Farb A, Weber DK, Kutys R, Finn AV, Gold HK. Pathologic assessment of the vulnerable human coronary plaque. *Heart*. 2004;90:1385-1391
68. Staub D, Patel MB, Tibrewala A, Ludden D, Johnson M, Espinosa P, Coll B, Jaeger KA, Feinstein SB. Vasa vasorum and plaque neovascularization on contrast-enhanced carotid ultrasound imaging correlates with cardiovascular disease and past cardiovascular events. *Stroke*. 2010;41:41-47
69. Ward MR, Pasterkamp G, Yeung AC, Borst C. Arterial remodeling : Mechanisms and clinical implications. *Circulation*. 2000;102:1186-1191
70. Smith SC, Jr. Risk-reduction therapy: The challenge to change : Presented at the 68th scientific sessions of the american heart association november 13, 1995 anaheim, california. *Circulation*. 1996;93:2205-2211
71. Farb A, Burke AP, Tang AL, Liang Y, Mannan P, Smialek J, Virmani R. Coronary plaque erosion without rupture into a lipid core : A frequent cause of coronary thrombosis in sudden coronary death. *Circulation*. 1996;93:1354-1363

72. Ruggeri ZM. Platelets in atherothrombosis. *Nat Med*. 2002;8:1227-1234
73. Davì G, Patrono C. Platelet activation and atherothrombosis. *New England Journal of Medicine*. 2007;357:2482-2494
74. Ajjan R, Grant PJ. Coagulation and atherothrombotic disease. *Atherosclerosis*. 2006;186:240-259
75. Virmani R, Burke AP, Kolodgie FD, Farb A. Pathology of the thin-cap fibroatheroma. *Journal of Interventional Cardiology*. 2003;16:267-272
76. Hansson GK. Inflammation, atherosclerosis, and coronary artery disease. *N Engl J Med*. 2005;352:1685-1695
77. Newby AC. Dual role of matrix metalloproteinases (matrixins) in intimal thickening and atherosclerotic plaque rupture. *Physiol. Rev.* 2005;85:1-31
78. Galis ZS, Khatri JJ. Matrix metalloproteinases in vascular remodeling and atherogenesis: The good, the bad, and the ugly. *Circ Res*. 2002;90:251-262
79. Libby P. Molecular and cellular mechanisms of the thrombotic complications of atherosclerosis. *Journal of Lipid Research*. 2009;50:S352-S357
80. van der Wal A, Becker A, van der Loos C, Das P. Site of intimal rupture or erosion of thrombosed coronary atherosclerotic plaques is characterized by an inflammatory process irrespective of the dominant plaque morphology. *Circulation*. 1994;89:36-44
81. Wang TJ, Gona P, Larson MG, Tofler GH, Levy D, Newton-Cheh C, Jacques PF, Rifai N, Selhub J, Robins SJ, Benjamin EJ, D'Agostino RB, Vasan RS. Multiple biomarkers for the prediction of first major cardiovascular events and death. *New England Journal of Medicine*. 2006;355:2631-2639
82. Calabro P, Willerson JT, Yeh ETH. Inflammatory cytokines stimulated c-reactive protein production by human coronary artery smooth muscle cells. *Circulation*. 2003;108:1930-1932
83. Burke AP, Tracy RP, Kolodgie F, Malcom GT, Zieske A, Kutys R, Pestaner J, Smialek J, Virmani R. Elevated c-reactive protein values and atherosclerosis in sudden coronary death: Association with different pathologies. *Circulation*. 2002;105:2019-2023
84. Schieffer B, Selle T, Hilfiker A, Hilfiker-Kleiner D, Grote K, Tietge UJF, Trautwein C, Luchtefeld M, Schmittkamp C, Heeneman S, Daemen MJAP, Drexler H. Impact of interleukin-6 on plaque development and morphology in experimental atherosclerosis. *Circulation*. 2004;110:3493-3500
85. Schieffer B, Schieffer E, Hilfiker-Kleiner D, Hilfiker A, Kovanen PT, Kaartinen M, Nussberger J, Harringer W, Drexler H. Expression of angiotensin ii and interleukin 6 in human coronary atherosclerotic plaques : Potential implications for inflammation and plaque instability. *Circulation*. 2000;101:1372-1378
86. Lindmark E, Diderholm E, Wallentin L, Siegbahn A. Relationship between interleukin 6 and mortality in patients with unstable coronary artery disease. *JAMA: The Journal of the American Medical Association*. 2001;286:2107-2113
87. Stampfer MJ, Ridker PM, Dzau VJ. Risk factor criteria. *Circulation*. 2004;109:IV-3-5
88. Fuster V, Lois F, Franco M. Early identification of atherosclerotic disease by noninvasive imaging. *Nat Rev Cardiol*. 2010;7:327-333
89. Jaffer FA, Libby P, Weissleder R. Molecular and cellular imaging of atherosclerosis: Emerging applications. *Journal of the American College of Cardiology*. 2006;47:1328-1338
90. Jaffer FA, Kim D-E, Quinti L, Tung C-H, Aikawa E, Pande AN, Kohler RH, Shi G-P, Libby P, Weissleder R. Optical visualization of cathepsin k activity in atherosclerosis with a novel, protease-activatable fluorescence sensor. *Circulation*. 2007;115:2292-2298
91. Gambhir SS. Molecular imaging of cancer with positron emission tomography. *Nat Rev Cancer*. 2002;2:683-693

92. Leuschner F, Nahrendorf M. Molecular imaging of coronary atherosclerosis and myocardial infarction: Considerations for the bench and perspectives for the clinic. *Circulation Research*. 2011;108:593-606

1.2 FIBROBLAST ACTIVATION PROTEIN

1.2.1 CLASSIFICATION OF FIBROBLAST ACTIVATION PROTEIN

FAP is a Serine Integral Membrane Protease

FAP is a serine protease shown to play a role in tissue remodeling during tumourogenesis, rheumatoid arthritis, and chronic inflammatory liver disease. As these diseases have similar inflammatory-mediated pathophysiology as atherogenesis, we hypothesized that FAP is also involved in the development of atherosclerotic lesions. FAP has been studied in different directions and under varying names including: Seprase, Fibroblast Activation Protein α, Serine peptidase, Antiplasmin Cleaving Enzyme, and Serine integral membrane protein. FAP belongs to the small family of serine integral membrane peptidases, called SIMPs.[3] SIMPs cleave proline-containing peptides and macromolecules and are active on the cell surface. Proline peptidases such as prolyl endopeptidase, dipeptidyl peptidase 8, and dipeptidyl peptidase IV-β have also been show to modify bioactive peptides and change their cellular functions, and play a critical role in tumourogenesis.[4, 5] FAP has similar behavior, and also plays an instrumental role in tumor formation and cellular function.

Similarity of FAP to Dipeptidyl Peptidase IV (CD26)

The most studied SIMP is dipeptidyl peptidase IV (DPPIV or CD26), which shows striking similarities to FAP. Several studies demonstrate the importance of DPPIV in regulating tumor stromal cell behavior and function, and FAP shows up to 52% homology to DPPIV.[6] Both FAP and DDPIV are also members of the S9b peptidase family, which is play an indirect role in anti-hyperglycaemia via degradation of the incretins, a group of gastrointestinal hormones that cause an increase in the amount of insulin released from pancreatic beta cells.[2] While all SIMPs cleave prolyl peptide (Pro-Xaa), FAP's predominant distinguishing feature is its potent gelatinase activity.[7, 8] Indeed, this a is key feature which differentiates the behavior of FAP from DPPIV.[7] While the exact physiological roles of FAP are only beginning to be understood, insight can be obtained from the vast amount of research already performed on DPPIV.

1.2.2 MOLECULAR STRUCTURE AND GENETIC CONSERVATION

Molecular Structure of FAP

Native expressed FAP is a 170kDa homodimer, and is often found as a type II integral membrane protein with a very large C-terminal extracellular domain (**Figure 21**). The native monomer form of FAP is 97 kDa and is N-glycosylated.[2] Transmembrane FAP can shed from the cell surface and, is indeed detectable in human blood. The circulating form of FAP has been investigated under the name Antiplasmin Cleaving Enzyme (APCE), and has an approximate molecular weight of 175kDa, as it retains the same homodimer structure as the transmembrane variant.[9] APCE also retains the same catalytic activity as trans-membrane FAP, whereas the FAP monomer exhibits no gelatinolytic activity. The FAP monomer contains three segments which are highly conserved in serine proteases and has five potential N-glycosylation sites. The cytoplamic tail of FAP on the N-terminus is only six amino acids long, and its biological role is not yet understood.[4] The structure of the FAP homodimer has recently been resolved (**Figure 21**), which provides valuable information regarding the enzyme's substrate specificity.[2]

Each FAP monomer contains two distinct domains: the β-propeller domain and the α/β-hydrolase domain; which contains FAP's catalytic site. The catalytic site is located directly at the interface of the β-propeller and the α/β-hydrolase domain. The β-propeller domain is located on top of the catalytic triad

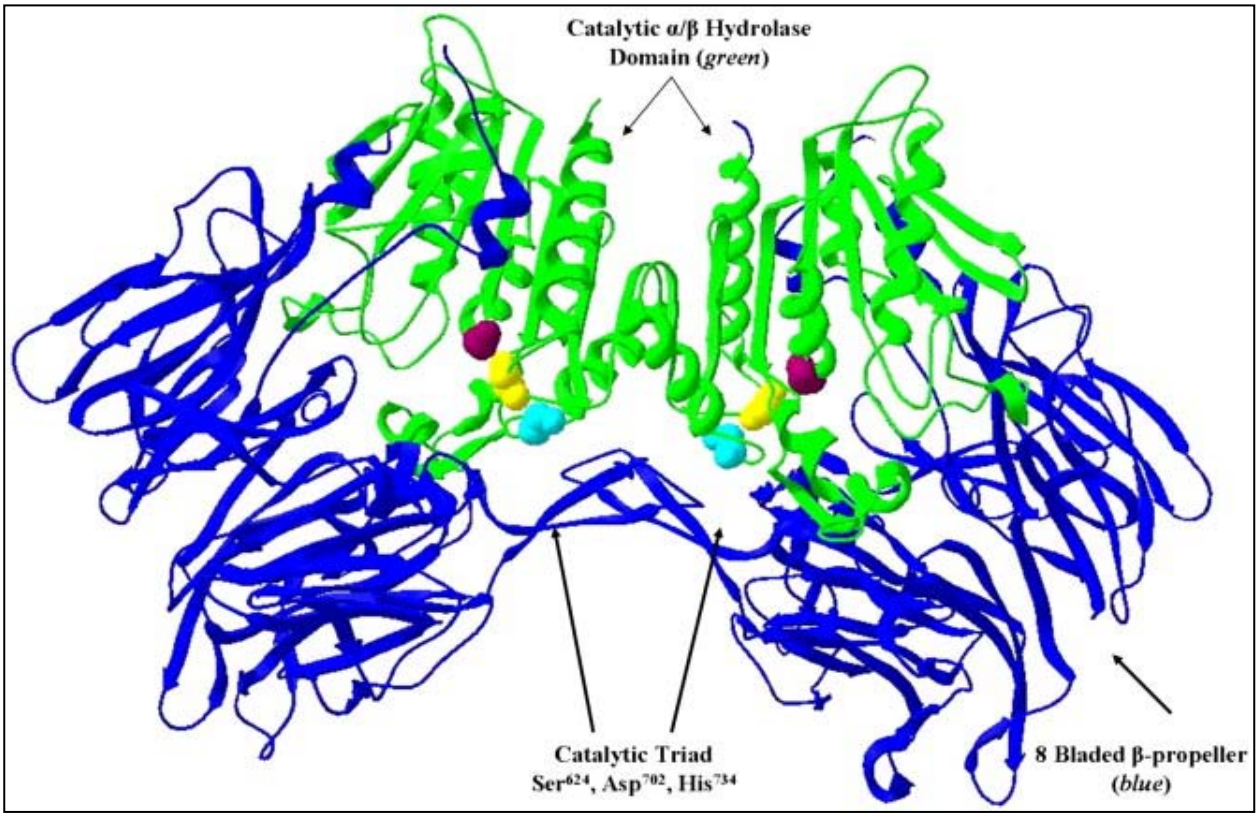

Figure 21. The Extracellular Domain of Fibroblast Activation Protein. The extracellular domain has an eight bladed β-propeller domain (blue) and an α/β hydrolase domain (green) that contains the catalytic triad. Catalytic residues are shown, purple (Serine 624), cyan (Aspartic Acid 702), yellow (Histidine 734). **Taken from [2].**

and appears to reduce protein access to the catalytic site. This notion is supports findings from previous studies of a related serine protease called prolyl oligopeptidase, which has a similar β-propeller domain that regulates proteolysis by excluding large proteins from the catalytic site.[10] The active site is theoretically accessible via the cavity formed between the β-propeller (about 24 Angstroms in diameter) or through the hydrolase domain (about 14 Angstroms in diameter). This notion is supported by further studies using recombinant FAP which indicate that proteolytic truncation of the β-propeller domain reduces steric hindrance for substrates, and results in a 7-fold increase in FAPs gelatinase activity.[11] However the dipeptidyl peptidase activity of truncated FAP remained identical to the native FAP.

Genetic Conservation of FAP Across Species

The FAP gene is relatively well conserved in different species including Homo sapiens, Mus musculus (89%), and Xenopus laevis (50%). Interestingly, the catalytic domain is much better conserved between species than is the β-propeller domain.[2] Studies of murine FAP identifies three different splice variants which have been detected in native tissues. Similarly, a single splice variant of FAP, called seprase-s, has also been identified in a human melanoma cell line and encodes a truncated 27kDa isoform. The Seprase-s isoform precisely overlaps 239 amino acids of native FAP's catalytic domain.[12] However the physiological role of seprase-s has not yet been investigated.

1.2.3 INDUCTION AND CATALYTIC ACTIVITY

Biochemical Properties of FAP

FAP undergoes significant post translational modifications such as N-glycosylation. Without glycosylation, FAP lacks all forms of detectable enzymatic activity.[13] Further reports show that the gelatinase activity of FAP is inhibited using standard serine protease inhibitors.[2] FAP exhibits total loss of its enzymatic activity upon dissociation of the dimer into its 97kDa subunits, confirming that FAP activity depends upon the association of its subunits to form an active dimer.[3, 14] The proteolytic optimum of FAP is at a neutral pH, and becomes inactive at under acidic conditions due to dissociation of the monodimer.[15]

Catalytic Activity of FAP

FAP has two known catalytic targets; gelatin and proline bearing peptides.[2] Few proteases are able to cleave proline-linked peptide bonds. Proline residues appear near the amino terminus of many biologically active peptides where they appear to protect the peptides against degradation.[16] Understanding the signaling effect of FAP-derived peptide fragments has not yet been investigated, but may identify additional physiological roles of FAP.

Zymography-based specificity studies reveal that FAP degrades gelatin and collagen type I and type IV collagens but not laminin, fibronectin, or fibrin.[3, 7] However, conflicting studies demonstrate that FAP does not cleave native collagen type I or III into smaller peptides. The same study concludes that FAP works in parallel with other proteinases to cleave partially degraded or denatured Collagen I and III as ECM is excavated from remodeling tissue.[17]

The Role of FAP in Cell Migration

FAP associates with $\alpha_3\beta_1$ integrin, DPPIV, MMP-2, membrane-type 1 MMP, and urokinase-type plasminogen activator receptor at the invadopodia of malignant human tumor cells. Therefore, FAP likely plays an interactive role with these proteinases, their receptors, and their associated signaling pathways.[2] Specifically, FAP has been hypothesized to work in concert with $\alpha_3\beta_1$ integrin and participate in the formation of functional invadopodia by tethering FAP to the ECM substrate (**Figure 22**).[1] FAP and DPPIV also have been shown to form a complex at the invadopodia of fibroblasts on collagenous fibers. This DPPIV–FAP complex, which exhibits both prolyl peptidase activity and gelatinase activity, is necessary for fibroblast migration on a collagen substrate *in vitro*.[18, 19]

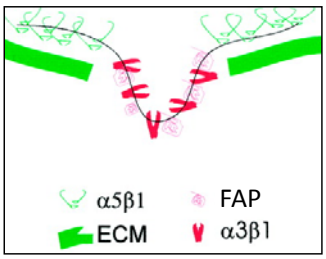

Figure 22. The Role of FAP and $\alpha_3\beta_1$. $\alpha_3\beta_1$ participates in the formation of functional invadopodia by docking Seprase. Taken from.[1]

Induction of FAP Expression

Fibroblast activation protein is expressed in migrating fibroblasts and tissues undergoing matrix remodeling during wound healing. Numerous studies show FAP expression primarily in "remodeling tissues," but not in quiescent tissues, which supports the notion of regulated FAP induction.[7, 8, 20, 21] Colocalization of FAP in inflamed tissues further suggests its induction by inflammatory cytokines. However, it was not until recently that induction of FAP expression had been addressed. In cancer cells, FAP could be induced by stimulation with tumor growth factor-β (TGF-β).[22] These finding are further

supported by additional investigations into the FAP promoter. This study found that early growth response 1 protein (EGR1) binds to the FAP promoter, and thereby regulates its transcription. [23] Interestingly, hallmark pro-inflammatory cytokine TNFα has been show to induce ERG1 expression in smooth muscle cells of experimental atherosclerotic lesions, suggesting a possible mechanism of FAP induction.[24]

FAP in Tissue Remodeling

Notions that FAP is involved in wound healing are supported by its expression in many tissues undergoing active remodeling. Perhaps even more definitive is another study involving the *Xenopus laevis* FAP homologue, which associates the enzyme's increased expression during hormone-induced tail resorption; a highly active tissue remodeling process.[25] Further support of this theory can be found in studies of mouse embryo development, where FAP is expressed in remodeling tissues.[26] To access FAP expression during embryonic development, mice deficient in FAP but expressing β-galactosidase under the control of the FAP promoter were developed. β-galactosidase strongly correlated with regions of active tissue remodeling during embryogenesis. However, it is important to note that FAP-deficient mice have no obvious developmental defects, which suggests that FAP may not play a critical role in embryonic tissue remodeling processes.

1.2.4 THE ROLE OF FAP IN CANCER AND INFLAMMATORY DISEASES

Cancer

Numerous studies show that FAP is expressed during wound healing and in reactive stroma of epithelial cancers and in multiple sarcomas.[27] However, malignant epithelial, neural and haematopoietic cells are generally FAP-negative, although it has been detected in astroglial tumours.[28] Additional studies describe FAP expression in the reactive mesenchyme of epithelial tumors (carcinomas). Further, FAP has been discovered in colon adenocarcinoma, lung adenocarcinoma, metastatic colon adenocarcinoma, ductal carcinoma in breast cancer, epithelial ovarian carcinoma, and cervical carcinoma.[2] *In-vivo* studies of epithelial-derived solid tumors in mice indicate a causal role of FAP in stromal cell mediated pathways including tumor cell proliferation and neovascularization.[29] Further studies show that immunization against the FAP inhibits tumor growth and increases survival in a murine model.[30]

Liver Disease

Stellate cells at the tissue remodeling interface of cirrhosis in humans have also been shown to express FAP.[8] Indeed hepatic stellate cells are largely responsible for hepatic tissue remodeling. From this work, it was concluded that FAP contributes hepatic stellate cell-induced ECM changes observed during chronic inflammatory liver disease. FAP expression was also detected in the similar pathophysiology of chronic hepatitis C virus infection, where it contributes significantly with the degree of hepatic fibrosis.[31]

Arthritis

FAP expression has been observed in osteoarthritis. This pioneering work identified the expression of FAP on chondrocyte membranes under conditions that promote cartilage

resorption, and also elevated expression in cartilage from osteoarthritis patients. FAP has also been detected in the similar pathophysilogy of rheumatoid arthritis, where it was reported that FAP is expressed in the lining layer of rheumatoid synovium. This study also reports a strong association of inflammatory synovitis with FAP expression.[32] While it is generally believed that FAP contributes the pathological breakdown of joint tissues in arthritic disease, conflicting pharmacological-inhibition studies in-vivo reveal that FAP actually protects articular cartilage against invasion by synovial fibroblasts.[33] Future *in-vivo* analyses using FAP knockout mice may clarify its *in-vivo* causal role in arthritic disease.[34]

1.2.5 THE ROLE OF FAP IN BLOOD COAGULATION

Lee et al. discovered that Antiplasmin Cleaving Enzyme (APCE) is actually a soluble form of FAP. APCE was shown to indirectly influence the cross-linking of fibrin via α_2-Antiplasmin (AP).[35] AP is a plasma glycoprotein of the Serpin (serine protease inhibitor) superfamily and is the primary physiological inhibitor of plasmin, a key enzyme in fibrin degradation. The fibrinolytic system leads to the generation of plasmin from plasminogen through the action of Tissue or Urokinase Plasminogen Activator (t-PA or uPA). FAP processes α2-antiplasmin (α2AP) from the less active "PRO" form (α2APPRO) into the more potent "ACT" form (α2APACT). The PRO-form has remarkably less capacity of cross-linking fibrin compared to the ACT form. α2APACT binds to fibrin during clot formation, effectively inhibiting plasmin and rendering the fibrin resistant to proteolysis (**Figure 23**).[9, 35] However, despite this behavior, the role or FAP in atherothrombosis is not understood.

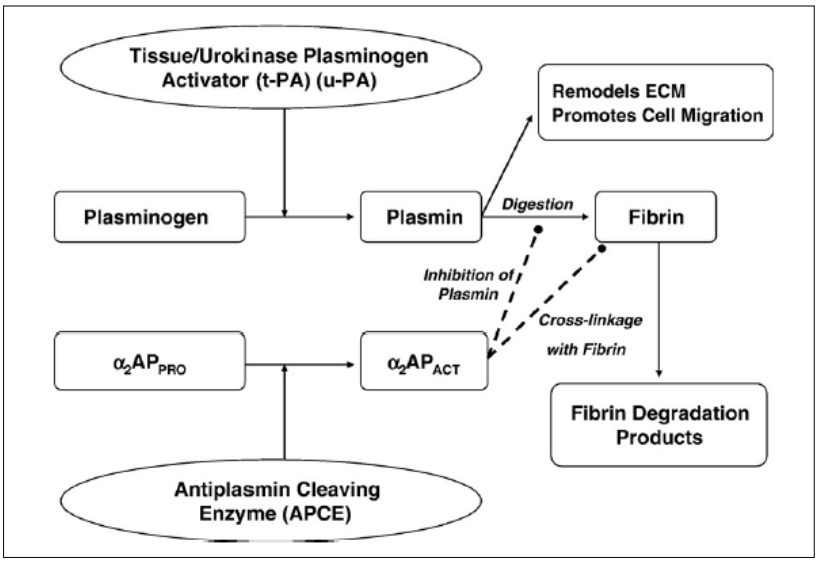

Figure 23. Impact of APCE (soluble FAP) on the fibrinolytic sytem. APCE impairs blood coagulation by activating α2-antiplasmin, which in turn inhibits plasmin-mediated cleavage of fibrin. Adapted from [2]

1.2.6 REFERENCES

1. Mueller SC, Ghersi G, Akiyama SK, Sang Q-XA, Howard L, Pineiro-Sanchez M, Nakahara H, Yeh Y, Chen W-T. A novel protease-docking function of integrin at invadopodia. *Journal of Biological Chemistry*. 1999;274:24947-24952
2. O'Brien P, O'Connor BF. Seprase: An overview of an important matrix serine protease. *Biochimica et Biophysica Acta (BBA) - Proteins & Proteomics*. 2008;1784:1130-1145
3. Piñeiro-Sánchez ML, Goldstein LA, Dodt J, Howard L, Yeh Y, Chen W-T. Identification of the 170-kda melanoma membrane-bound gelatinase (seprase) as a serine integral membrane protease. *Journal of Biological Chemistry*. 1997;272:7595-7601
4. Chen W-T, Kelly T. Seprase complexes in cellular invasiveness. *Cancer and Metastasis Reviews*. 2003;22:259-269-269
5. Busek P, Malík R, Sedo A. Dipeptidyl peptidase iv activity and/or structure homologues (dash) and their substrates in cancer. *The International Journal of Biochemistry & Cell Biology*. 2004;36:408-421
6. Bauvois B. Transmembrane proteases in cell growth and invasion: New contributors to angiogenesis? *Oncogene*. 0000;23:317-329
7. Park JE, Lenter MC, Zimmermann RN, Garin-Chesa P, Old LJ, Rettig WJ. Fibroblast activation protein, a dual specificity serine protease expressed in reactive human tumor stromal fibroblasts. *Journal of Biological Chemistry*. 1999;274:36505-36512
8. Levy MT, McCaughan GW, Abbott CA, Park JE, Cunningham AM, Müller E, Rettig WJ, Gorrell MD. Fibroblast activation protein: A cell surface dipeptidyl peptidase and gelatinase expressed by stellate cells at the tissue remodelling interface in human cirrhosis. *Hepatology*. 1999;29:1768-1778
9. Lee KN, Jackson KW, Christiansen VJ, Lee CS, Chun J-G, McKee PA. Antiplasmin-cleaving enzyme is a soluble form of fibroblast activation protein. *Blood*. 2006;107:1397-1404
10. Fülöp V, Böcskei Z, Polgár L. Prolyl oligopeptidase: An unusual [beta]-propeller domain regulates proteolysis. *Cell*. 1998;94:161-170
11. Chen D, Kennedy A, Wang J-Y, Zeng W, Zhao Q, Pearl M, Zhang M, Suo Z, Nesland JM, Qiao Y, Ng A-K, Hirashima N, Yamane T, Mori Y, Mitsumata M, Ghersi G, Chen W-T. Activation of edta-resistant gelatinases in malignant human tumors. *Cancer Research*. 2006;66:9977-9985
12. Goldstein LA, Chen W-T. Identification of an alternatively spliced seprase mrna that encodes a novel intracellular isoform. *Journal of Biological Chemistry*. 2000;275:2554-2559
13. Sun S, Albright CF, Fish BH, George HJ, Selling BH, Hollis GF, Wynn R. Expression, purification, and kinetic characterization of full-length human fibroblast activation protein. *Protein Expression and Purification*. 2002;24:274-281
14. Aertgeerts K, Levin I, Shi L, Snell GP, Jennings A, Prasad GS, Zhang Y, Kraus ML, Salakian S, Sridhar V, Wijnands R, Tennant MG. Structural and kinetic analysis of the substrate specificity of human fibroblast activation protein α. *Journal of Biological Chemistry*. 2005;280:19441-19444
15. Birney YA, O'Connor BF. Purification and characterization of a z-pro-prolinal-insensitive z-gly-pro-7-amino-4-methyl coumarin-hydrolyzing peptidase from bovine serum--a new proline-specific peptidase. *Protein Expression and Purification*. 2001;22:286-298
16. García-Horsman JA, Männistö PT, Venäläinen JI. On the role of prolyl oligopeptidase in health and disease. *Neuropeptides*. 2007;41:1-24
17. Christiansen VJ, Jackson KW, Lee KN, McKee PA. The effect of a single nucleotide polymorphism on human {alpha}2-antiplasmin activity. *Blood*. 2007;109:5286-5292

18. Ghersi G, Dong H, Goldstein LA, Yeh Y, Hakkinen L, Larjava HS, Chen W-T. Regulation of fibroblast migration on collagenous matrix by a cell surface peptidase complex. *Journal of Biological Chemistry*. 2002;277:29231-29241
19. Ghersi G, Zhao Q, Salamone M, Yeh Y, Zucker S, Chen W-T. The protease complex consisting of dipeptidyl peptidase iv and seprase plays a role in the migration and invasion of human endothelial cells in collagenous matrices. *Cancer Research*. 2006;66:4652-4661
20. Rettig WJ, Garin-Chesa P, Beresford HR, Oettgen HF, Melamed MR, Old LJ. Cell-surface glycoproteins of human sarcomas: Differential expression in normal and malignant tissues and cultured cells. *Proceedings of the National Academy of Sciences of the United States of America*. 1988;85:3110-3114
21. Wolfgang J. Rettig, Sai L. Su, Sheila R. Fortunato, Matthew J. Scanlan, B. K. Mohan Raj, Pilar Garin-Chesa, John H. Healey, Lloyd J. Old. Fibroblast activation protein: Purification, epitope mapping and induction by growth factors. *International Journal of Cancer*. 1994;58:385-392
22. Chen H, Yang W-W, Wen Q-T, Xu L, Chen M. Tgf-[beta]-induced fibroblast activation protein expression, fibroblast activation protein expression increases the proliferation, adhesion, and migration of ho-8910pm. *Experimental and Molecular Pathology*. 2009;87:189-194
23. Zhang J, Valianou M, Cheng JD. Identification and characterization of the promoter of fibroblast activation protein. *Front Biosci (Elite Ed)*. 2010;2:1154-1163
24. Goetze S, Kintscher U, Kaneshiro K, Meehan WP, Collins A, Fleck E, Hsueh WA, Law RE. Tnf[alpha] induces expression of transcription factors c-fos, egr-1, and ets-1 in vascular lesions through extracellular signal-regulated kinases 1/2. *Atherosclerosis*. 2001;159:93-101
25. Brown DD, Wang Z, Furlow JD, Kanamori A, Schwartzman RA, Remo BF, Pinder A. The thyroid hormone-induced tail resorption program during xenopus laevis metamorphosis. *Proceedings of the National Academy of Sciences*. 1996;93:1924-1929
26. Niedermeyer J, Garin-Chesa P, Kriz M, Hilberg F, Mueller E, Bamberger U, Rettig WJ, Schnapp A. Expression of the fibroblast activation protein during mouse embryo development. *Int. J. Dev. Biol.* 201:445–447.
27. Garin-Chesa P, Old LJ, Rettig WJ. Cell surface glycoprotein of reactive stromal fibroblasts as a potential antibody target in human epithelial cancers. *Proceedings of the National Academy of Sciences*. 1990;87:7235-7239
28. Mentlein R, Hattermann K, Hemion C, Jungbluth AA, Held-Feindt J. Expression and role of the cell surface protease seprase/fibroblast activation protein-α (fap-α) in astroglial tumors. *Biological Chemistry*. 2010;392:199-207
29. Santos AM, Jung J, Aziz N, Kissil JL, Puré E. Targeting fibroblast activation protein inhibits tumor stromagenesis and growth in mice. *The Journal of Clinical Investigation*. 2009;119:3613-3625
30. Wen Y, Wang C-T, Ma T-T, Li Z-Y, Zhou L-N, Mu B, Leng F, Shi H-S, Li Y-O, Wei Y-Q. Immunotherapy targeting fibroblast activation protein inhibits tumor growth and increases survival in a murine colon cancer model. *Cancer Science*. 2010;101:2325-2332
31. Levy MT, McCaughan GW, Marinos G, Gorrell MD. Intrahepatic expression of the hepatic stellate cell marker fibroblast activation protein correlates with the degree of fibrosis in hepatitis c virus infection. *Liver*. 2002;22:93-101
32. Bauer S, Jendro M, Wadle A, Kleber S, Stenner F, Dinser R, Reich A, Faccin E, Godde S, Dinges H, Muller-Ladner U, Renner C. Fibroblast activation protein is expressed by rheumatoid myofibroblast-like synoviocytes. *Arthritis Research & Therapy*. 2006;8:R171
33. Ospelt C, Mertens JC, Jüngel A, Brentano F, Maciejewska-Rodriguez H, Huber LC, Hemmatazad H, Wüest T, Knuth A, Gay RE, Michel BA, Gay S, Renner C, Bauer S. Inhibition of fibroblast activation protein and dipeptidylpeptidase 4 increases cartilage invasion by rheumatoid arthritis synovial fibroblasts. *Arthritis & Rheumatism*. 2010;62:1224-1235

34. Milner J, Kevorkian L, Young D, Jones D, Wait R, Donell S, Barksby E, Patterson A, Middleton J, Cravatt B, Clark I, Rowan A, Cawston T. Fibroblast activation protein alpha is expressed by chondrocytes following a pro-inflammatory stimulus and is elevated in osteoarthritis. *Arthritis Research & Therapy*. 2006;8:R23
35. Lee KN, Jackson KW, Christiansen VJ, Chung KH, McKee PA. A novel plasma proteinase potentiates {alpha}2-antiplasmin inhibition of fibrin digestion. *Blood*. 2004;103:3783-3788

1.3 AIM OF THE THESIS

Fibroblast activation protein (FAP) contributes to the pathophysiology of tumor formation, arthritis, and liver disease. Atherosclerosis follows similar pathophysiology to these diseases; however the role of FAP in atherosclerosis has never been investigated. Given the unmet need for improved diagnostic and therapeutic targets against atherosclerosis, the aim of this thesis is to (a) characterize FAP expression in atherosclerosis and examine its association with plaque instability, (b) to determine the induction and catalytic mechanisms of FAP as it relates to plaque complication, and (c) to evaluate the role of FAP in atherothrombosis.

1.4 OUTLINE OF THE THESIS

The experimental portion of this thesis begins with the description of an image analysis algorithm developed to quantify FAP expression in human carotid fibrous caps. The presented image analysis algorithm quantifies the association of smooth muscle cell-specific FAP expression with carotid fibrous cap thickness (**Chapter 2**). The next section investigates the role of FAP in human atherosclerosis. Experimental evidence is shown, which indicates that vascular smooth muscle cells express FAP in response to macrophage-derived TNFα. The same section goes on to show that FAP associates with thin-cap human coronary fibroatheromata, and contributes to type I collagen breakdown in fibrous caps (**Chapter 3**). The role of FAP in atherogenesis, and data indicating FAP-mediated acceleration of blood coagulation are shown (**Chapter 4**). The final section provides a discussion directed at the future diagnostic and therapeutic potential of FAP in cardiovascular disease (**Chapter 5**).

CHAPTER 2

FAP QUANTIFICATION IN CAROTID FIBROUS CAPS

Partially Based on

Novel Image Analysis Reveals Increased Fibroblast Activation Protein in Thin Carotid Fibrous Caps

Brokopp CE, Weber B, Emmert MY, Winnik S, Baumgartner L, Frimmel SAF, Neurnberg J, Burkhardt JK, Lüscher TF, Sütsch G, Kiowski W, Matter CM, Hoerstrup SP

Submitted to Atherosclerosis May, 2011

2.1 ABSTRACT

Background – Proteins expressed in "rupture-prone" thin-cap vs. "stable" thick-cap fibroatheromata of carotid plaques may be visualized by diagnostic imaging to identify patients at risk of stroke. Fibroblast Activation Protein (FAP), a Type I collagenase, is increased in thin vs. thick coronary fibrous caps. However, its role in carotid plaques, and a quantitative method linking fibrous cap thickness to cell-specific protein expression remains unavailable.

Methods and Results – We describe a novel image analysis algorithm that associates protein expression to human carotid fibrous cap thickness. Image analysis reveals that FAP is increased in thin (≤65μm) vs. thick (>65 μm) carotid fibrous caps (n=5 patients; p=0.035) and colocalizes with vascular smooth muscle cells, but not endothelial cells or macrophages. Finally, the presented algorithm reveals increased smooth muscle cell-specific FAP expression in thin vs. thick fibrous caps (n=5, p=0.026).

Conclusions – The presented novel image analysis algorithm identifies enhanced smooth muscle cell-specific FAP expression in thin carotid fibrous caps. This method may be applied to identify future molecular targets of thin-cap fibroatheromata, and also to investigate cell-specific protein regulation associated with fibrous cap thinning.

2.2 INTRODUCTION

Carotid plaque rupture is more prevalent in patients with a history of ischemic neurological events.[1] Moreover, studies of advanced carotid plaques indicate that fibrous cap thinning associates with lesion rupture.[2] Therefore, identification of high-risk lesions is of utmost importance in neurology and cardiovascular medicine.

Whereas currently applied imaging modalities identify the overall morphology of carotid plaques, molecular imaging of targets specific for unstable fibrous caps may specifically identify rupture-prone lesions.[3] Thus, the identification of targets that are enhanced in "rupture-prone" thin vs. "stable" thick carotid fibrous caps may identify patients at increased risk for stroke. However identification of these targets has proven difficult, in part because no method currently exists to associate protein levels of imaging targets to fibrous cap thickness.

Here we present a novel image analysis algorithm to quantify cell-specific protein expression in thick vs. thin human carotid fibrous caps *ex vivo*. Fibroblast Activation Protein (FAP) is a constitutively active serine protease that degrades collagen type I, a primary load-bearing component in fibrous caps, and thereby likely contributes to plaque destabilization.[4] The presented image analysis algorithm is applied to quantify smooth muscle cell-specific FAP expression, and examine its association with fibrous cap thickness.

2.3 METHODS

2.3.1 CHARACTERIZATION OF CAROTID PLAQUES

Patients with severe carotid plaque burden, as diagnosed by carotid doppler, underwent carotid endarterectomy and had the following characteristics: *n = 5, age (y): 74 ±14.1 , BMI: 28.7 ± 5.5, diabetes mellitus: 3/5; pre-operative CRP (mg/L):73.5±143.9*. Approval from the local Ethics Committee was obtained for collections of all patient specimens. Carotid plaques were cryosectioned, and stained with Masson against collagen for characterization of fibrous cap thickness. Fibrous caps were identified as the collagen-rich tissue separating the lumen and the necrotic core. Fibrous caps with a minimum thickness

of less than 65µm were classified as *thin-cap*, whereas those 65µm or greater in thickness were classified as *thick-cap* fibroatheromata.[5]

2.3.2 IMMUNOFLUORESCENCE

Carotid plaque sections were fixed in ice-cold acetone for 5 min and stained for FAP using mouse monoclonal F19 IgG antibody and a Cy5 goat anti-mouse secondary antibody (115-175-008; Jackson ImmunoResearch).[6] Actin was stain using a rabbit anti-human/mouse antibody (Sigma; A2066) and labeled with a Cy2 secondary antibody (111-225-047; Jackson ImmunoResearch). FAP colocalization with macrophages, endothelial cells, and smooth muscle cells was determined using a rabbit antibodies directed against CD68 (SC-9139; Santa Cruz, Santa Cruz, CA), von Willebrand factor (vWF; F3520; Sigma-Aldrich, Carlsbad, CA), and alpha-smooth muscle actin (αSMA; Ab5694; Abcam). Subsequent fluorescent labeling was performed using a Cy2-labeled anti-rabbit IgG (111-225-047; Jackson ImmunoResearch) in three adjacent sections of each biopsy specimen. DAPI (D9542; Sigma-Aldrich) was used for fluorescent counterstaining of nuclei. Isotype control antibodies were used to address antigen-binding specificity. Stained samples were cover-slipped with Tris-buffered glycerol (a 3:7 mixture of 0.1 M Tris-HCl at pH 9.5 and glycerol supplemented with 50 mg/mL *n*-propyl-gallate).

2.3.3 IMMUNOHISTOCHEMISTRY

Cryosections of carotid plaques were fixed in ice-cold acetone for 5 min and stained using a mouse monoclonal against FAP (clone F19, Provided by ATCC, Molsheim Cedex, France) and the appropriate mouse isotype control (401401; BioLegend, San Diego, CA).[7, 8] Primary antibodies were detected with biotin-labeled goat anti-mouse (115-066-003; Jackson ImmunoResearch, West Grove, PA) and biotin-labeled goat anti-rabbit (111-066-003; Jackson ImmunoResearch) and stained using an ABC staining kit (Vector Labs, Burlingame, CA) and counterstained with Mayer's haematoxylin to visualize cell nuclei.

2.3.4 IMAGE ACQUISITION

For low power imaging at spatial resolutions above 1 µm/pixel, a fluorescent microscope (DM60000B; Leica, Wetzlar, Germany) equipped with a fluorescent camera (DFC350 FX; Leica) was used. Colocalization analyses, and quantification of FAP expression in smooth muscle cells were performed at higher magnifications using a multichannel confocal microscope (TCS SP2, Leica) on a single optical plane**.**

To address variability due to focusing inconsistencies during image acquisition, a murine aortic arch was harvested, sectioned at 10µm thickness, and stained for actin with a fluorescently Cy5 labeled secondary antibody. The specimen was brought into manual focus and an image was taken as the baseline focus level and analyzed for average pixel intensity. Auto-focusing was then performed on the same specimen to identify changes in the resulting average pixel intensity. The specimen was moved ±4, ±8, and ±16µm away from the focused plane and an image was captured before and after auto-focusing to determine the range at which auto-focusing provides consistency (**Figure 25**).

2.3.5 IMAGE ANALYSIS

For quantification of FAP and actin, three single-channel fluorescent images were taken for each specimen at constant camera settings at an auto-focused plane, in tagged image file format (TIFF) at a binary pixel intensity between 0-255; a sample image (with target-specific primary antibodies), a

background image (taken 200µm below the specimen), and an isotype control image (an adjacent section stained with non-specific isotype control antibodies; Figure 1A). In each patient, three sets of three images (sample, background, and isotype control) were taken and the signals analyzed (nine images in total). The image analysis was performed in custom developed code in Matlab (R2007b, Mathworks, Novi, MI). The complete software code for the algorithm is provided in the appendix section of this thesis (Chapter 6). To minimize variability due to focusing inconsistencies, all images were auto-focused by the image capture software; a method validated to provide consistent image readouts (**Figure 25**).

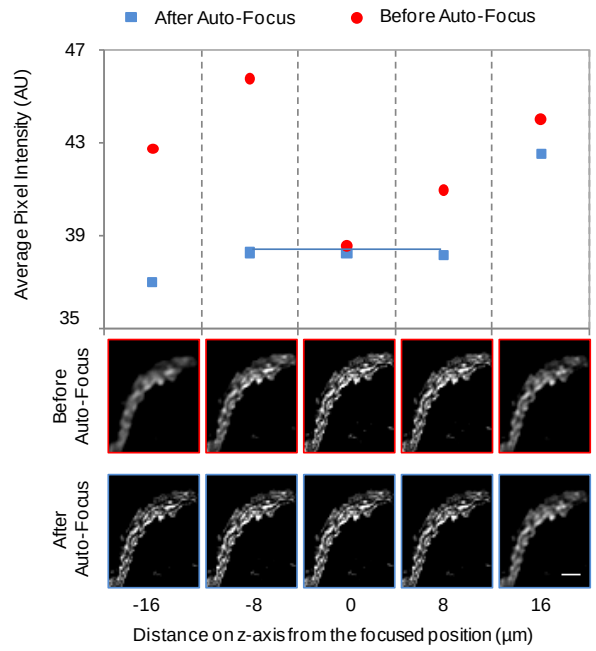

Figure 25. Software auto-focus generates reproducible pixel intensity readouts. Top; Graph reveals the values (red) derived from images of fluorescent actin-stained murine aortae captured within 8µm of the focused position (0µm). Auto-focus generates reproducible readouts (blue). Bottom; Representative images at specified distances (-16µm to 16µm) away from the plane of focus before (red) and after auto-focusing (blue; bar = 100µm).

To objectively remove the background signal from the image, a threshold is calculated as the pixel intensity below which 95% of the pixels exist in both the background and isotype control images.[9, 10] Pixels below both thresholds are removed from the sample image and excluded.[10] After sub-threshold subtraction, the mean pixel intensity is calculated for the entire image as the sum of all super-threshold pixel intensities divided by the total number of super-threshold pixels. To calculate a normalized value of FAP expression relative to cell quantity, the mean signal of the FAP fluorescent channel was divided by the mean signal of actin channel. Three sections with matching control images were averaged for each fibrous cap.

To calculate colocalization coefficients, super-threshold pixels positive for FAP that were also were positive for cell-specific markers (alpha smooth muscle actin, CD68, and von Wildbrand Factor) were calculated. The percentage of FAP positive pixels also positive for a cell-specific marker were reported as the colocalization coefficient. A qualitative impression of colocalization was generated by two-dimensional scattergram, which plot pixels on the x-axis according to their expression of FAP and on the y-axis according to their expression of cell-specific markers.[11] The amount of pixels in each position is quantified by the color of the pixels in the scattergram.

To quantify FAP expression in smooth muscle cells, images were taken of carotid specimens stained for FAP with αSMA, FAP with αSMA-isotype control, and FAP-isotype contol with αSMA-isotype control. The background threshold for αSMA is determined as the pixel intensity below which 95% of the pixels exist in both the background and isotype control confocal images. Pixels above the αSMA threshold were quantified for FAP expression in both the FAP with αSMA and FAP with αSMA-isotype control images. From these images, the mean pixel intensities were calculated for FAP and the FAP-isotype control. The difference between the FAP signal and the FAP-isotype signal in αSMA-positive pixels is calculated as the difference in mean fluorescent intensity (ΔMFI; Figure 2E).

For validation of linearity between actin concentration and the calculated signal, HEK293 cells were cytospun onto glass slides at a density of 1, 10, 100, and 1000 cells per cm^2 and stained for actin-specific antibodies, and relevant isotype control antibodies. Purchased recombinant human FAP (Origene, Rockville, MD) was also plated at a density of 1, 10, 100, and 1000 ng/cm^2 onto a glass slide and allowed

to dry overnight before staining for FAP and relevant isotype control antibodies. Background images were taken at 200µm below the sample plane. The emitted signals were correlated to the concentration of plated FAP and cells (actin).

2.3.5 Statistical Analyses

Associations for the linearity validations were calculated by Pearson's correlation coefficient. Paired Student's T-test was used for comparisons of immunofluorescent images in thick vs. thin fibrous caps. All statistical analyses were performed using MatLab (Version, R2007b, Mathworks, Novi, MI). Data are presented as mean±SD. Significance was accepted at the level of $p<0.05$.

2.4 Results

2.4.1 Image Analysis Algorithm Quantifies FAP and Actin Within a Linear Range

Signals calculated from the image analysis algorithm are linear with the pre-defined protein concentrations of FAP and actin (**Figure 26**).

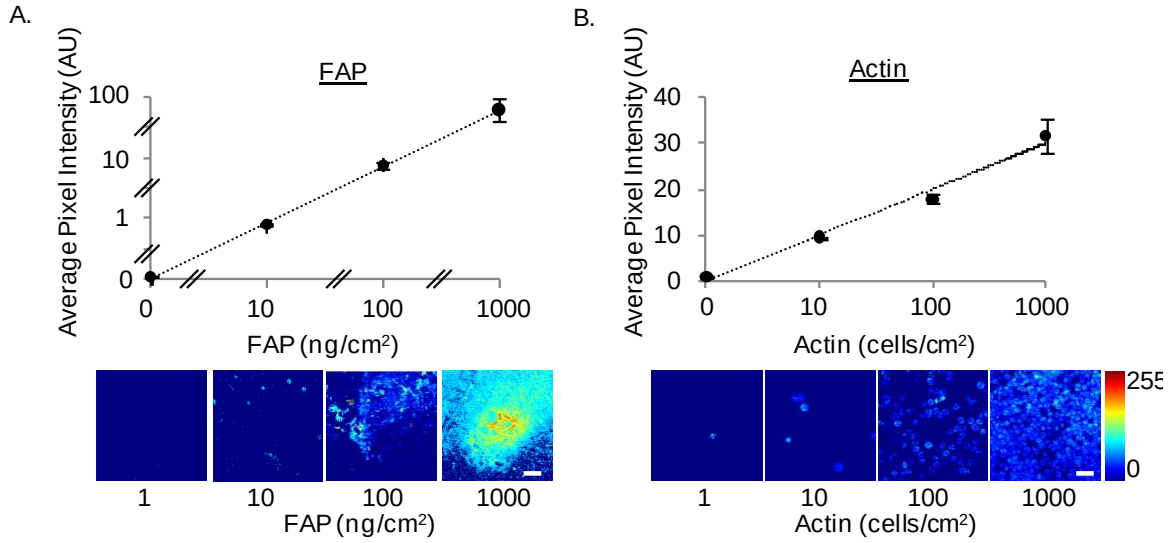

Figure 26. Calculated signal is linear to FAP and actin protein concentration. A. The average pixel intensity of Fibroblast Activation Protein is linear to the protein concentration (n=4, R^2=0.9996, p=0.0004; bar=20µm) and the average pixel of actin (B) is linear to the concentration of HEK293 cells (n=4, R^2=0.9852, p=0.0148; bar=20µm).

2.4.2 BACKGROUND CORRECTION PROVIDES OBJECTIVE QUANTIFICATION OF FAP IN FIBROUS CAPS

FAP expression in carotid fibrous caps (**Figure 27A**) is quantified by correction of background and isotype control signals from a sample image (**Figure 27B**) followed by calculating the mean pixel intensity of the resulting FAP-specific signal (**Figure 27C**).

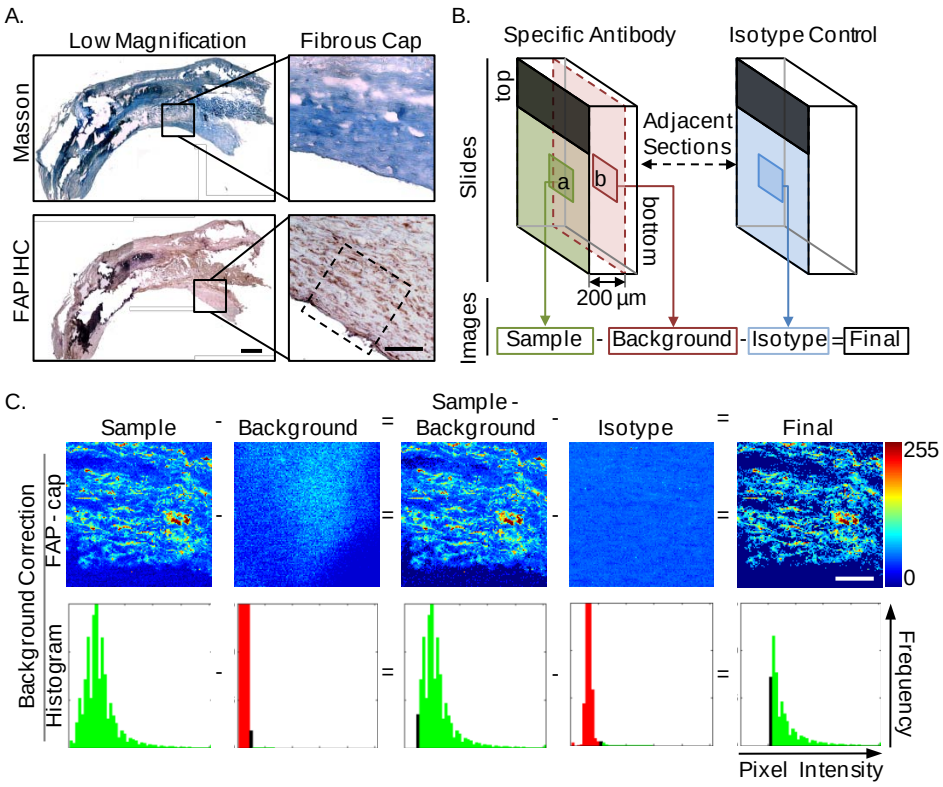

Figure 27. Image analysis algorithm quantifies fibroblast activation protein expression in carotid fibrous caps. A. Representative stainings of a fibrous cap (by Masson) and FAP in an adjacent section (bar low magnification = 200µm, bar high magnification = 50µm). B. The "sample image" is taken of a carotid plaque specimen stained with a target-specific antibody (a) and a "background image" (b; taken at an optical plane 200µm below the carotid specimen), and an "isotype image" (c; adjacent section of the carotid plaque stained with an isotype control antibody) is subtracted. C. Representative FAP stainings of the fibrous cap (top; bar = 20µm) are shown in A. (dashed black box) with corresponding histogram readouts showing the frequency of pixel intensities (bottom). Super-threshold pixels (green), sub-threshold pixels (red), and pixels equal to the threshold (black) are shown.

2.4.3 FAP Colocalizes with Smooth Muscle Cells in Carotid Fibrous Caps

Confocal image analyses reveals FAP expression by smooth muscle cells, but not by macrophages or endothelial cells in human carotid fibrous caps using scattergram and colocalization coefficient calculations (**Figure 29**).

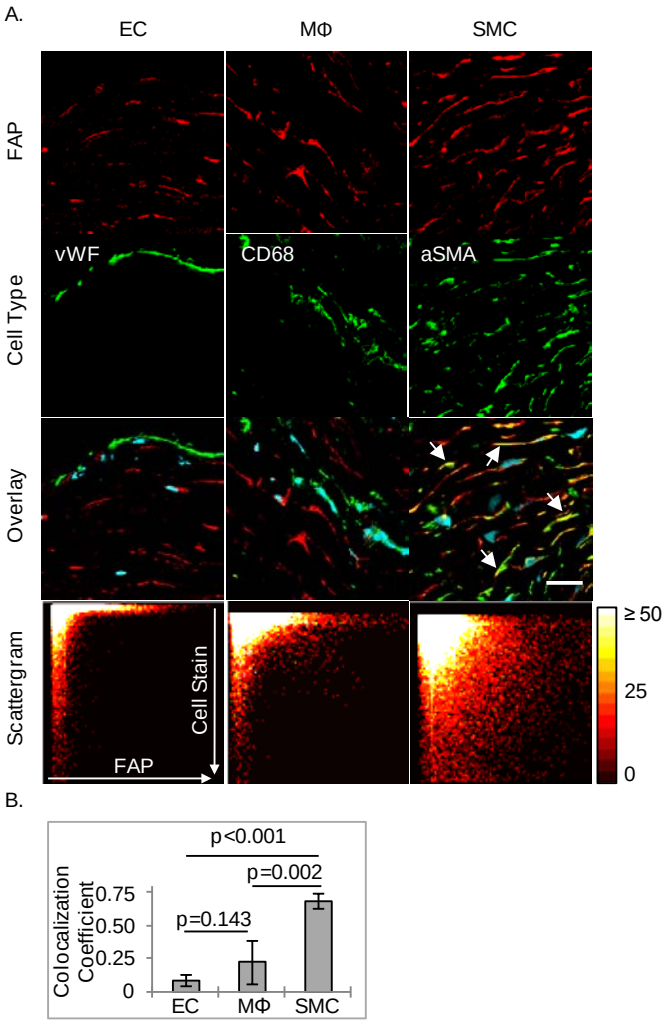

Figure 29. FAP expression colocalizes with smooth muscle cells, but not with macrophages or endothelial cells in carotid fibrous caps. A, Overlays of confocal images of FAP (red) and DAPI (blue) with cell-specific stainings of αSMA, CD68, and vWF (green) in representative sections illustrate FAP colocalization (arrows) with smooth muscle cells (bar=20 μm). B, The graph quantifies an increased colocalization of FAP with smooth muscle cells (αSMA), compared with endothelial cells (vWF), and macrophages (CD68) in carotid fibrous caps (n=5).

2.4.4 SMOOTH MUSCLE CELLS EXPRESS INCREASED FAP IN THIN- VS THICK-CAP HUMAN CAROTID FIBROATHEROMATA

To determine carotid fibrous cap thickness, we labeled collagen in carotid fibroatheromata by Masson Trichrome staining. Immunohistological analysis reveals qualitatively enhanced FAP expression in thin vs. thick fibrous caps within the same plaque specimens (**Figure 2A**). Finally, FAP expression is enhanced in smooth muscle cells of thin vs. thick fibrous caps (**Figure 2B-C)**.

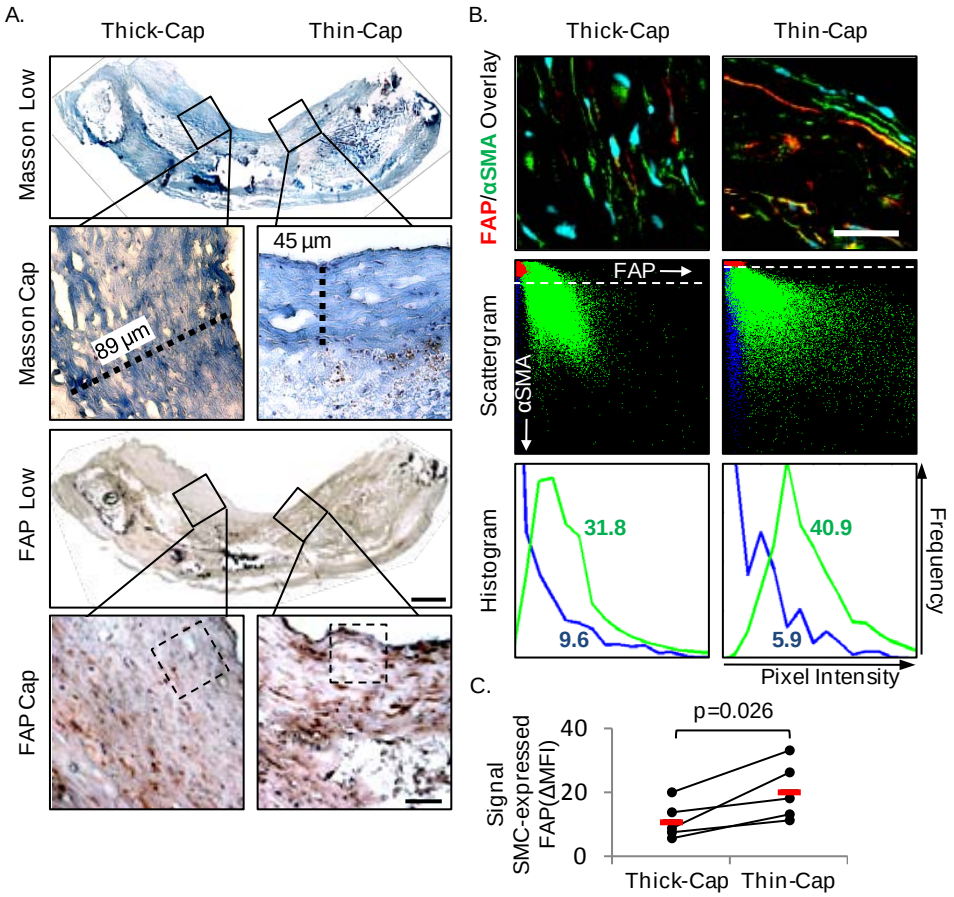

Figure 30. Fibroblast activation protein expression is enhanced in smooth muscle cells of thin vs. thick carotid fibrous caps. A. top; Representative histology of a carotid fibroatheroma (as stained by Masson for collagen) reveals enhanced FAP expression in thick (>65µm) vs. ≤65µm) fibrous caps (bar low magnification = 200µm, bar high magnification = 20µm). B. top; Immunofluorescent stainings of FAP (red), αSMA (green), and cell nuclei (DAPI, blue) are shown for thick vs. thin cap regions. B. Middle; scattergrams are shown for specimens stained with FAPctrl/αSMActrl (red), FAPctrl/αSMA (blue), and FAP/αSMA(green). Pixels above the threshold for αSMA-positive staining (white dotted line) are analyzed for FAP expression. Histograms (bottom) reveal the frequency of super-αSMA threshold pixels for FAPctrl/αSMA (blue) and FAP/αSMA (green). Mean pixel intensities are shown. C. The graph reveals enhanced expression of FAP in smooth muscle cells of thin vs. thick carotid fibrous caps from single plaques taken from 5 different patients (mean in red, p=0.026 by paired Student's T-Test).

2.4.5 TOTAL FAP IS ENHANCED IN THIN VS. THICK CAROTID FIBROUS CAPS

Immunofluorescent stainings and subsequent image analyses in adjacent sections reveal enhanced FAP expression normalized to cellular content (actin) in thin vs. thick fibrous caps (**Figure 28)**.

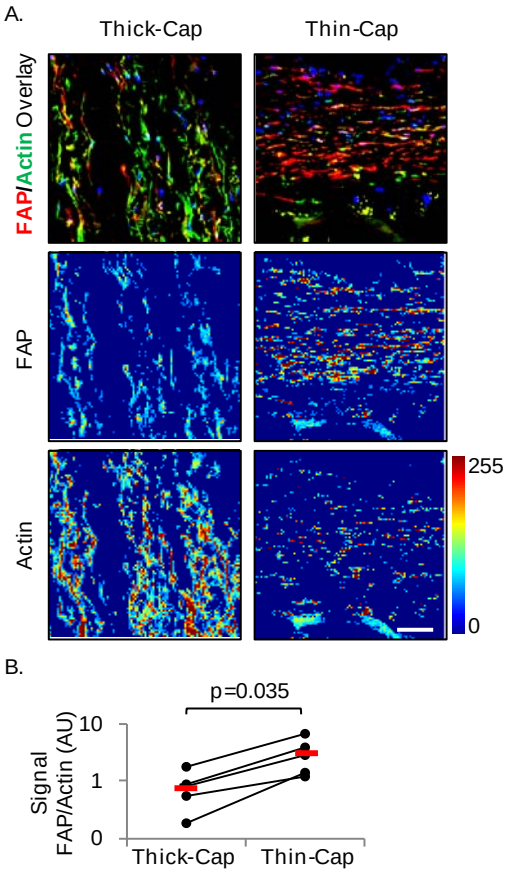

Figure 28. Fibroblast activation protein is enhanced in thin vs. thick carotid fibrous caps. A. top, Representative immunofluorescent images the region displayed in FAP Cap images (Figure 27A) show expression of FAP (red), actin (green), DAPI (blue) in thick vs. thin caps (bar=20µm). Heatmap rendered images are shown for FAP (middle) and actin (bottom). B. Quantification of FAP normalized to actin reveals a significant increase of FAP in thick vs. thin caps taken as paired samples from single plaques taken from 5 different patients (mean in red, n=5, p=0.035).

2.5 DISCUSSION

The fibrous cap is a tissue barrier between the blood stream in the vessel lumen and the thrombogenic plaque core, and fibrous cap thinning has been associated with plaque disruption, and atherothrombotic events.[1, 12] Therefore, specific targets which discriminate "rupture-prone" thin fibrous caps from "stable" thick fibrous caps may hold potential as diagnostic imaging targets in patients with carotid atherosclerosis. Here, a novel image analysis algorithm associates smooth muscle cell-specific FAP expression with fibrous cap thickness.

Applying the presented two-step image analysis algorithm, we quantify cell-specific protein expression and associate the expression pattern of our target protein with fibrous cap thickness. After objective subtraction of unspecific background signals, cell-specific FAP expression could be reliably quantified. As such, this presented algorithm identifies enhanced expression of FAP by smooth muscle cells in thin vs. thick carotid fibrous caps. Congruent with other matrix-degrading collagenases such as MMPs and cathepsins, the collagenolytic activity of FAP may promote fibrous cap remodeling and rupture.[4, 13] These findings warrant future investigations to identify a causal role of FAP in fibrous cap thinning *in vivo*.

Taken together, our work validates a novel image analysis method to associate cell-specific protein expression with fibrous cap thickness. Our data suggest FAP as a potential diagnostic target in thin-capped carotid plaques. Moreover, the presented algorithm may be applied to identify future targets specific for thin-cap fibroatheromata, and to investigate cell-specific protein expression as it relates to fibrous cap thinning.

2.6 ACKNOWLEDGEMENTS

This work was supported by grants from the Hartmann Müller Foundation, and the University Research Priority Program "Integrative Human Physiology", both at the University of Zurich. Further support was provided by the Special Program University Medicine (SPUM) by the Swiss National Science Foundation. We would like to also thank Ursula Steckholzer for her careful preparation of the tissue specimens.

2.7 REFERENCES

1. Carr S, Farb A, Pearce WH, Virmani R, Yao JST. Atherosclerotic plaque rupture in symptomatic carotid artery stenosis. *Journal of vascular surgery : official publication, the Society for Vascular Surgery [and] International Society for Cardiovascular Surgery, North American Chapter*. 1996;23:755-766
2. Redgrave JN, Gallagher P, Lovett JK, Rothwell PM. Critical cap thickness and rupture in symptomatic carotid plaques: The oxford plaque study. *Stroke*. 2008;39:1722-1729
3. Jaffer FA, Weissleder R. Molecular imaging in the clinical arena. *JAMA: The Journal of the American Medical Association*. 2005;293:855-862
4. Brokopp CE, Schoenauer R, Richards P, Bauer S, Lohmann C, Emmert MY, Weber B, Winnik S, Aikawa E, Graves K, Genoni M, Vogt P, Lüscher TF, Renner C, Hoerstrup SP, Matter CM. Fibroblast activation protein is induced by inflammation and degrades type i collagen in thin-cap fibroatheromata. *European Heart Journal*.
5. Virmani R, Burke AP, Farb A, Kolodgie FD. Pathology of the vulnerable plaque. *Journal of the American College of Cardiology*. 2006;47:C13-C18
6. Levy MT, McCaughan GW, Abbott CA, Park JE, Cunningham AM, Müller E, Rettig WJ, Gorrell MD. Fibroblast activation protein: A cell surface dipeptidyl peptidase and gelatinase expressed by stellate cells at the tissue remodelling interface in human cirrhosis. *Hepatology*. 1999;29:1768-1778
7. Rettig WJ, Pilar G-C, Beresford HR, Oettgen HF, Melamed MR, Old LJ. Cell-surface glycoproteins of human sarcomas: Differentialexpression in normal and malignant tissues and cultured cells. *Proc. Natl. Acad. Sci. USA*. 1988;85:3110-3114
8. Dippold WG, Lloyd KO, Li Lucy TC, Ikeda H, Oettgen HF. Cell surface antigens of human malignant melanoma: Definition of six antigenic systems with mouse monoclonal antibodies. *Proc. Nati. Acad. Sci. USA*. 1980;77:6114-6118
9. Smith PD, McLean KJ, Murphy MA, Wilson Y, Murphy M, Turnley AM, Cook MJ. A brightness-area-product-based protocol for the quantitative assessment of antigen abundance in fluorescent immunohistochemistry. *Brain Research Protocols*. 2005;15:21-29
10. Landmann L, Marbet P. Colocalization analysis yields superior results after image restoration. *Microscopy Research and Technique*. 2004;64:103-112
11. Zinchuk V, Zinchuk O, Okada T. Quantitative colocalization analysis of multicolor confocal immunofluorescence microscopy images: Pushing pixels to explore biological phenomena. *Acta Histochem Cytochem*. 2007;40:101-111
12. Burke AP, Farb A, Malcom GT, Liang Y-h, Smialek J, Virmani R. Coronary risk factors and plaque morphology in men with coronary disease who died suddenly. *New England Journal of Medicine*. 1997;336:1276-1282
13. Chatzizisis YS, Baker AB, Sukhova GK, Koskinas KC, Papafaklis MI, Beigel R, Jonas M, Coskun AU, Stone BV, Maynard C, Shi G-P, Libby P, Feldman CL, Edelman ER, Stone PH. Augmented expression and activity of extracellular matrix-degrading enzymes in regions of low endothelial shear stress colocalize with coronary atheromata with thin fibrous caps in pigs. *Circulation*. 2011;123:621-630

CHAPTER 3

FAP IS INDUCED BY INFLAMMATION AND DEGRADES TYPE-I COLLAGEN IN THIN-CAP FIBROATHEROMATA

Based on

Fibroblast activation protein is induced by inflammation and degrades type I collagen in thin-cap fibroatheromata.

Brokopp CE, Schoenauer R, Richards P, Bauer S, Lohmann C, Emmert MY, Weber B, Winnik S, Aikawa E, Graves K, Genoni M, Vogt P, Lüscher TF, Renner C, Hoerstrup SP, Matter CM.

European Heart Journal. 2011; doi: 10.1093/eurheartj/ehq519. Published online: February 2, 2011

3.1 ABSTRACT

Background – Collagen degradation in atherosclerotic plaques with thin fibrous caps renders them more prone to rupture. Fibroblast Activation Protein (FAP) plays a role in arthritis and tumor formation through its collagenase activity. However, the significance of FAP in thin-cap human fibroatheromata remains unknown.

Methods and Results – We detected enhanced FAP expression in type IV-V human aortic atheromata (n=12), compared with type II-III lesions (n=9; $p<0.01$) and healthy aortae (n=8; $p<0.01$) by immunostaining and western blot analyses. FAP was also increased in thin (<65µm) versus thick cap (≥65µm) human coronary fibroatheromata (n=12; $p<0.01$). FAP was expressed by human aortic smooth muscle cells (HASMC) as shown by colocalization on immunofluorescent aortic plaque stainings (n=10; $p<0.01$) and by flow cytometry in cell culture. While macrophages did not express FAP, macrophage burden in human aortic plaques correlated with FAP expression (n=12; $R^2=0.763$; $p<0.05$). ELISAs showed a time- and dose-dependent upregulation of FAP in response to human TNFα in HASMC (n=6; $p<0.01$). Moreover, supernatants from peripheral blood-derived macrophages induced FAP expression in cultured HASMC (n=6; $p<0.01$), an effect abolished by blocking tumor necrosis factor alpha (TNFα; n=6; $p<0.01$). FAP associated with collagen-poor regions in human coronary fibrous caps and digested type I collagen and gelatin *in vitro* (n=6; $p<0.01$). Zymography revealed that FAP-mediated collagenase activity was neutralized by an antibody directed against the FAP catalytic domain both in HASMC (n=6; $p<0.01$) and in fibrous caps of atherosclerotic plaques (n=10; $p<0.01$).

Conclusions – FAP expression in HASMC is induced by macrophage-derived TNFα. FAP associates with thin-cap human coronary fibroatheromata, and contributes to type I collagen breakdown in fibrous caps.

3.2 INTRODUCTION

Rupture of the fibrous cap in advanced atherosclerotic plaques is a critical trigger of acute coronary syndromes (ACS) that may lead to myocardial infarction and sudden cardiac death. One of the key events in promoting plaque instability is the degradation of the fibrous cap, which exposes the underlying thrombogenic plaque core to the bloodstream, thereby causing thrombosis and subsequent vessel occlusion.[1-3] Fibrous cap rupture is facilitated by proteases which cleave type I collagen, the primary load-bearing molecule in fibrous caps, leading to fibrous cap thinning and destabilization.[4-7] Therefore, activated proteases, which localize to thin fibrous caps, have attracted attention as potential diagnostic and therapeutic targets.

Candidate targets include matrix metalloproteinases (MMP)-2 and 9 and the cysteine protease cathepsin K; each of which are enhanced in both stable and unstable lesions.[8-11] MMP-2 and cathepsin K staining reveal diffuse localization throughout the plaque, whereas MMP-9 has been shown to colocalize with macrophages beneath the fibrous cap.[12-14] While these proteases have shown potential as markers of atherosclerotic plaques, their diffuse expression in all lesions warrant careful assessment of their targeting potential toward clinically relevant unstable plaques. An ideal protease target would be specific to the rupture-prone fibrous cap; a site perhaps more easily accessible by intravenously injected targeting agents. While MMPs and cysteine proteases have been well characterized as protease targets, the role of serine proteases in this context has not been investigated.

Fibroblast activation protein (FAP) is a membrane-bound, constitutively active serine protease expressed by activated fibroblasts in epithelial tumor stroma, arthritis, and wound healing, but remains virtually undetectable in healthy tissues.[15-17] FAP exhibits dipeptidyl peptidase IV activity, prolyl endopeptidease activity, and specificity for type I collagen and gelatin.[17-19] However, the role of FAP in

atherosclerosis is unknown. The aim of this study was to characterize FAP expression in human atherosclerosis and examine its association with features of plaque instability. Moreover, we sought to determine the mechanism of FAP induction, its downstream effects, and the capacity of a neutralizing FAP-specific antibody.

3.3 METHODS

3.3.1 AORTIC AND CORONARY ARTERY SPECIMENS

Ascending aortic plaque biopsies were placed into sterile Dulbecco's Modified Eagle Medium (DMEM; Gibco, Carlsbad, CA), pre-chilled to 4°C, and transferred on ice to the laboratory and frozen in Optimal Cutting Temperature Compound (Tissue-Tek, Torrance, CA) for tissue zymography. Coronary arteries were obtained from patients that died after an acute myocardial infarction. Approval from the local Ethics Committee was obtained for collections of all patient specimens.

3.3.2 CHARACTERIZATION OF ATHEROSCLEROTIC PLAQUES

Biopsies of normal and plaque bearing ascending aortae were obtained from patients undergoing surgical aortic valve replacement secondary to aortic stenosis (n = 20, age (y): 63 ± 14.5, BMI: 27.8 ± 5.4, diabetes mellitus 3/20; CRP (mg/L): 2.1 ± 1.8, Triglycerides (mmol/L): 2.2 ± 1.6, LDH (IU/L): 218.9 ± 37.8). Aortic plaques were sectioned and graded according the American Heart Association (AHA) criteria[20, 21] using Movat pentachrome, Oil-Red-O, anti-CD68, and von Kossa staining (data not shown). Coronary arteries were obtained from patients that died after an acute myocardial infarction and embedded in paraffin for sectioning. Collagen in coronary artery plaques was characterized by Masson staining. Fibrous caps were identified as the collagen-rich tissue separating the lumen and the necrotic core.[2] Plaques with a minimum fibrous cap thickness of less than 65 µm were classified as *thin-cap*, whereas plaques with a fibrous cap thickness equal or greater than 65 µm were classified as *thick-cap* atheromata.[2]

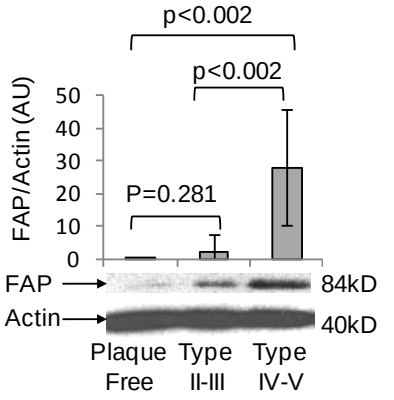

Figure 31. FAP is enhanced in Type IV-V aortic atherosclerotic plaques as shown by Western Blot. The graph shows a significant increase FAP signal compared to an all actin loading control in plaque-free aortae (n=8) compared to type II-III (n=8), and type IV-V plaques (n=7).

3.3.3 FAP IMMUNOBLOTTING

Characterized plaques and plaque-free aortic tissue samples were snap-frozen in liquid nitrogen, homogenized and blotted according to standard procedures. The following antibodies were used: FAP was labeled using rabbit A246, actin (**Figure 31**) was labeled using a polyclonal rabbit anti–human antibody [Sigma-Aldrich]) and αSMA was identified using a rabbit polyclonal against alpha-smooth muscle actin (αSMA; Ab5694; Abcam). Densiometry was performed using a FluorChem Q Imaging System (Alpha Innotech).

3.3.4 IMMUNOFLUORESCENCE AND IMMUNOHISTOCHEMISTRY

Cross sections from human ascending aortae (10 µm thickness) and paraffin-embedded sections of coronary plaques (4 µm thickness) were mounted on glass slides. Paraffin-embedded coronary sections

were labeled with A246 and subsequently by Cy5-labeled secondary goat anti-mouse IgG (115-175-146; Jackson ImmunoResearch). FAP colocalization with macrophages, endothelial cells, and smooth muscle cells was determined using a rabbit antibodies directed against CD68 (SC-9139; Santa Cruz, Santa Cruz, CA), von Willebrand factor (vWF; F3520; Sigma-Aldrich, Carlsbad, CA), alpha-smooth muscle actin (αSMA; Ab5694; Abcam), or type I collagen (Ab292; Abcam); subsequent fluorescent labeling was performed using a Cy3-labeled anti-rabbit IgG (111-165-144; Jackson ImmunoResearch) in three adjacent sections of each biopsy specimen. DAPI (D9542; Sigma-Aldrich) was used for fluorescent counterstaining of nuclei. Isotype control antibodies were used to address antigen-binding specificity. Stained samples were cover-slipped with Tris-buffered glycerol (a 3:7 mixture of 0.1 M Tris-HCl at pH 9.5 and glycerol supplemented with 50 mg/mL *n*-propyl-gallate).

Antigen retrieval in paraffin-embedded sections of coronary plaques was performed after 20 min incubation in 95ºC retrieval buffer (2 mM Sodium Citrate, pH 7.6). FAP was stained using a rabbit polyclonal antibody raised against the catalytic insert of FAP (A246; Ab28246; Abcam, Cambridge, MA) and a rabbit isotype control (Ab37415; Abcam). Cryosections of aortic plaques were fixed in ice-cold acetone for 5 min and stained using a mouse monoclonal against FAP (F19, Provided by Sloan-Kettering Institute, New York, NY) and the appropriate mouse isotype control (401401; BioLegend, San Diego, CA).[22, 23] Primary antibodies were detected with biotin-labeled goat anti-mouse (115-066-003; Jackson ImmunoResearch, West Grove, PA) and biotin-labeled goat anti-rabbit (111-066-003; Jackson ImmunoResearch) and stained using an ABC staining kit (Vector Labs, Burlingame, CA).

3.3.5 IMAGE ANALYSIS

For low power imaging at spatial resolutions above 1 µm/pixel, we used a fluorescent microscope (DM60000B; Leica, Wetzlar, Germany) equipped with a fluorescent camera (DFC350 FX; Leica). Colocalization analyses were performed at higher magnifications using a multichannel confocal microscope (TCS SP2, Leica) on a single optical plane**.**

Single-channel fluorescent images (nine images per section in three adjacent sections) of aortic tissue sections were taken at constant camera settings in tagged image file format (TIFF) at a binary pixel intensity between 0-255. In each group, additional adjacent tissue sections were stained with isotype control antibodies to determine the background threshold. The background intensity threshold for each channel was set at the intensity under which 95% of the pixels emitted in control staining. [24, 25] Pixels below the background intensity threshold were excluded from quantification.[25] The remaining pixels were summed and divided by the total number of pixels to calculate the mean pixel intensity. Positive pixels were summed to calculate positive area using image analysis software by Matlab (Mathworks, Novi, MI). [26] Quantitative colocalization analyses were performed using a confocal microscope at high resolution on a single plane. Two TIFF images were captured from distinct fluorescent channels on each tissue section, and background signal was subtracted as previously described. Colocalization coefficients were calculated as the sum of FAP-positive pixels, which colocalized with pixels positive for cell-specific markers.[27, 28]

3.3.6 CELL CULTURES

Human aortic endothelial cells (HAEC) were isolated from biopsies of ascending aortae without macroscopic lesions obtained from patients undergoing operations for valve repair, human aortic smooth muscle cells were purchased (HASMC; Promocell); peripheral blood-derived monocytes were isolated from healthy subjects**.** Foam cells were generated by stimulating macrophages with 100 µg/mL of oxidized low-density lipoprotein (BT-910; BioConcept, Allschwil, Switzerland) for 48 h in Serum-Free Macrophage Medium (SFM; Gibco). Lipid uptake was assessed by Oil-red-O staining (O0624; Sigma-Aldrich).

For endothelial cell isolation, aortic lumens were washed with PBS and incubated in DMEM containing collagenase type 2 (350 U/mL; Worthington, Lakewood, NJ) for 30 min, and agitated gently to dissociate the endothelium from the vessel wall. Endothelial cells were further purified by magnetic bead separation against CD34 (130-046-702**;** Miltenyi Biotec**,** Gladbach, Germany). HAEC were expanded in endothelial cell growth medium (EGM2; Gibco) and characterized by FACS analysis for vWF expression (>98%). To isolate phagocytic monocytes, 50 mL of peripheral venous blood was collected from healthy probands in EDTA collection tubes, diluted 2x in Hank's buffered salt solution and spun on a Ficoll gradient (20 min, 400 G, 24°C).

Monocytes were selected from the buffy coat by magnetic bead sorting for CD14 **(**130-050-201; Miltenyi Biotec), to yield a final purity over 94% (FACS against CD64). Monocytes were differentiated into macrophages in polystyrene six well plates over seven days in RPMI-1640 (Gibco) containing 10% heat-inactivated, low-endotoxin fetal bovine serum (Gibco) and 50nM recombinant human macrophage colony stimulating factor (AF-300-03; Peprotech, Rocky Hill, NJ), replacing the media every 48 h. Macrophage differentiation was validated using anti-CD68 FACS analysis. FAP was measured in all cell types using F19 in unfixed cells and a Cy5-conjugated secondary antibody for FACS analyses, and the appropriate murine IgG isotype control antibody.

3.3.7 FAP INDUCTION ASSAYS

Peripheral blood-derived macrophages were incubated for 48 h in SFM (2mL/well in a 6 well plate) and the supernatant was sterile filtered, aliquoted, and frozen at -80ºC. Purchased human aortic smooth muscle cells (HASMC; Promocell) were validated by FACS analyses for αSMA (purity>96%), and plated at passage 4 into a 96-well black cell culture test plate at a density of $5x10^4$ cells/cm^2 in DMEM (10938; Gibco) supplemented with 10% Fetal Calf Serum (3302-P250302; PAN Biotech, Aidenbach, Germany) and allowed to attach for 24 h before rendered quiescent overnight in Advanced DMEM (12491-015; Invitrogen, Carlsbad, CA) with 1% bovine serum albumin (starvation medium). Quiescent HASMCs were treated with starvation media supplemented with 3, 5, 10, 20, 40% macrophage-conditioned SFM for 48 h. To determine the effects of TNFα on FAP expression, quiescent HASMCs were treated with starvation media supplemented with 20% macrophage-conditioned SFM and a TNFα-neutralizing antibody (Ab6671; Abcam) or an IgG isotype control (Ab27478; Abcam) antibody. Recombinant human TNFα (300-01A; Peprotech) was used to induce FAP expression in quiescent HASMC in a dose- and time-dependant manner. For quantifications, cells were

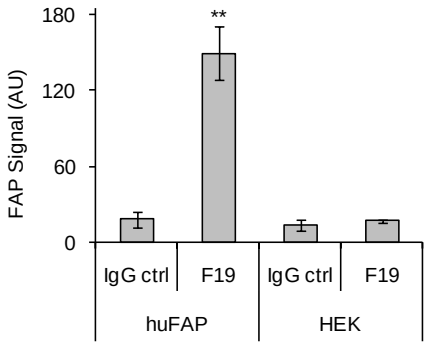

Figure 32. Membrane-bound FAP is detected by indirect ELISA on cell membranes. The graph shows a significant increase FAP signal in F19-labelled huFAPs compared with HEKs or IgG labeled controls

washed with PBS, fixed in 4% formalin for 30 min, and labeled against FAP with F19. Cultures were enzymatically labeled using a Horseradish Peroxidase ELISA kit (Anaspec, Fremont, CA) and the enzymatic product quantified with a fluorescent plate reader. Background values were subtracted, and all values were normalized to untreated/unconditioned control groups.

Validation of the FAP ELISA was performed using HEK293 as a negative control, and HEK293 cells stably transfected with an FAP plasmid as a positive control. An unspecific murine IgG antibody was used as a negative control detection antibody and the anti-FAP F19 antibody was used as a positive control antibody (**Figure 32**).

3.3.8 ZYMOGRAPHY ASSAYS

In situ zymography was performed on (5µm) cryosections of human aortic atherosclerotic plaques which had been stained against FAP using non-inhibitory F19 and Cy5 labeled secondary antibody, and then treated with A246 or an isotype control at 50 nM concentration overnight.[17] Treated and untreated sections were then mounted in warm 1% Agarose in PBS with 10% direct quenched type I collagen from bovine skin (D12060; Invitrogen) and imaged after 2 h at 37ºC by confocal microscopy. For quantification, background signals were subtracted from isotype control images and pixels which were positive for both FAP cleaved Type I collagen were quantified as the average of nine images from three adjacent sections per biopsy.

Direct-quenched porcine gelatin (DQ gelatin; D12054; Invitrogen) was diluted to a final concentration of 100 µg/mL in reaction buffer (0.5 M Tris-HCl, 1.5 M NaCl, 50 mM $CaCl_2$, and 2 mM sodium azide at pH 7.6) and 0, 10, 20, 40 nM of recombinant human FAP in a black 96-well plate. Cleaved gelatin was quantified, at 0.5, 8, and 24 h, and background fluorescence subtracted (**Figure 33**).

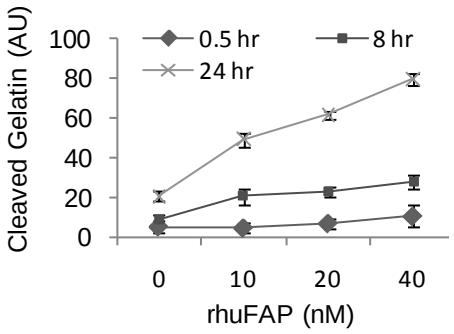

Figure 33. rhuFAP degrades DQ-collagen. The graphs shows rhuFAP cleavage of DQ-gelatin (n=6/group) *in vitro.*

A246 raised against FAP's catalytic insert and a matching isotype control IgG (Ab27478; Abcam) were added to 20 mM recombinant human FAP and 100 µg/mL DQ gelatin or DQ type I collagen in reaction buffer and analyzed after 24 h, to determine blocking efficacy. A246 is a rabbit polyclonal raised against an FAP-specific peptide, immunogen affinity purified, and recognizes fibroblast activation protein specifically, but not other dipeptidyl peptidases family members (Abcam; Ab28246). Confluent HASMC at passage 4 were treated with A246 or an antibody control for 30 min, washed with PBS, and then placed under 100 µL of 100 µg/mL DQ gelatin in reaction solution for 4 h before fluorescence analysis with a plate reader (**Figure 34**).

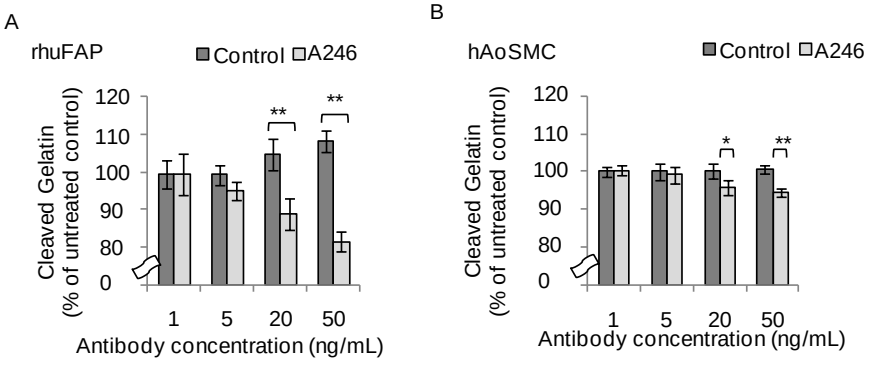

Figure 34. A246 reduces gelatinase activity of recombinant human FAP (rhuFAP) and HASMC in vitro. A. The graph reveals dose-dependent inhibition of rhuFAP gelatinase activity by A246 (n=6/group; ** = p<0.01; * = p<0.05). B. The graph reveals dose-dependent inhibition of FAP in HASMC (n=6/group; ** = p<0.01; * = p<0.05).

3.3.9 FAP-MEDIATED TYPE I COLLAGEN DEGRADATION ASSAYS

To evaluate the FAP-mediated type I collagen-specific cleavage, full-length native human type I collagen isolated from human placenta (purity >90%) was used (288; Yo Proteins). Type I collagen (100ng/mL) was treated with recombinant human FAP (200nM) for 18 h at 37°C in PBS (pH = 7.2) and compared to an untreated collagen control. A246 (50ng/mL) was added to the solution and compared to an isotype control antibody IgG (Ab27478; Abcam) to validate the neutralizing capacity of A246. Samples were separated by gel electrophoresis and visualized by silver staining (ProteoSilver Silver Stain Kit, Sigma).

3.3.10 STATISTICAL ANALYSES

Histological and cell culture results were compared using one-way ANOVA and associations calculated by Pearson's correlation coefficient. Student's T-test was used for comparisons of zymography. All statistical analyses were performed using MatLab (Version, R2007b). Data are presented as mean±SD. Significance was accepted at the level of $p<0.05$.

3.4 RESULTS

3.4.1 FAP EXPRESSION IS ENHANCED IN ADVANCED HUMAN AORTIC PLAQUES

Immunofluorescent stainings for FAP in adjacent cryosections revealed enhanced expression of FAP in fibroatheromata vs. plaque-free aortae (**Figure 35A**). Positive staining for FAP was virtually absent in healthy ascending aortae, whereas a step-wise increase was observed in Type II-III and Type IV-V plaques by western blot analyses (**Figure 35B**) and quantitative image analysis (**Figure 35C-D**).

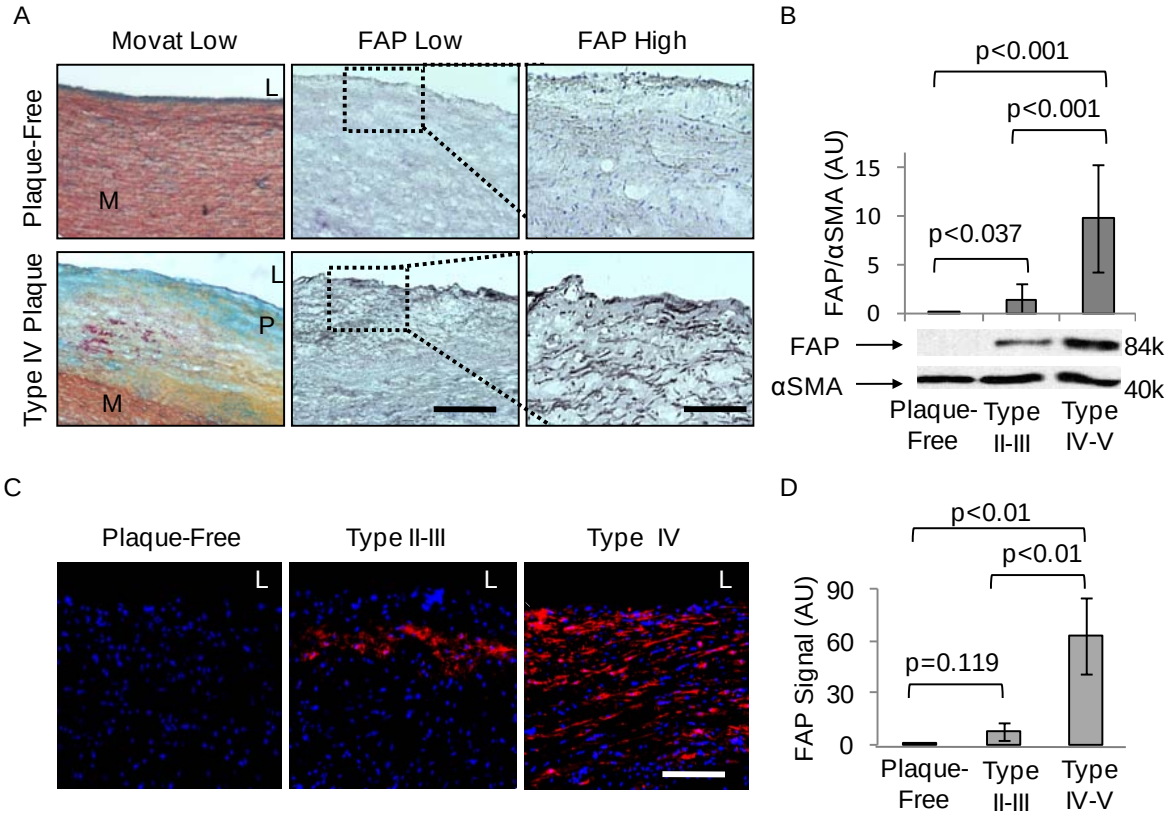

Figure 35. FAP expression is enhanced in human atherosclerotic aortic plaques. A, Movat and FAP stainings show cross-sections of representative plaque-free aortae and Type IV aortic atherosclerotic plaques (L=lumen, M=media, P=atherosclerotic plaque; bar=400 µm). Dotted boxes indicate regions of interest in adjacent sections at high magnification (bar=50 µm). **B**, Western blot analysis of FAP normalized to αSMA in plaque-free aortae (n=8), type II-III plaques (n=8), and type IV-V plaques (n=7) show a significant increase in FAP in advanced type IV-V plaques by immunoblot densitometry. **C**, Immunofluorescent stainings in representative tissue sections of plaque-free aortae, type II-III plaque, and type IV plaque show FAP expression in red (DAPI in blue; bar=50 µm). **D**, The graph reveals a significant increase in FAP expression in Type II-III aortic plaques (n=9) and in Type IV-V plaques (n=12) compared with plaque-free aortae (n=8).

3.4.2 FAP IS EXPRESSED BY SMOOTH MUSCLE CELLS IN ADVANCED HUMAN AORTIC PLAQUES

To characterize FAP-expressing cell types in human atherosclerotic plaques, we performed immunofluorescent co-stainings of FAP in macrophages (identified as CD68-positive cells), smooth muscle cells (αSMA-positive cells), and endothelial cells (vWF-positive cells) (**Figure 36A)**. Confocal image analyses revealed FAP expression by smooth muscle cells, but not by macrophages or endothelial cells (**Figure 36B**).

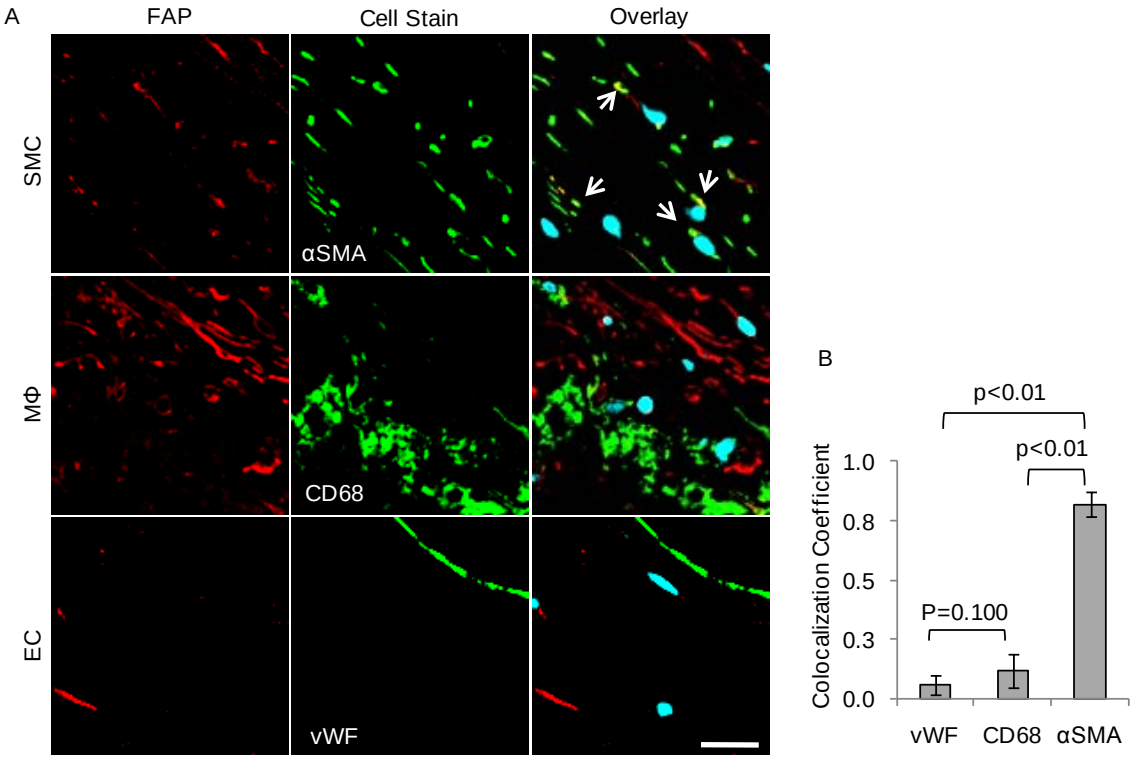

Figure 36. FAP expression in human aortic plaques colocalizes with smooth muscle cells, but not with macrophages or endothelial cells. A, Overlays of confocal images of FAP (red) and DAPI (blue) with cell-specific stainings of αSMA, CD68, and vWF (green) in representative sections illustrate FAP colocalization (arrows) with smooth muscle cells (bar=20 μm). **B**, The graph quantifies an increased colocalization of FAP with smooth muscle cells (αSMA), compared with endothelial cells (vWF) and macrophages (CD68) in type IV-V atherosclerotic plaques (n=10).

3.4.3 SMOOTH MUSCLE CELLS EXPRESS FAP *IN-VITRO*

To validate FAP expression by vascular cells *in vitro*, we performed FACS analyses of FAP in HASMC (αSMA-positive cells), HAEC (vWF-positive cells), peripheral blood derived-monocytes (CD64-positive), macrophages (CD68-positive), and foam cells (Oil-Red-O-positive macrophages). FACS analyses revealed high constitutive FAP expression in HASMC, slight expression in HAEC, but no expression by peripheral blood-derived monocytes, macrophages or foam cells (**Figure 37**).

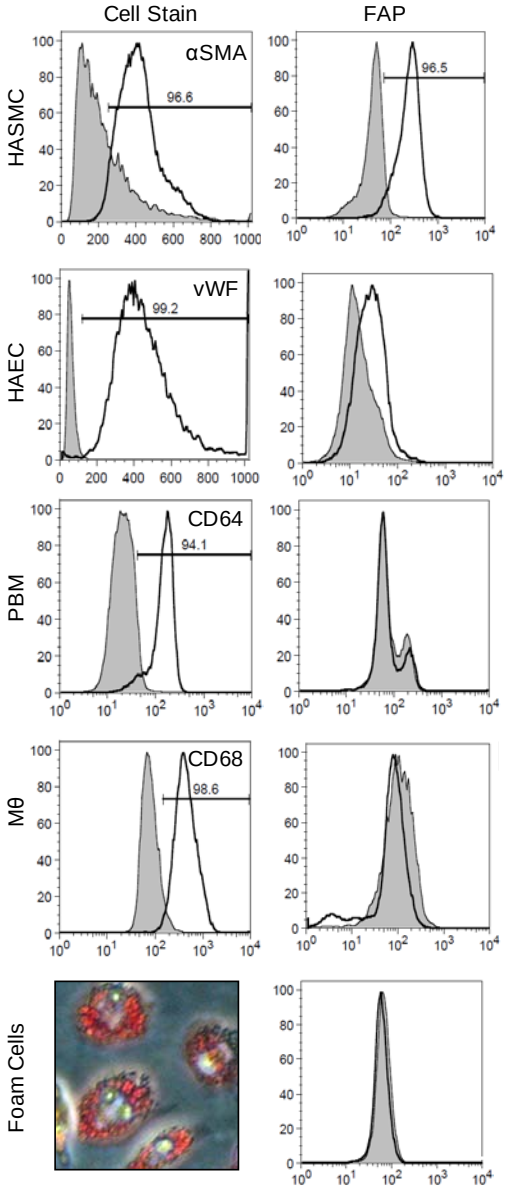

Figure 37. FAP is constitutively expressed in cultured human aortic smooth muscle cells (HASMC) and endothelial cells (HAEC), but not in peripheral blood-derived monocytes (PBM), macrophages (MΦ), or foam cells. FACS analyses and Oil-Red-O staining of peripheral blood derived-macrophages laden with oxidized low-density lipoprotein (oxLDL) characterize cells populations (left) and their respective FAP expression (right).

3.4.4 FAP EXPRESSION IS ENHANCED IN THIN-CAP VERSUS THICK-CAP HUMAN CORONARY ATHEROMATA

In order to determine the association of FAP with coronary fibrous cap thickness, we stained collagen applying the Masson method (stains collagen in blue) in rupture-prone human coronary arteries obtained from patients that died after myocardial infarction. Based on fibrous cap thickness these specimens were characterized as thin-cap (<65 µm) or thick-cap (≥65 µm) fibroatheromata. Immunohistological and immunofluorescent stainings and subsequent confocal image analyses in adjacent sections revealed enhanced FAP expression in thin compared with thick fibrous caps (**Figure 38)**.

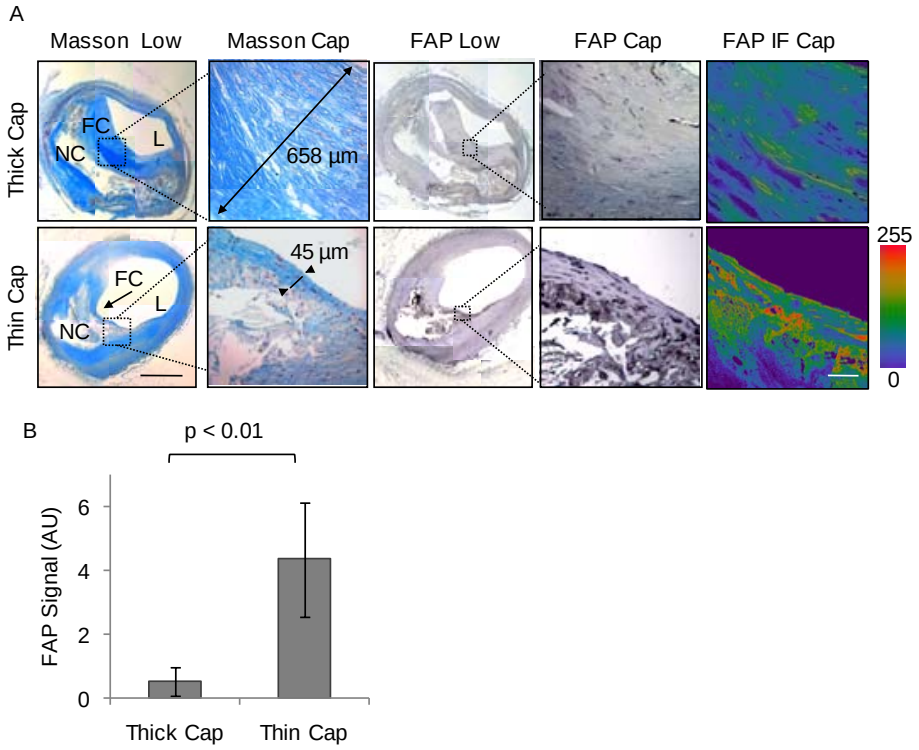

Figure 38. FAP expression is enhanced in thin-cap versus thick-cap human coronary fibroatheromata. A, Masson staining shows collagen-rich thick (658 µm) versus thin (45 µm) fibrous caps (L=lumen, FC=fibrous cap, NC=necrotic core; bar=1 mm). FAP immunohistochemistry and immunofluorescence (intensity scale; bar=50 µm) shows FAP expression in representative thin vs. thick caps. Dotted boxes indicate regions of interest in adjacent sections at high magnification. **B,** The graph reveals a significant increase in FAP expression in thin vs. thick fibrous caps (n=12 each).

3.4.5 FAP Associates with Macrophage Burden in Human Aortic Atherosclerotic Plaques

Immunofluorescence stainings revealed FAP expression in medial cells adjacent to macrophages in aortic fatty streaks (**Figure 39A**). To characterize the relationship between FAP and inflammation, we compared FAP and macrophage immunofluorescent signal intensity in human aortic plaques (**Figure 39B**). We observed a positive correlation between macrophage burden and FAP expression with plaque progression (R^2=0.763; n=12; **Figure 39C**).

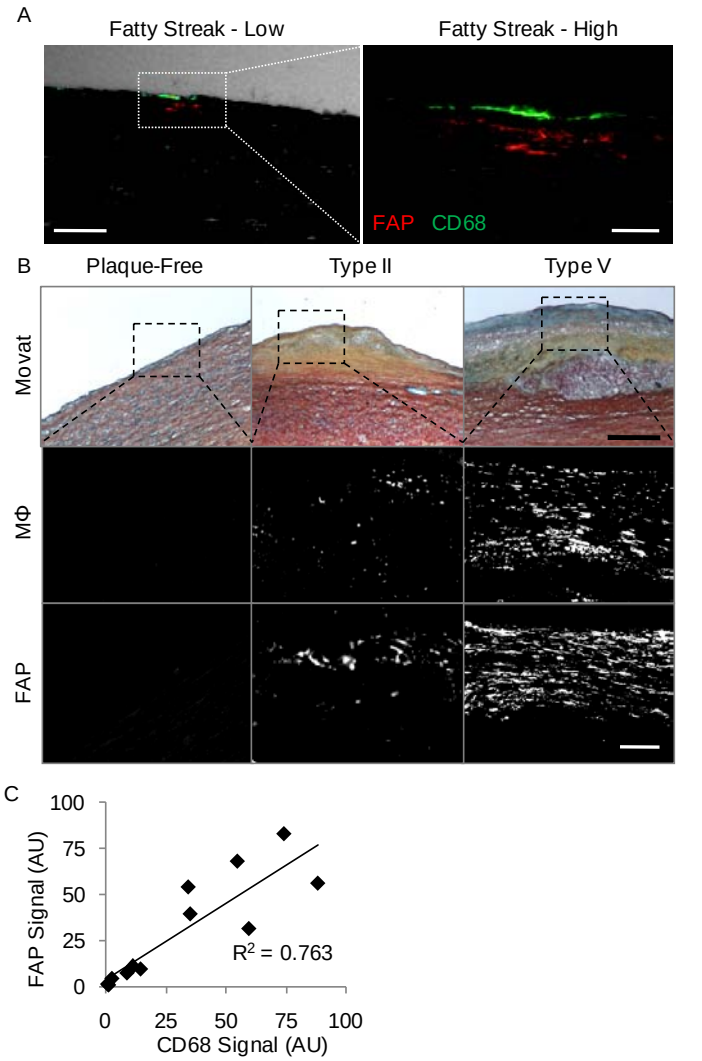

Figure 39. FAP expression correlates with macrophage burden in human aortic plaques. A, Confocal immunofluorescent photomicrograph of an aortic fatty streak reveals FAP expression (red) adjacent to macrophages (CD68; green) at low (phase-contrast, white; bar=100 µm) and high magnification (bar=25 µm). **B**, Movat staining (bar=400 µm), FAP, or macrophage (CD68) immunofluorescent stainings in plaque-free aortae, Type II, and Type V atherosclerotic plaques show enhanced FAP expression with increasing macrophage burden (bar=50 µm). **C**, Comparisons of FAP and macrophage expression in serial adjacent sections from aortic plaques demonstrate a significant positive correlation (R^2=0.763; n=12; $p<0.05$); AU, arbitrary units.

3.4.6 MACROPHAGE-DERIVED TNFα INDUCES FAP EXPRESSION IN SMOOTH MUSCLE CELLS

To elucidate a signaling mechanism between macrophages and FAP expressing HASMC, we exposed HASMC to macrophage-conditioned media for 48 h to simulate conditions applicable to plaque inflammation. Cultured HASMC showed a dose-dependent increase in FAP expression in response to the macrophage-conditioned media with a maximal effect observed at 20% media concentration (**Figure 40A**) after 48 h. This effect was abolished when macrophage-conditioned media was supplemented with a TNFα-neutralizing antibody (**Figure 40B)**. To confirm this paracrine effect of TNFα on FAP expression, experiments were repeated using recombinant human TNFα. TNFα-mediated FAP expression was observed in a dose- and time-dependent manner, with a maximum response at 30 ng/mL after 48 h (**Figure 40C-D**).

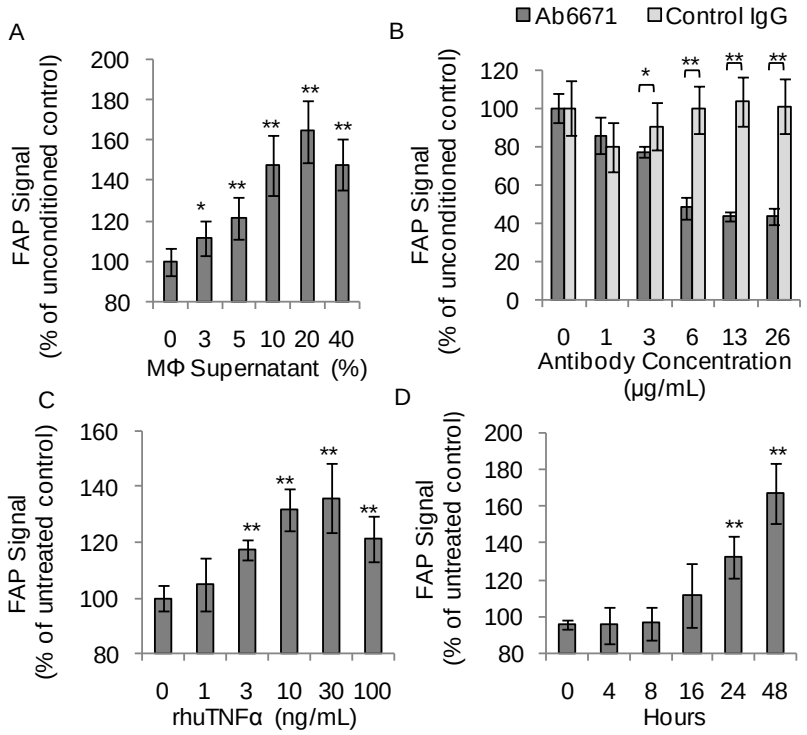

Figure 40. Macrophage-derived TNFα induces FAP expression in HASMC. A, Macrophage-conditioned supernatant induces FAP in HASMC in a concentration-dependent manner following 48 h exposure (n=6). **B**, Using the same macrophage-conditioned medium, TNFα-blocking antibody (Ab6671) decreases FAP expression by 40% in HASMC compared with an isotype control antibody (n=6). **C**, Recombinant human TNFα induces FAP in HASMC in a dose-dependent manner after 48 h incubation (n=6). **D**, Recombinant human TNFα induces FAP in HASMC in a time-dependent manner (30 ng/mL). AU, arbitrary units (*=p<0.05, **=p<0.01).

3.4.7 FAP IS INHIBITED BY AN FAP NEUTRALIZING ANTIBODY IN FIBROUS CAPS

Immunofluorescence analyses revealed enhanced FAP expression in Type I collagen-poor regions of aortic fibrous caps (**Figure 41A)**. Aortic fibrous caps treated with an IgG control antibody showed a colocalization of FAP with cleaved DQ type I collagen, whereas Ab246-treated plaques demonstrated a significantly reduced colocalization of FAP with type I collagenase activity (**Figure 41B)**. Confocal image analyses revealed that A246-treated fibrous caps exhibited decreased cleaved type I collagen at sites of FAP expression (**Figure 41C**). Type I collagenase activity of rhuFAP and the neutralizing capacity of A246 were demonstrated by incubation of native human type I collagen with rhuFAP in the presence of inhibiting antibody or isotype control (**Figure 41D**).

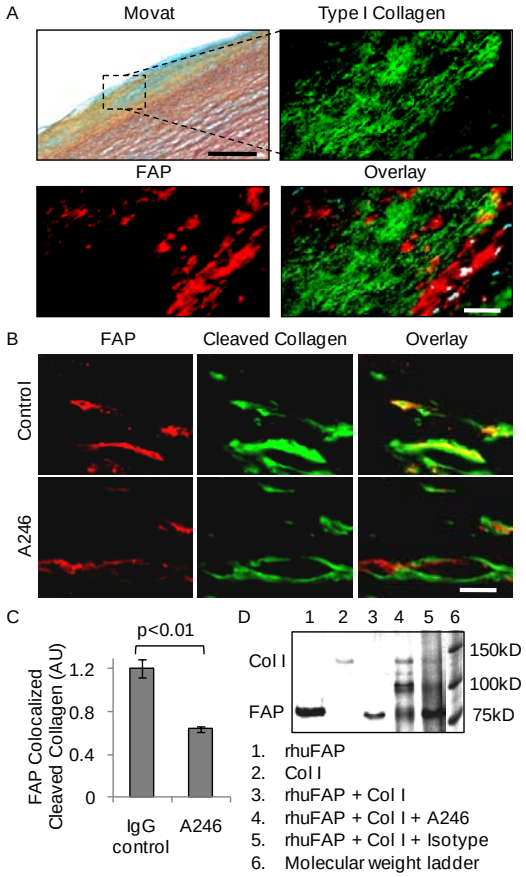

Figure 41. Type I collagenase activity is inhibited in human aortic fibrous caps by the FAP-blocking antibody A246. A, Movat staining of a fibrous cap in human aortic plaque. The region of interest (black box) is shown at higher magnification in an adjacent section stained for FAP (red), type I collagen (green), and overlay (DAPI=blue; bar=150 µm). B, Confocal images of *in situ* zymography show FAP (red) and cleaved DQ type I collagen (green) in fibrous caps shown by Movat (7A) of aortic plaque treated with a control IgG antibody or neutralizing antibody A246 (bar=10 µm). C, The graph reveals a significant reduction of cleaved type I collagen colocalized with FAP expression by *in situ* zymography (n=10/group). D, Type I Collagenase activity of rhuFAP and the neutralizing capacity of A246 was demonstrated by incubation of native human type I collagen with rhuFAP in the presence of inhibiting or isotype control antibodies (Lanes 1 rhuFAP, 2 collagen, 3 rhuFAP + collagen, 4 rhuFAP + collagen + A246, 5 rhuFAP + collagen + isotype control antibody, 6 molecular weight marker).

3.5 DISCUSSION

The fibrous cap of an atherosclerotic plaque is essential for separating the blood stream in the vessel lumen from the its thrombogenic necrotic core. The mechanical strength of the fibrous cap is provided primarily by type I collagen, which is degraded by MMPs and cysteine proteases, both of which are associated with plaque instability and occurrence of acute thrombotic events.[29-33]

This study links the constitutively active serine protease FAP to plaque progression and fibrous cap thinning and provides evidence that: (1) FAP expression is enhanced in human aortic atheromata and in fibrous caps of thin-cap coronary plaques, (2) FAP is expressed in HASMC and its expression correlates with macrophage burden, (3) FAP expression is induced in HASMC by macrophage-derived TNFα via paracrine signaling, (4) FAP cleaves collagen in fibrous caps of human atheromata, and (5) FAP-mediated type I collagenase activity is inhibited by a FAP-neutralizing antibody.

Numerous studies implicate matrix-degrading collagenases such as MMP1, 2, and 9 as well as cysteine proteases such as cathepsins S and K in vascular remodeling and plaque rupture.[13, 30, 34] Our findings provide evidence that FAP is the first known smooth muscle cell-derived serine protease involved in collagen degradation in human atherosclerosis. FAP expression was particularly enhanced in fibrous caps of thin-cap human coronary plaques isolated from patients that died after myocardial infarction. Indeed, thin fibrous caps (<65µm) have been associated with sudden cardiac death.[2, 35] The type I collagenase activity of FAP is demonstrated by both FAP-mediated collagenolysis in fibrous caps and the association of FAP with collagen-poor fibrous cap tissue in image analyses. These observations underline the potential clinical relevance of FAP as a diagnostic and / or therapeutic target in patients with plaques prone to rupture, i.e. patients at risk for ACS or stroke.

Inflammation constitutes a key feature of plaque vulnerability and inflammatory processes have been shown to induce collagenases in atherosclerotic plaques.[4, 36, 37] Consistent with this paradigm, we demonstrate that FAP expression in HASMC is associated with macrophage burden in intermediate and advanced human atherosclerotic plaques. FAP was not expressed by macrophages. However, macrophage-derived TNFα induced a dose- and time-dependent increase in FAP expression in cultured smooth muscle cells. These data indicate that a paracrine inflammatory pathway can induce FAP expression in smooth muscle cells. Thereby, our findings contribute to a growing body of evidence that supports the notion of inflammation-induced collagenase expression in atherosclerosis.[6, 11, 29, 38] Such findings could motivate future studies to investigate putative atheroprotective interventions involving either key anti-inflammatory mechanisms, such as the TNFα pathway, collagen-degrading enzymes themselves such as FAP, or both.

In addition to its expression in smooth muscle cells, we detected constitutive FAP expression in human aortic endothelial cells *in vitro*. Endothelial activation is a critical step in atherogenesis.[39] Activated endothelial cells express fibrous cap-degrading collagenases, and have also been shown to act in concert with fibrous cap-degrading smooth muscle cells.[5, 32, 40] Indeed, the observed capacity of endothelial cells to express FAP in-vitro supports the notion of a coordinated remodeling of the fibrous cap by both endothelial and smooth muscle cells. Furthermore, by recruiting blood-borne inflammatory cells to the plaque, activated endothelial cells may also enhance macrophage-derived cytokine release, activate smooth muscle cells, and thus induce FAP expression and / or activity.

Distinct from MMPs FAP combines several unique properties: MMPs exhibit diffuse expression throughout both intermediate and advanced atherosclerotic plaques.[14] In contrast, FAP expression is associated specifically with thin-cap atheromata. Moreover, MMP activity is modified by tissue inhibitors of metalloproteinases (TIMPs), whereas no natural inhibitors of the constitutively active FAP are identified. It is therefore plausible that FAP expression associates with its activity, rendering FAP a

potential diagnostic target. Furthermore, we demonstrate that FAP is mainly expressed in activated smooth muscle cells in thin fibrous caps of advanced atherosclerotic plaques. Given its localization in the fibrous cap close to the blood stream, FAP may be more accessible than MMPs by circulating targeting agents.

Taken together, we found that FAP expression is induced by macrophage-derived TNFα in human aortic smooth muscle cells, associates with thin-cap human coronary plaques, and contributes to type I collagen breakdown in fibrous caps. Thus, FAP expression in thin-cap coronary plaques and endothelial cells renders this target attractive for further investigation in patients with ACS. Along this line, we plan to investigate whether soluble FAP may be a biomarker for ACS. Moreover, our present findings demonstrate that FAP-mediated collagenolysis is induced by inflammatory cues and may be blocked by neutralizing antibodies. At the experimental level, studies using genetic or pharmacological modulation of FAP will shed light onto the causal role of FAP in atherogenesis and its potential use as a target in atherosclerosis and other inflammatory diseases such as rheumatoid arthritis and tumor formation.

3.6 ACKNOWLEDGEMENTS

We thank Sonja Matter, Stephan Keller, and Matthias Stein for their excellent support, the Zurich Center for Integrative Human Physiology (ZIHP), Andres Kaech at the Center for Microscopy and Image Analysis at the University of Zurich for access to imaging facilities, Thomas Wüest for his help in preparing targeting agents, and Irina Agarkova for providing expertise on immunofluorescent imaging.

This work was supported by grants from the Swiss National Science Foundation 31-114094/1, 310030_130626/1 (CMM) and 3100-068118 (TFL), the Herzog-Egli Foundation (CEB, CMM) and the Hartmann Müller Foundation (CEB, CMM), both at the University of Zürich, the University Research Priority Program “Integrative Human Physiology” at the University of Zurich (CEB, PR, SS, TFL, SPH, CMM). Further support was provided by unrestricted grants from the MERCATOR Foundation Switzerland.

3.7 REFERENCES

1. Farb A, Burke AP, Tang AL, Liang Y, Mannan P, Smialek J, Virmani R. Coronary plaque erosion without rupture into a lipid core : A frequent cause of coronary thrombosis in sudden coronary death. *Circulation*. 1996;93:1354-1363
2. Virmani R, Burke AP, Farb A, Kolodgie FD. Pathology of the vulnerable plaque. *Journal of the American College of Cardiology*. 2006;47:C13-C18
3. van der Wal A, Becker A, van der Loos C, Das P. Site of intimal rupture or erosion of thrombosed coronary atherosclerotic plaques is characterized by an inflammatory process irrespective of the dominant plaque morphology. *Circulation*. 1994;89:36-44
4. Shah P, Falk E, Badimon J, Fernandez-Ortiz A, Mailhac A, Villareal-Levy G, Fallon J, Regnstrom J, Fuster V. Human monocyte-derived macrophages induce collagen breakdown in fibrous caps of atherosclerotic plaques. Potential role of matrix-degrading metalloproteinases and implications for plaque rupture. *Circulation*. 1995;92:1565-1569
5. Rajavashisth TB, Xu X-P, Jovinge S, Meisel S, Xu X-O, Chai N-N, Fishbein MC, Kaul S, Cercek B, Sharifi B, Shah PK. Membrane type 1 matrix metalloproteinase expression in human atherosclerotic plaques. *Circulation*. 1999;99:3103-3109
6. Crisby M, Nordin-Fredriksson G, Shah PK, Yano J, Zhu J, Nilsson J. Pravastatin treatment increases collagen content and decreases lipid content, inflammation, metalloproteinases, and cell death in human carotid plaques : Implications for plaque stabilization. *Circulation*. 2001;103:926-933
7. Herman MP, Sukhova GK, Libby P, Gerdes N, Tang N, Horton DB, Kilbride M, Breitbart RE, Chun M, Schonbeck U. Expression of neutrophil collagenase (matrix metalloproteinase-8) in human atheroma: A novel collagenolytic pathway suggested by transcriptional profiling. *Circulation*. 2001;104:1899-1904
8. Aikawa E, Nahrendorf M, Figueiredo J-L, Swirski FK, Shtatland T, Kohler RH, Jaffer FA, Aikawa M, Weissleder R. Osteogenesis associates with inflammation in early-stage atherosclerosis evaluated by molecular imaging in vivo. *Circulation*. 2007;116:2841-2850
9. Jaffer FA, Kim D-E, Quinti L, Tung C-H, Aikawa E, Pande AN, Kohler RH, Shi G-P, Libby P, Weissleder R. Optical visualization of cathepsin k activity in atherosclerosis with a novel, protease-activatable fluorescence sensor. *Circulation*. 2007;115:2292-2298
10. Schafers M, Riemann B, Kopka K, Breyholz H-J, Wagner S, Schafers KP, Law MP, Schober O, Levkau B. Scintigraphic imaging of matrix metalloproteinase activity in the arterial wall in vivo. *Circulation*. 2004;109:2554-2559
11. Deguchi J-o, Aikawa M, Tung C-H, Aikawa E, Kim D-E, Ntziachristos V, Weissleder R, Libby P. Inflammation in atherosclerosis: Visualizing matrix metalloproteinase action in macrophages in vivo. *Circulation*. 2006;114:55-62
12. Herman MP, Sukhova GK, Kisiel W, Foster D, Kehry MR, Libby P, Schönbeck U. Tissue factor pathway inhibitor-2 is a novel inhibitor of matrix metalloproteinases with implications for atherosclerosis. *The Journal of Clinical Investigation*. 2001;107:1117-1126
13. Sukhova GK, Shi GP, Simon DI, Chapman HA, Libby P. Expression of the elastolytic cathepsins s and k in human atheroma and regulation of their production in smooth muscle cells. *The Journal of Clinical Investigation*. 1998;102:576-583
14. Kong Y-Z, Yu X, Tang J-J, Ouyang X, Huang X-R, Fingerle-Rowson G, Bacher M, Scher LA, Bucala R, Lan HY. Macrophage migration inhibitory factor induces mmp-9 expression: Implications for destabilization of human atherosclerotic plaques. *Atherosclerosis*. 2005;178:207-215

15. Bauer S, Jendro M, Wadle A, Kleber S, Stenner F, Dinser R, Reich A, Faccin E, Godde S, Dinges H, Muller-Ladner U, Renner C. Fibroblast activation protein is expressed by rheumatoid myofibroblast-like synoviocytes. *Arthritis Research & Therapy*. 2006;8:R171
16. Edosada CY, Quan C, Wiesmann C, Tran T, Sutherlin D, Reynolds M, Elliott JM, Raab H, Fairbrother W, Wolf BB. Selective inhibition of fibroblast activation protein protease based on dipeptide substrate specificity. *J. Biol. Chem.* 2006;281:7437-7444
17. Park JE, Lenter MC, Zimmermann RN, Garin-Chesa P, Old LJ, Rettig WJ. Fibroblast activation protein, a dual specificity serine protease expressed in reactive human tumor stromal fibroblasts. *Journal of Biological Chemistry*. 1999;274:36505-36512
18. Levy MT, McCaughan GW, Abbott CA, Park JE, Cunningham AM, Müller E, Rettig WJ, Gorrell MD. Fibroblast activation protein: A cell surface dipeptidyl peptidase and gelatinase expressed by stellate cells at the tissue remodelling interface in human cirrhosis. *Hepatology*. 1999;29:1768-1778
19. Aertgeerts K, Levin I, Shi L, Snell GP, Jennings A, Prasad GS, Zhang Y, Kraus ML, Salakian S, Sridhar V, Wijnands R, Tennant MG. Structural and kinetic analysis of the substrate specificity of human fibroblast activation protein α. *Journal of Biological Chemistry*. 2005;280:19441-19444
20. Stary HC, Chandler AB, Dinsmore RE, Fuster V, Glagov S, Insull W, Jr, Rosenfeld ME, Schwartz CJ, Wagner WD, Wissler RW. A definition of advanced types of atherosclerotic lesions and a histological classification of atherosclerosis : A report from the committee on vascular lesions of the council on arteriosclerosis, american heart association. *Circulation*. 1995;92:1355-1374
21. Stary HC, Chandler AB, Dinsmore RE, Fuster V, Glagov S, Insull W, Jr, Rosenfeld ME, Schwartz CJ, Wagner WD, Wissler RW. A definition of advanced types of atherosclerotic lesions and a histological classification of atherosclerosis : A report from the committee on vascular lesions of the council on arteriosclerosis, american heart association. *Arterioscler Thromb Vasc Biol*. 1995;15:1512-1531
22. Rettig WJ, Pilar G-C, Beresford HR, Oettgen HF, Melamed MR, Old LJ. Cell-surface glycoproteins of human sarcomas: Differential expression in normal and malignant tissues and cultured cells. *Proc. Natl. Acad. Sci. USA*. 1988;85:3110-3114
23. Dippold WG, Lloyd KO, Li Lucy TC, Ikeda H, Oettgen HF. Cell surface antigens of human malignant melanoma: Definition of six antigenic systems with mouse monoclonal antibodies. *Proc. Nati. Acad. Sci. USA*. 1980;77:6114-6118
24. Smith PD, McLean KJ, Murphy MA, Wilson Y, Murphy M, Turnley AM, Cook MJ. A brightness-area-product-based protocol for the quantitative assessment of antigen abundance in fluorescent immunohistochemistry. *Brain Research Protocols*. 2005;15:21-29
25. Landmann L, Marbet P. Colocalization analysis yields superior results after image restoration. *Microscopy Research and Technique*. 2004;64:103-112
26. Mosedale D, Metcalfe J, Grainger D. Optimization of immunofluorescence methods by quantitative image analysis. *J. Histochem. Cytochem.* 1996;44:1043-1050
27. Zinchuk V, Zinchuk O, Okada ^{T}. Quantitative colocalization analysis of multicolor confocal immunofluorescence microscopy images: Pushing pixels to explore biological phenomena. *Acta Histochem Cytochem*. 2007;40:101-111
28. Agnati LF, Fuxe K, Torvinen M, Genedani S, Franco R, Watson S, Nussdorfer GG, Leo G, Guidolin D. New methods to evaluate colocalization of fluorophores in immunocytochemical preparations as exemplified by a study on a2a and d2 receptors in chinese hamster ovary cells. *J. Histochem. Cytochem.* 2005;53:941-953
29. Hansson GK. Inflammation, atherosclerosis, and coronary artery disease. *N Engl J Med*. 2005;352:1685-1695

30. Galis ZS, Khatri JJ. Matrix metalloproteinases in vascular remodeling and atherogenesis: The good, the bad, and the ugly. *Circ Res*. 2002;90:251-262
31. Newby AC. Dual role of matrix metalloproteinases (matrixins) in intimal thickening and atherosclerotic plaque rupture. *Physiol. Rev.* 2005;85:1-31
32. Sluijter JPG, Pulskens WPC, Schoneveld AH, Velema E, Strijder CF, Moll F, de Vries J-P, Verheijen J, Hanemaaijer R, de Kleijn DPV, Pasterkamp G. Matrix metalloproteinase 2 is associated with stable and matrix metalloproteinases 8 and 9 with vulnerable carotid atherosclerotic lesions: A study in human endarterectomy specimen pointing to a role for different extracellular matrix metalloproteinase inducer glycosylation forms. *Stroke*. 2006;37:235-239
33. Sukhova GK, Schonbeck U, Rabkin E, Schoen FJ, Poole AR, Billinghurst RC, Libby P. Evidence for increased collagenolysis by interstitial collagenases-1 and -3 in vulnerable human atheromatous plaques. *Circulation*. 1999;99:2503-2509
34. Lutgens SPM, Cleutjens KBJM, Daemen MJAP, Heeneman S. Cathepsin cysteine proteases in cardiovascular disease. *FASEB J.* 2007;21:3029-3041
35. Burke AP, Farb A, Malcom GT, Liang Y-h, Smialek J, Virmani R. Coronary risk factors and plaque morphology in men with coronary disease who died suddenly. *New England Journal of Medicine*. 1997;336:1276-1282
36. Brown DL, Hibbs MS, Kearney M, Loushin C, Isner JM. Identification of 92-kd gelatinase in human coronary atherosclerotic lesions : Association of active enzyme synthesis with unstable angina. *Circulation*. 1995;91:2125-2131
37. Aikawa M, Rabkin E, Sugiyama S, Voglic SJ, Fukumoto Y, Furukawa Y, Shiomi M, Schoen FJ, Libby P. An hmg-coa reductase inhibitor, cerivastatin, suppresses growth of macrophages expressing matrix metalloproteinases and tissue factor in vivo and in vitro. *Circulation*. 2001;103:276-283
38. Spagnoli LG, Bonanno E, Mauriello A, Palmieri G, Partenzi A, Sangiorgi G, Crea F. Multicentric inflammation in epicardial coronary arteries of patients dying of acute myocardial infarction. *J Am Coll Cardiol*. 2002;40:1579-1588
39. Szmitko PE, Wang C-H, Weisel RD, de Almeida JR, Anderson TJ, Verma S. New markers of inflammation and endothelial cell activation: Part i. *Circulation*. 2003;108:1917-1923
40. Skinner MP, Raines EW, Ross R. Dynamic expression of alpha 1 beta 1 and alpha 2 beta 1 integrin receptors by human vascular smooth muscle cells. Alpha 2 beta 1 integrin is required for chemotaxis across type i collagen-coated membranes. *The American Journal of Pathology*. 1994:1070-1081

CHAPTER 4

FAP IS ENHANCED IN ATHEROTHROMBOSIS AND ACCELERATES BLOOD COAGULATION

Based on

Fibroblast Activation Protein is Enhanced in Atherothrombosis and Accelerates Blood Coagulation

Brokopp CE, Nürnberg J, Emmert MY, Weber B, Ackmedov A., Lüscher TF, Renner C, Hoerstrup SP, Matter CM.

Manuscript in Preparation

4.1 ABSTRACT

Background – Fibroblast Activation Protein (FAP) contributes to plaque disruption via its collagenase activity and plays a known role in impaired fibrinolysis. However, the significance of FAP in atherothrombosis and acute coronary syndromes (ACS) remains unknown.

Methods and Results – We detected enhanced FAP expression in occluding human coronary thrombi compared to peripheral blood by immunohistochemistry and RT-PCR (n=6; $p<0.01$). Confocal image analysis revealed FAP expression by thrombus neutrophils. FAP was increased in coronary thrombus neutrophils (n=6; $p<0.01$), compared to peripheral blood neutrophils, but not in monocytes or leukocytes. FAP expression could also be detected in thin-cap coronary fibroatheromata. Acutely formed coronary thrombi showed increased expression of FAP compared to chronic peripheral artery derived thrombi ($p<0.01$). Native rotational thromboelastometry indicated a dose and time-dependant effect of FAP on accelerated blood coagulation and clot thickness.

Conclusions – FAP is expressed by neutrophils during acute coronary thrombus formation. FAP also associates with the endothelium in coronary thin-cap fibroatheromata, and contributes to hyperthrombosis.

4.2 INTRODUCTION

Atherothrombosis is characterized by atherosclerotic lesion disruption superimposed with thrombus formation, and is the primary cause of myocardial infarction. A key trigger of atherothrombosis is disruption of the fibrous cap, which exposes thrombogenic plaque components to the bloodstream. Therefore, atherothrombosis is governed by factors involved in both plaque rupture and blood coagulation.

While collagenases play a hallmark role in fibrous cap destabilization and plaque rupture, they do not directly contribute a hyperthrombogenic state in the blood.[1-4] Atherosclerotic plaque-derived factors involved in systemic hyperthrombosis have therefore also drawn attention, particularly in cases of atherothrombosis due to superficial intimal erosion. Circulating tissue factor for example has been associated with increased blood thrombogenicity in patients with unstable angina.[5] However the role of tissue factor in atherosclerotic plaque rupture and superficial intimal erosion *per se* is minimal. Still, proteases which promote plaque rupture while simultaneously accelerating blood thrombosis may hold potential as diagnostic and therapeutic targets.

Fibroblast activation protein (FAP) is a constitutively active serine protease that associates with thin-cap coronary fibroatheromata. FAP contributes to fibrous cap destabilization via its collagenolytic activity, and also to hyperthrombosis via activation of α_2-Antiplasmin; a coagulation factor which inhibits plasmin-mediated thrombolysis.[6, 7] The aim of this study was to characterize FAP expression in human coronary atherothrombosis and to also determine the causal role of FAP in accelerated blood coagulation.

4.3 METHODS

4.3.1 THROMBUS AND PERIPHERAL BLOOD SPECIMENS

Thrombi from the coronary and femoral arteries were aspirated from patients who suffered a myocardial infarction or peripheral artery occlusive disease, respectively. 5mL of peripheral blood was

drawn from each patient into the citrated tube prior to thrombus aspiration. The thrombi and blood specimens were placed in phosphate buffered saline and transferred to the laboratory for immediate processing. Thrombi analyzed by immunohistochemistry were fixed for 24hr in formalin, specimens for immunohistochemistry were embedded for cryosectioning and frozen @ -80°C, and specimens for RT-PCR analysis were snap frozen.

4.3.2 IMMUNOHISTOCHEMISTRY

Cross sections from human paraffin-embedded thrombi and peripheral blood sections (4 µm thickness) of coronary plaques were mounted on glass slides. Antigen retrieval in paraffin-embedded sections of coronary thrombi and peripheral blood was performed after 20 min incubation in 95°C retrieval buffer (2 mM Sodium Citrate, pH 7.6). FAP was stained using a rabbit polyclonal antibody raised against the catalytic insert of FAP (A246; Ab28246; Abcam, Cambridge, MA) and a rabbit isotype control (Ab37415; Abcam). CD31 was stained using a mouse monoclonal antibody (303108; Biolegend) and matching isotype control (400123; Biolegend). Primary antibodies were detected with biotin-labeled goat anti-mouse (115-066-003; Jackson ImmunoResearch, West Grove, PA) and biotin-labeled goat anti-rabbit (111-066-003; Jackson ImmunoResearch) and stained using an ABC staining kit (Vector Labs, Burlingame, CA).

4.3.3 REAL-TIME POLYMERASE CHAIN REACTION

Thrombi and peripheral blood were lysed in RLT buffer, and total RNA was isolated using an RNeasy Mini kit (Qiagen). Total RNA was reverse transcribed using random hexamers and MultiScribe reverse transcriptase (Applied Biosystems). Non–reverse-transcribed samples were used as negative controls. Single-reporter real-time PCR was performed using the ABI Prism 7700 Sequence Detection system (Applied Biosystems). The primer sequence for FAP was forward 5'-CAAGAA-TGT-TTC-GGT-CCT-GT-3' and reverse 5'-GTC-TGCCAG-TCT-TCC-CTG-AA-3'. Eukaryotic 18S ribosomal RNA, measured with a predeveloped primer/probe system (Applied Biosystems), served as endogenous controls for relative quantification.

4.3.4 IMMUNOFLUORESCENCE

Cryosections of aortic plaques were fixed in ice-cold acetone for 5 min and stained using a mouse monoclonal against FAP (F19, Provided by Sloan-Kettering Institute, New York, NY) and the appropriate mouse isotype control (401401; BioLegend, San Diego, CA).[8, 9] F19 was then labeled with a Cy5 goat anti-mouse IgG (115-175-146; Jackson ImmunoResearch). Sections were then washed in PBS and stained for granulocytes, monocytes, and T-Lymphocytes with a FITC-labelled mouse antibodies directed against CD66b (555724, BD Pharmingen), CD14 (555397, BD Pharmingen), CD3 (555332, BD Pharmingen). Non-specific staining was addressed using a FITC labeled mouse isotype control (555748, BD Pharmingen) antibody. DAPI (D9542; Sigma-Aldrich) was used for fluorescent counterstaining of nuclei. Isotype control antibodies were used to address antigen-binding specificity. Stained samples were cover-slipped with Tris-buffered glycerol (a 3:7 mixture of 0.1 M Tris-HCl at pH 9.5 and glycerol supplemented with 50 mg/mL *n*-propyl-gallate). Colocalization analyses were performed using a multichannel confocal microscope (TCS SP2, Leica) on a single optical plane**.**

4.3.5 NATIVE THROMBOELASTOMETRY

Peripheral blood was harvested from healthy probands into citrate collection tubes. All healthy probands were shown to have plasma FAP levels of less than 5ng/mL by ELISA. Recombinant human FAP (Enzo, BML-SE409) was diluted into sterile saline and added to proband blood such that the final concentration of rhuFAP in the blood was 0, 0.175, 1.75, and 3.5µg/mL of blood. NATAM (Axon Lab, Baden-Dättwil, Switzerland) analysis was performed according to the manufacturer's instructions by using STAR-TEM reagent after incubation times of 0, 2.5, and 5hrs before beginning the analysis. All analyses were performed on the same machine.

4.3.6 FLOW CYTOMETRY

Peripheral blood (1mL) and thrombi were placed into 1mL of Acutase with 50 µL Actilyse, and shaken gently at 37°C for 1 hr. Cell aggregates were further dissociated by sifting through a cell strainer (40µm pore size) using the soft rubber from a syringe. Both samples were then spun at 400 G for 5 min and the supernatant removed. Cell pellets were then resuspended in FACS buffer (PBS with 1% FCS and 5 mM EDTA) with 1 µg/mL for Fc receptor blocking agent and incubated for 30 min at 4°C. Cells were subsequently labeled with fluorescently tagged antibodies presented in Table 1, and in the combinations presented in Table 2. Representative cell population gatings and histograms are shown in Figures 42-48.

Antigen	Label	Source
CD66b	FITC	555724 BD Pharmingen
CD45	PER-CP	345809 BD Pharmingen
CD14	FITC	555397 BD Pharmingen
CD125	PE	555902 BD Pharmingen
CD3	FITC	555332 BD Pharmingen
FAP	Alexa 647	ATCC-CRL-2733
IgG control	Alexa 647	557783 BD Pharmingen

Table 1. Antibodies used for flow cytometry.

Cell Population	Stainings
T (thymus) Cells	CD3+ CD45+
Granulocytes	CD66b+ CD45+
Eosinophils	CD66b+ CD125+ SSC (side scatter) high CD45+
Neutrophils	CD66b+ CD125- SSC high CD45+
Basophils	CD66b+ CD125- SSC low CD45+
Monocytes	CD14 low and high CD45+

Table 2. Antibody profiles for cell population gating.

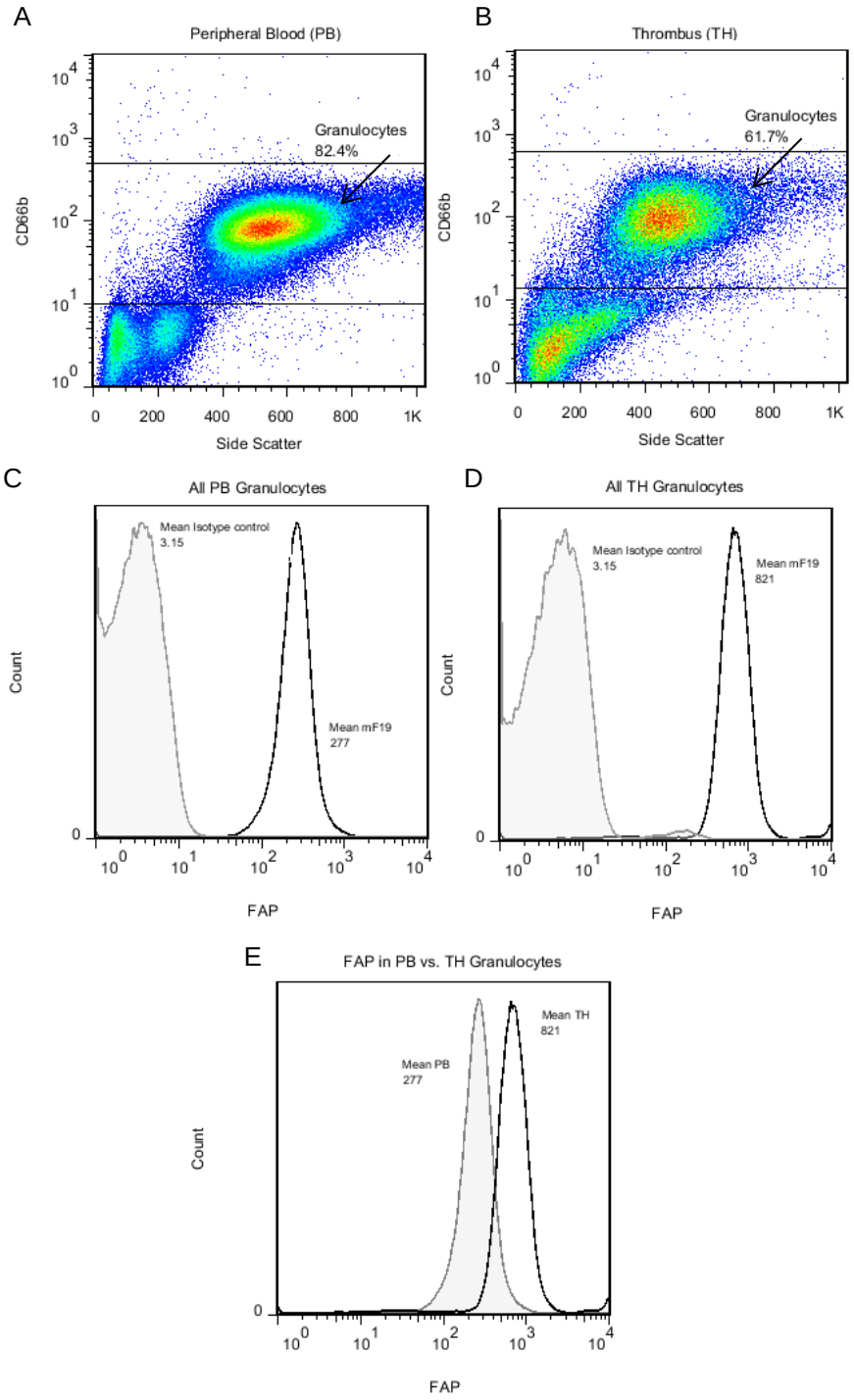

Figure 42. Representative granulocyte gating for cell population-associated FAP expression, illustrates enhanced FAP expression in granulocytes. Granulocytes are first gated by CD66b expression and side scatter in peripheral blood (A) and thrombi specimens (B). C. Granulocyte-specific FAP expression is quantified as the mean fluorescent intensity from the histogram generated by F19 (black) and a matching isotype control antibody (grey) stainings in both peripheral blood (C) and thrombi (D). E. The increase of granulocyte-specific FAP expression is shown by the change of mean fluorescent intensity between peripheral blood (grey) and thrombi (black).

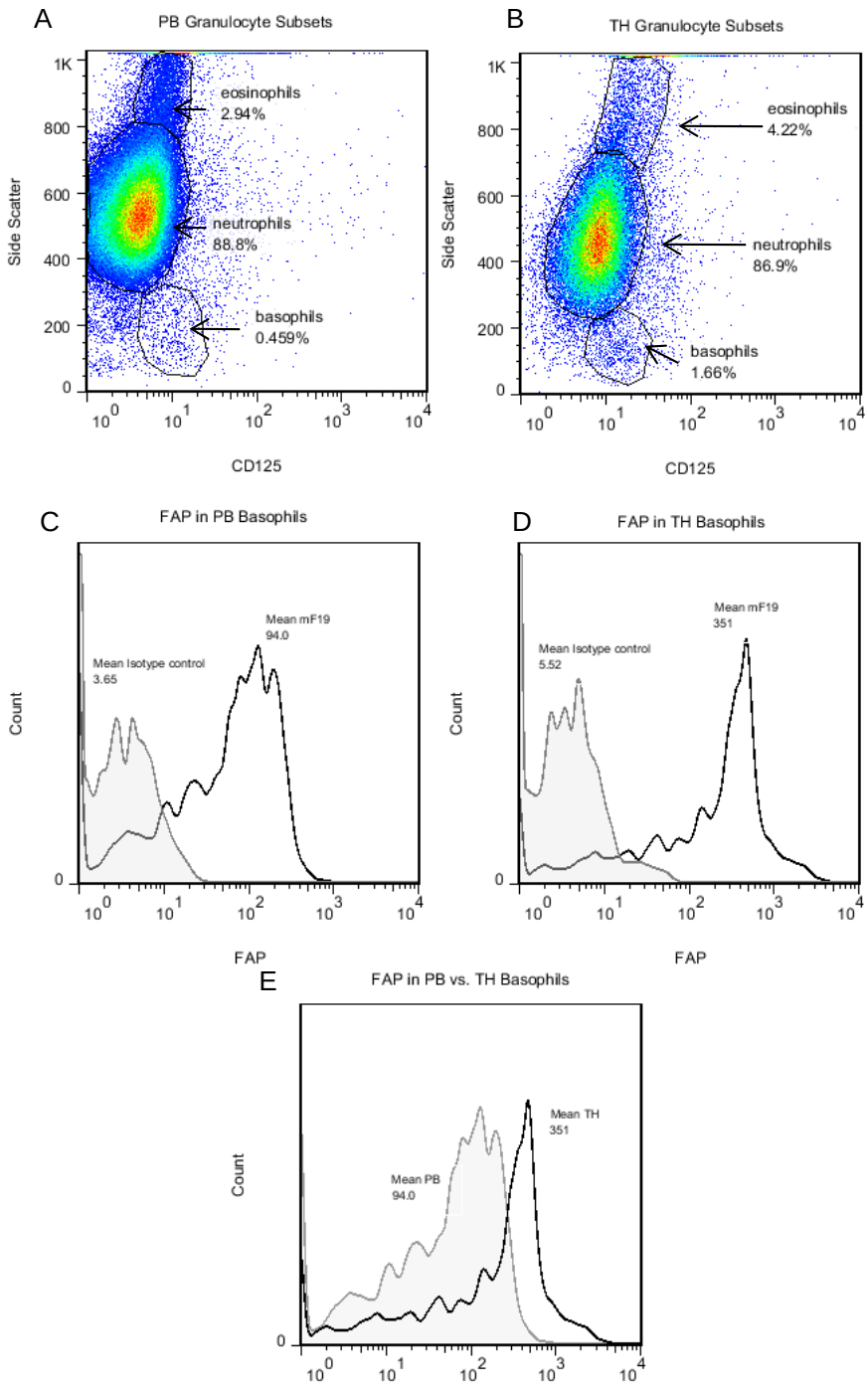

Figure 43. Representative granulocyte subset gating for cell sub-population-associated FAP expression illustrates enhanced FAP expression in thrombus basophils. Granulocytes pre-gated by CD66b/side scatter, are further gated into granulocyte subsets by CD125 and side scatter in peripheral blood (A) and thrombus specimens (B). Basophil-specific FAP expression is quantified as the mean fluorescent intensity from the histogram generated by FAP-specific staining (black) and a matching isotype control antibody (grey) for both peripheral blood (C) and thrombi (D). E. The increase of basophil-specific FAP is shown by the change of mean fluorescent intensity of peripheral blood (grey) vs. thrombi (black).

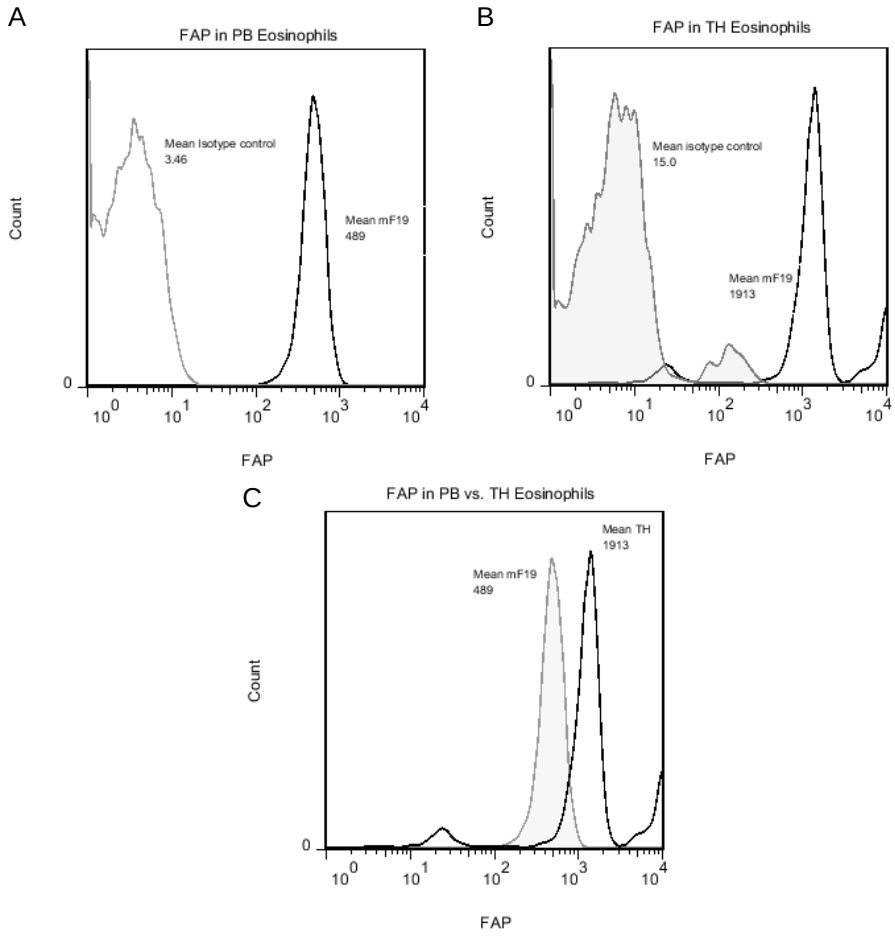

Figure 44. Eosinophil-associated FAP expression is enhanced in peripheral blood (PB) vs. coronary (TH) thrombi. FAP expression in eosinophils pre-gated by side scatter and CD125 (Figure 43), is quantified as the mean fluorescent intensity from the histogram generated by FAP-specific antibody F19 (black) and a matching isotype control antibody (grey) for both peripheral blood (A) and thrombi (B). C. The increase of eosinophil-specific FAP expression is shown by the change of mean fluorescent intensity of the F19 histogram for peripheral blood (grey) and thrombi (black).

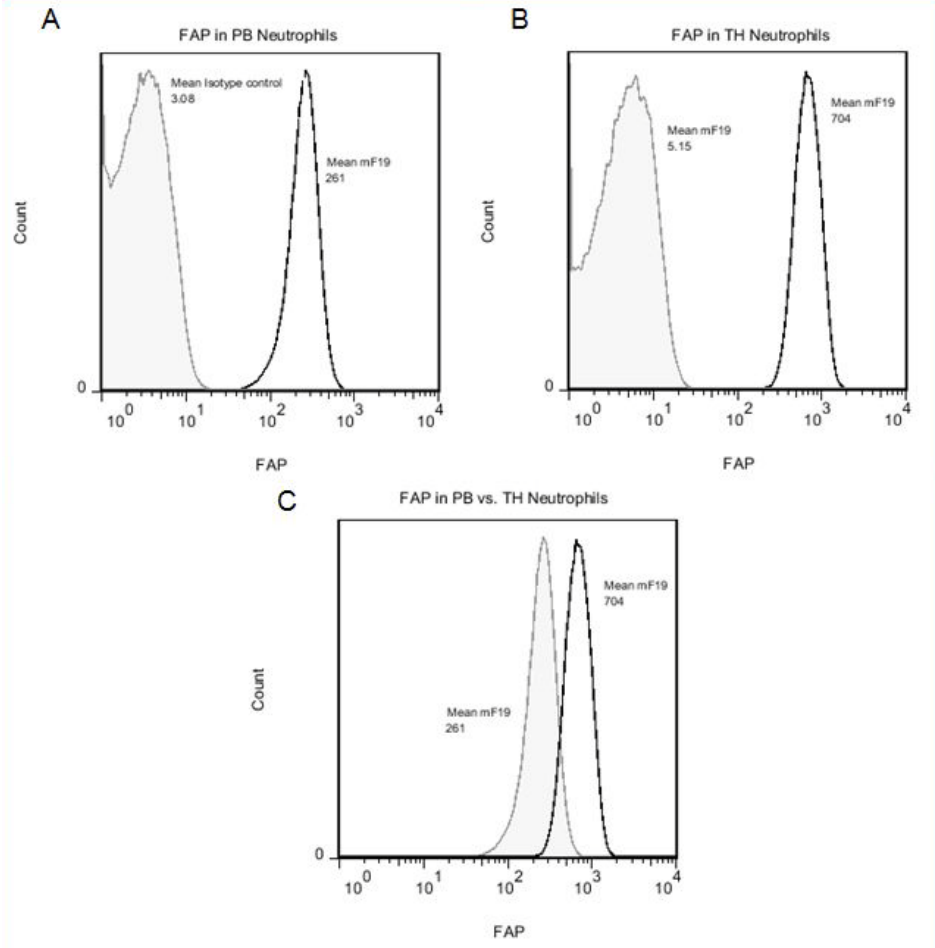

Figure 45. Neutrophil-associated FAP expression is enhanced in peripheral blood (PB) vs. coronary thrombi (TH). A-B. FAP expression in neutrophils pre-gated by side scatter and CD125 (Figure 43) is quantified as the change in mean fluorescent intensity generated by FAP-specific F19 (black) and a matching isotype control antibody (grey) for both peripheral blood (A) and coronary thrombi (B). C. The increase of neutrophil-specific FAP binding is shown by the change of mean fluorescent intensity for F19 binding in peripheral blood (grey) and coronary thrombi (black).

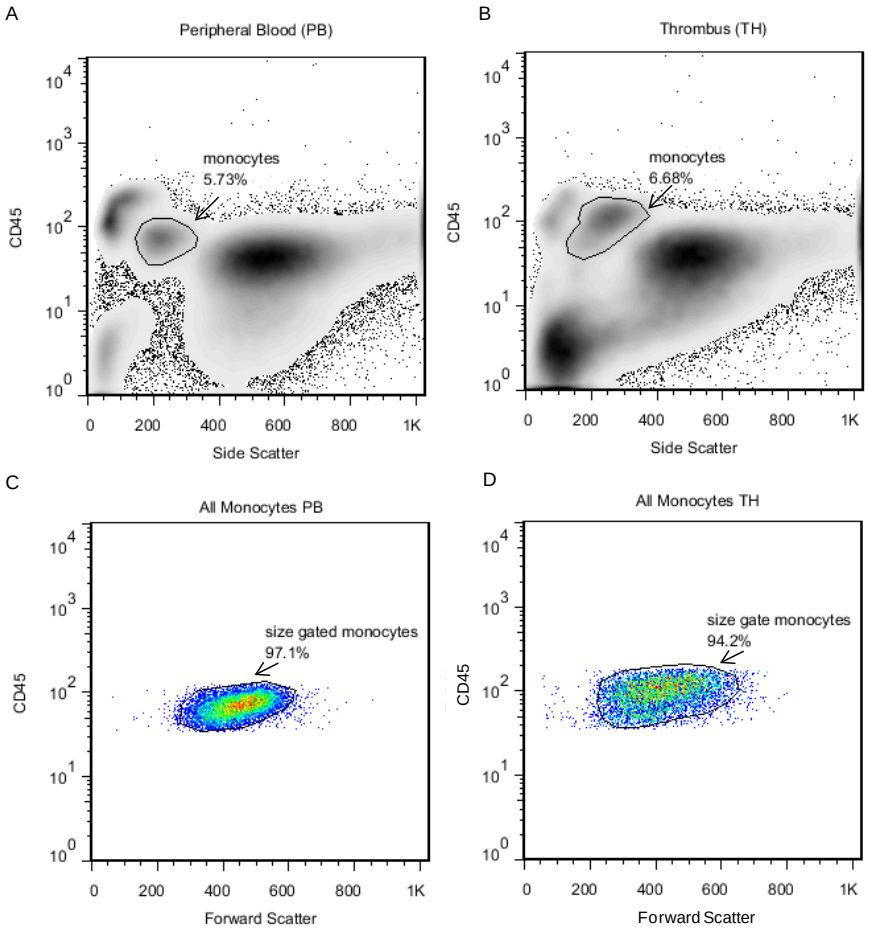

Figure 46. Representative monocyte gating for cell population-associated FAP protein expression. Monocytes are first gated by CD45 expression and side scatter in peripheral blood (A) and thrombi specimens (B) and then by CD45 expression and size (Forward Scatter; C-D).

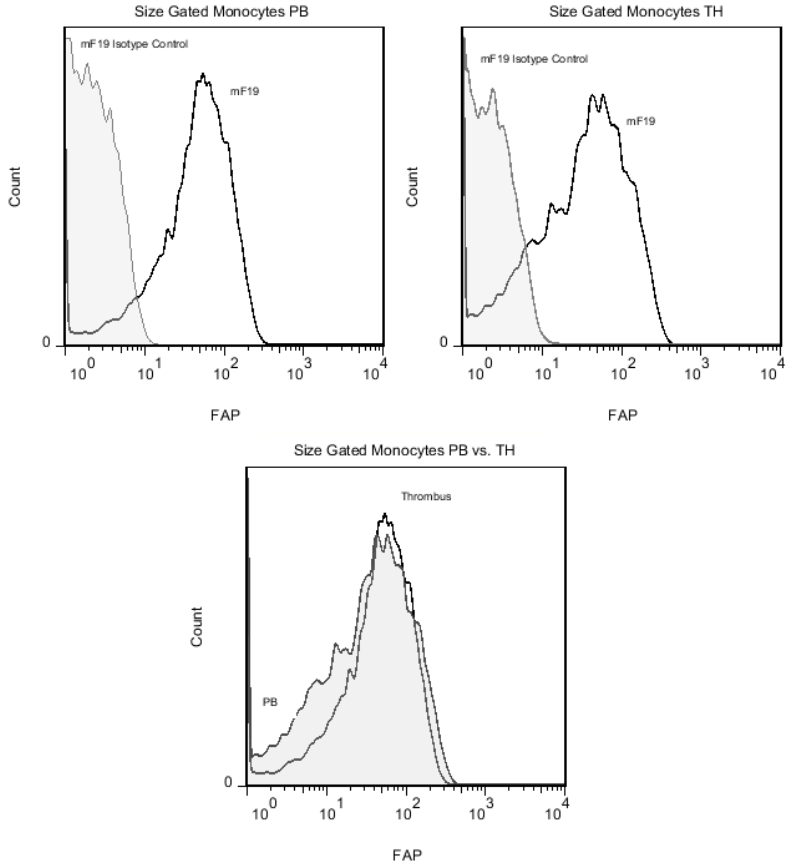

Figure 47. Monocyte-associated FAP expression is unchanged in peripheral blood (PB) vs. coronary thrombi (TH). FAP expression in monocytes is quantified as the mean fluorescent intensity from the histogram of F19 binding (black) and a matching isotype control antibody (grey) for both peripheral blood (A) and thrombi (B). C. The monocyte-specific FAP expression in thrombi is shown by the change of mean fluorescent intensity of F19 staining in peripheral blood (grey) vs. thrombi (black).

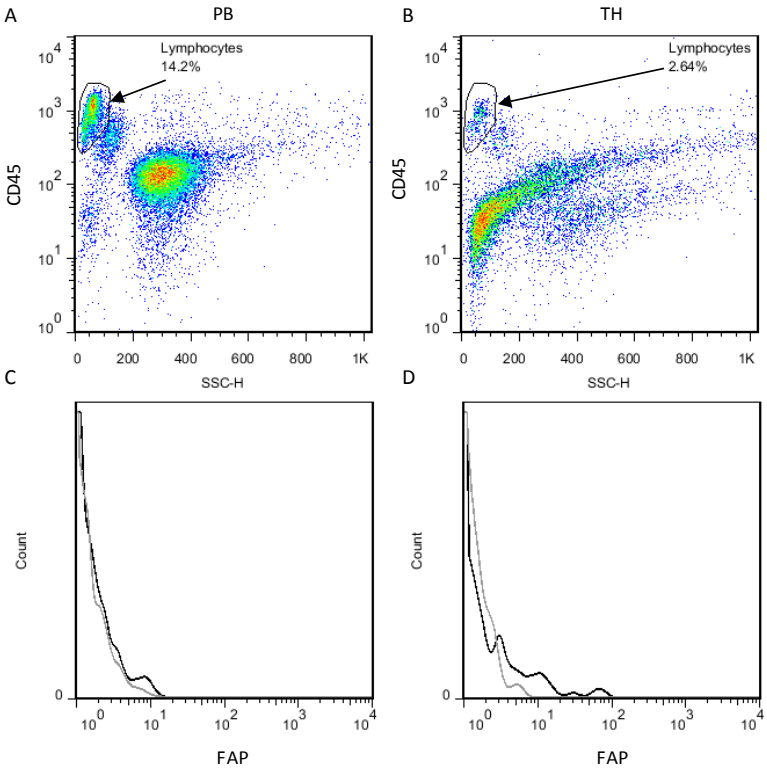

Figure 48. Lymphocyte-associated FAP expression is unchanged in peripheral blood (PB) vs. coronary thrombi (TH). FAP binding in lymphocytes pre-gated by side scatter (SSC-H) and CD45 in peripheral blood and matching thrombus is quantified as the mean fluorescent intensity from the histogram generated by F19 (black) and a matching isotype control antibody (grey) for both peripheral blood (A) and thrombi (B). The increase of lymphocyte-specific FAP expression is shown by the change of mean fluorescent intensity between FAP-specific F19 binding (black) and an isotype control antibody (grey) for peripheral blood (C) and thrombi (D).

4.4 RESULTS

4.4.1 FAP EXPRESSION IS ENHANCED IN HUMAN CORONARY THROMBI

Immunohistochemical stainings for FAP in adjacent paraffin-embedded sections reveal enhanced FAP expression in human coronary thrombi vs. peripheral blood (**Figure 49A**). Positive staining for FAP is virtually absent in peripheral blood, and FAP mRNA is increased in coronary thrombi by RT-PCR analysis (**Figure 49B**).

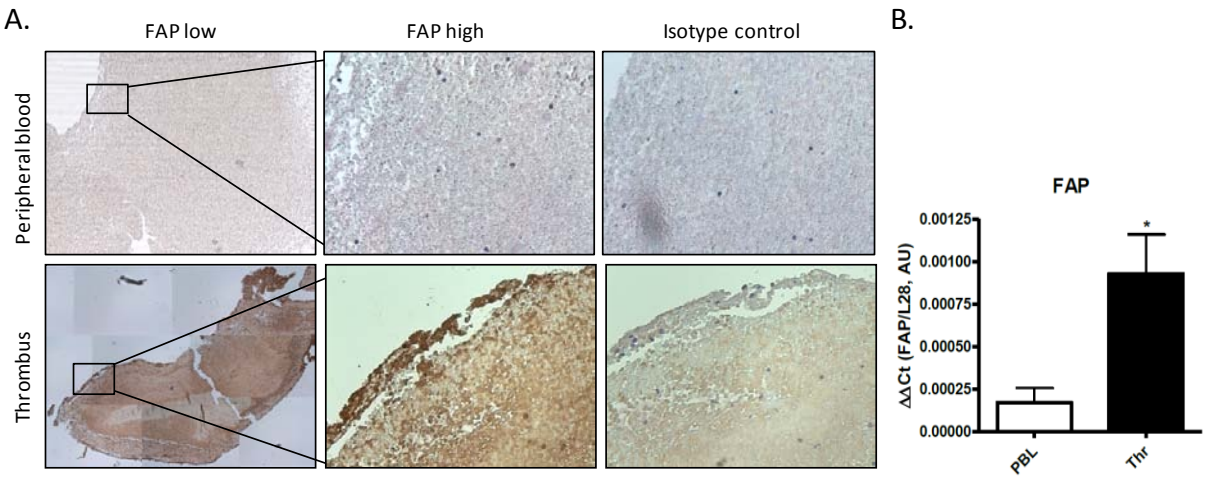

Figure 49. FAP is enhanced in human coronary thrombi vs. peripheral blood in STEMI patients. A. Representative immunohistological stainings illustrate enhanced FAP in coronary thrombi vs. peripheral blood. **B.** FAP mRNA is enhanced in coronary thrombi (Thr) vs. peripheral blood leukocytes (PBL). (* = $p < 0.05$, n=6)

4.4.2 FAP IS EXPRESSED BY GRANULOCYTES IN HUMAN CORONARY THROMBI

To characterize FAP-expressing cell types in human thrombi, we performed immunofluorescent co-stainings of FAP in monocytes/macrophages (identified as CD14-positive cells), granulocytes (CD68-positive cells), and T-Lymphocytes (CD3-positive cells). Confocal image analyses revealed FAP expression by granulocytes, but not by macrophages or endothelial cells (**Figure 50**).

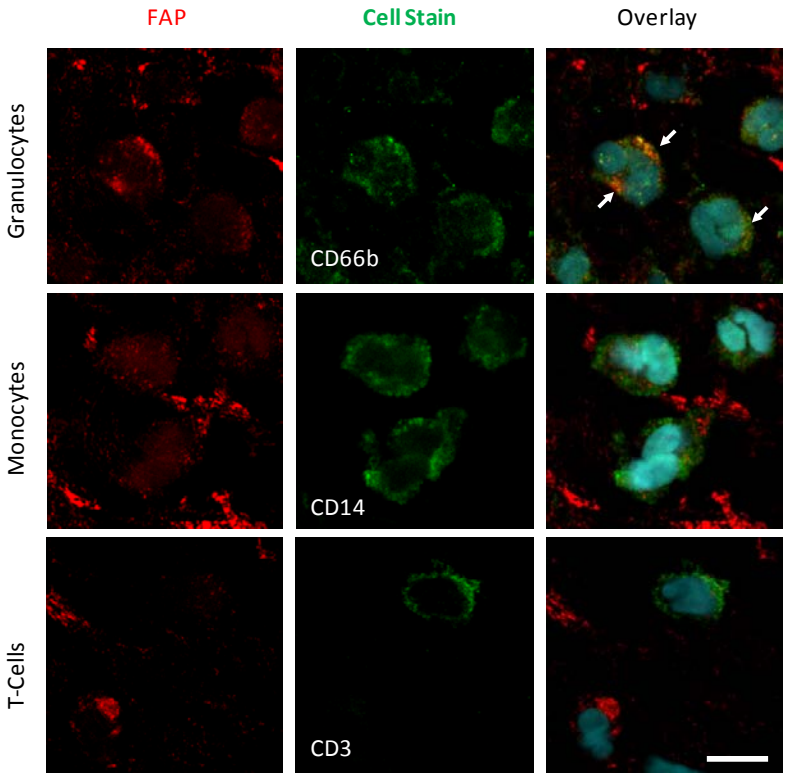

Figure 50. FAP expression in human coronary thrombi colocalizes with granulocytes, but not with monocytes/macrophages or T-cells. Overlays of confocal images of FAP (red) and DAPI (blue) with cell-specific stainings of CD66b, CD14, and CD3 (green) in representative cryosections of human coronary thrombi illustrate FAP colocalization (arrows) with granulocytes (bar=5 µm).

4.4.3 FAP EXPRESSION IS INCREASED IN CORONARY THROMBUS NEUTROPHILS

We used flow cytometry to quantify FAP expression in human peripheral blood vs. thrombus leukocyte cell populations including; monocytes, T-Cells, granulocytes, neutrophils, eosinophils, and basophils. Quantitative analyses revealed enhanced FAP expression in thrombus granulocytes and neutrophils, but in none of the other analyzed cell populations (**Figure 51**).

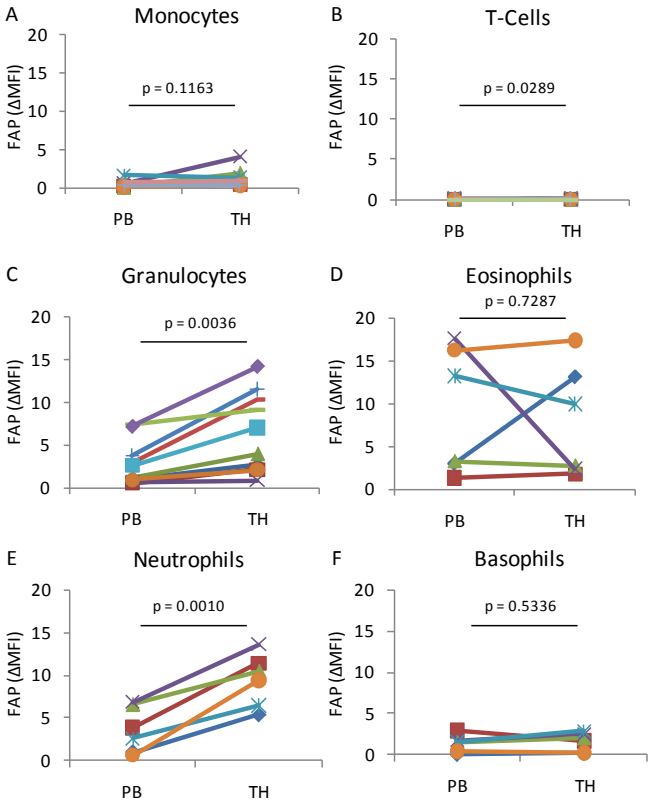

Figure 51. FAP expression is enhanced in thrombus neutrophils and granulocytes in STEMI patients suffering myocardial infarction. FAP expression is quantified in peripheral blood (PB) vs. coronary thrombus (TH) derived monocytes (A), T-Cells (B), and granulocytes (C), eosinophils (D), neutrophils (E), and basophils (F). FAP is enhanced in thrombus all granulocytes and in the neutrophil sub-population.

4.4.4 NEUTROPHIL-SPECIFIC FAP EXPRESSION IS ENHANCED IN STEMI BUT NOT PAOD PATIENTS

To access whether neutrophil-specific FAP expression associates with acute atherothrombosis, we used flow cytometry to quantify FAP expression in peripheral blood and occluding thrombi from patients suffering from STEMI (coronary artery thrombi) and PAOD (femoral artery thrombi). Acutely formed coronary thrombi showed increased expression of FAP compared to chronic peripheral artery derived thrombi (**Figure 52**).

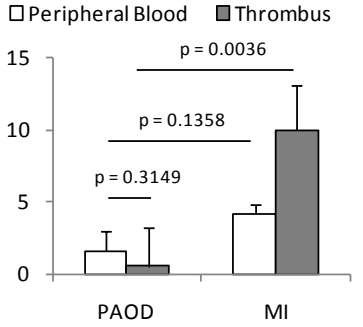

Figure 52. Neutrophil FAP expression is enhanced in acute, but not chronic atherothrombosis. Neutrophil FAP expression is enhanced in peripheral blood (white bar) and occluding thrombi (grey bar) from patients with myocardial infarction (MI, n=9) compared to patients with peripheral artery occlusive disease (PAOD, n=5).

4.4.5 FAP IS EXPRESSED IN THE ENDOTHELIUM OF HUMAN CORONARY THIN-CAP FIBROATHEROMATA

In order to determine FAP expression in the endothelium of human coronary fibrous caps, we stained H&E stainings in rupture-prone human coronary arteries obtained from patients that died after myocardial infarction and healthy internal mammary arteries as control. Immunohistological stainings revealed FAP expression in the fibroatheromata endothelium (**Figure 53)**.

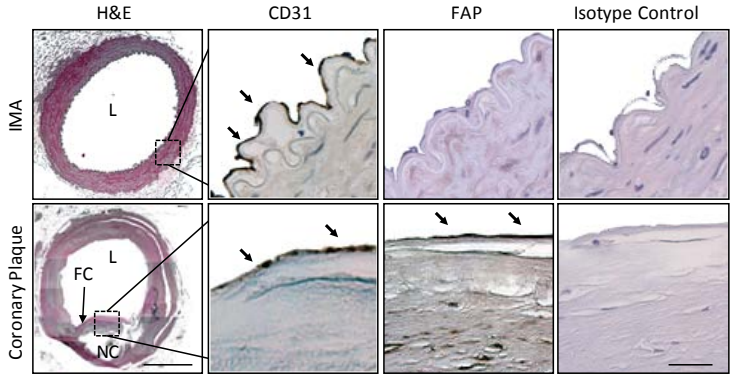

Figure 53. FAP is expressed in the endothelium of human thin-cap coronary fibroatheromata. H&E staining shows an internal mammary artery and a thin-cap coronary fibroatheromata (L=lumen, FC=fibrous cap, NC=necrotric core; bar=1mm). FAP and CD31 immunohistochemistry (bar = 50µm) shows FAP expression in the endothelium (arrows). Dotted boxes indicate regions of interest in adjacent sections at high magnification, and stainings with isotype control antibodies are shown.

4.4.6 FAP Accelerates Human Blood Coagulation and Increases Clot Thickness

To determine the role of FAP in accelerated blood coagulation and clot thickness, healthy human blood was treated with 1.75µg/mL recombinant FAP with the optimal dosage (1.75µg/mL) for the optimal incubation time (5hr). FAP was found to accelerate blood clotting time and clot formation compared to a vehicle control, time while increasing the alpha angle and maximum clot firmness by NATEM (**Figure 54**).

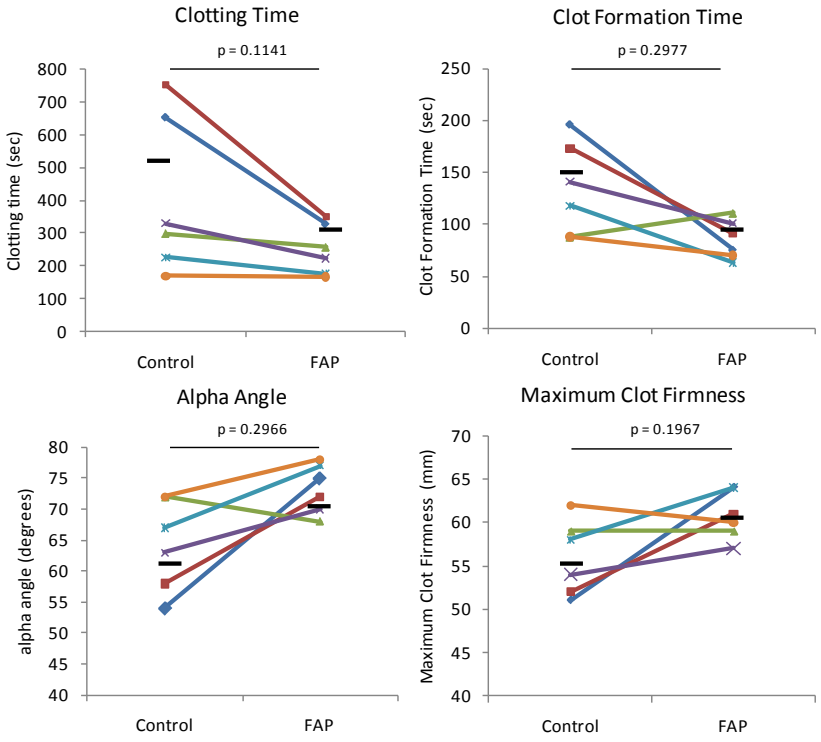

Figure 54. FAP accelerates blood clotting time and clot formation time while increasing the alpha angle and maximum clot firmness by NATEM analysis. Absolute clotting time and clot formation time decreased in 5/6 probands, alpha angle increased in 5/6 patients, and maximum clot thickness increased in 4/6 probands when conditioned with 1.75ug/mL of FAP at 5hr incubation compared to vehicle treated control. Averages are shown indicated by the black line.

4.4.7 FAP PROMOTES BLOOD COAGUATION IN A DOSE AND TIME-DEPENDANT MANNER

To determine a causal role of FAP in thrombus formation, the dose and time-dependant effects of recombinant human FAP on healthy human blood coagulation was assessed ex-vivo by NATEM analysis. The effect of FAP was both time and dose dependant (**Figure 55**).

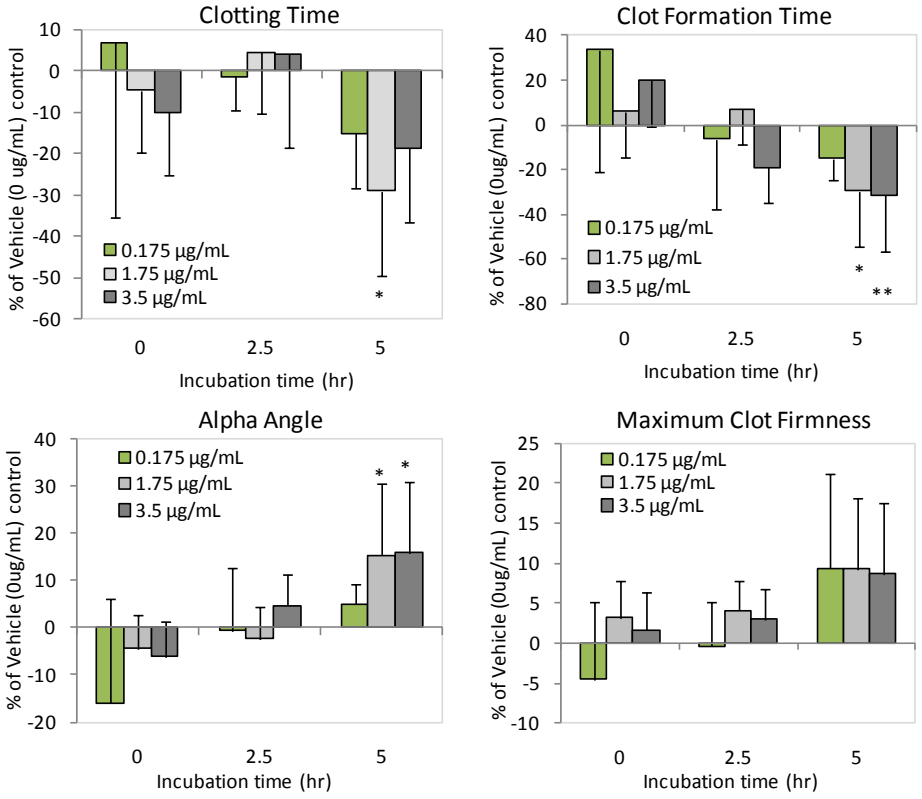

Figure 55. FAP promotes blood coagulation in a time and dose-dependent manner ex-vivo by NATEM. Blood from healthy probands (n=6) was conditioned with recombinant human FAP at 0.175 (green), 1.75 (grey), and 3.5 µg/mL (black) for 0, 2.5, 5hr incubation. Average values and standard deviations compared to unconditioned controls 0µg/mL are shown (*, $p<0.05$; **, $p<0.01$, Student's T-test).

4.5 DISCUSSION

Atherothrombosis is caused by plaque disruption via fibrous cap rupture and also by superficial erosion of the intima. The severity of the thrombotic complications is governed by both the thrombotic components of the disrupted plaque, and also the systemic thrombogenic state of the blood.

This study links the constitutively active serine protease FAP to coronary atherothrombosis and provides evidence that: (1) FAP is enhanced in occlusive coronary thrombi, (2) FAP is expressed by neutrophils during acute thrombus formation, (3) FAP is expressed in the endothelium of thin-cap fibroatheromata, (4) FAP accelerates blood coagulation and clot thickness.

Numerous studies implicate elevated systemic levels of plaque-derived prothrombogenic factors such as tissue factor, von Willebrand factor, and factor VIII in atherothrombosis.[10, 11] However, these hallmark coagulation factors play no known role in plaque destabilization and fibrous cap rupture. FAP expression was particularly enhanced in the endothelium of thin-cap coronary fibroatheromata and in coronary thrombus neutrophils. Moreover, FAP was shown to accelerate blood coagulation. Taken together, our findings provide evidence that FAP is the first known collagenase contributing to both plaque destabilization and atherothrombosis. These observations underline the potential clinical relevance of FAP and a diagnostic and/or therapeutic target in patients with advanced atherosclerotic plaques.

Neutrophil levels have also been shown to associate with future cardiovascular events.[12] However, the causal role of neutrophils in atherothrombosis remains largely conjectural. In rupture-prone carotid plaque, neutrophils have been shown to release destabilizing proteases, and associate with intraplaque hemorrhage.[13] Recent work by *Massberg et al* also identifies a role of neutrophils in thrombosis via releasing neutrophil serine proteases, which degrade the anticoagulant tissue-factor pathway inhibitor (TFPI), thereby enhancing coagulation and thrombus formation.[14] Our findings show further contribution of neutrophils to atherothrombosis via expression of FAP, and thereby adds to this growing body of evidence which supports the notion of neutrophil involvement in atherothrombosis.

We also found constitutive FAP expression in endothelial cells of thin-cap fibroatheromata. Endothelial activation dysfunction plays a central role in atherothrombosis.[15] Activated endothelial cells express fibrous cap-degrading collagenases, and have also been shown to act in concert with fibrous cap-degrading smooth muscle cells.[16-18] FAP expression in the endothelium of thin capped fibroatheromata may indicate a role of FAP in superficial intimal erosion. Moreover FAP expression in the endothelium may indicate its long-term interaction with blood, which could promote a chronic hyperthrombogenic state.

Taken together, we found that FAP expression is enhanced in human coronary thrombi, and in the endothelium of thin-cap coronary fibroatheromata. FAP was also found to and accelerate blood coagulation. Thus, FAP expression in thin-cap coronary plaques and coronary thrombi renders it an attractive diagnostic target for further investigation in patients with ACS. Along this line, the ability of FAP to accelerate blood coagulation may also draw attention to its potential as a therapeutic target. We now aim to investigate the effect of FAP in atherothrombosis *in vivo* via genetic and pharmacological modulation, and to also investigate the mechanism of FAP induction in both endothelial cells and neutrophils. On a clinical level, associations of soluble FAP levels to inflammatory diseases such as rheumatoid arthritis and chronic liver disease may shed light on its potential clinical use as a diagnostic biomarker.

4.6 ACKNOWLEDGEMENTS

We thank Ursula Steckholzer for help in preparation of the tissue specimens. This work was supported by grants from the Swiss National Science Foundation, the Herzog-Egli Foundation, and the Hartmann Müller Foundation at the University of Zürich. Further support was provided by the Special Program University Medicine (SPUM) by the Swiss National Science Foundation

4.7 REFERENCES

1. Aikawa E, Nahrendorf M, Figueiredo J-L, Swirski FK, Shtatland T, Kohler RH, Jaffer FA, Aikawa M, Weissleder R. Osteogenesis associates with inflammation in early-stage atherosclerosis evaluated by molecular imaging in vivo. *Circulation*. 2007;116:2841-2850
2. Jaffer FA, Kim D-E, Quinti L, Tung C-H, Aikawa E, Pande AN, Kohler RH, Shi G-P, Libby P, Weissleder R. Optical visualization of cathepsin k activity in atherosclerosis with a novel, protease-activatable fluorescence sensor. *Circulation*. 2007;115:2292-2298
3. Schafers M, Riemann B, Kopka K, Breyholz H-J, Wagner S, Schafers KP, Law MP, Schober O, Levkau B. Scintigraphic imaging of matrix metalloproteinase activity in the arterial wall in vivo. *Circulation*. 2004;109:2554-2559
4. Deguchi J-o, Aikawa M, Tung C-H, Aikawa E, Kim D-E, Ntziachristos V, Weissleder R, Libby P. Inflammation in atherosclerosis: Visualizing matrix metalloproteinase action in macrophages in vivo. *Circulation*. 2006;114:55-62
5. Kaikita K, Ogawa H, Yasue H, Takeya M, Takahashi K, Saito T, Hayasaki K, Horiuchi K, Takizawa A, Kamikubo Y, Nakamura S. Tissue factor expression on macrophages in coronary plaques in patients with unstable angina. *Arterioscler Thromb Vasc Biol*. 1997;17:2232-2237
6. Lee KN, Jackson KW, Christiansen VJ, Chung KH, McKee PA. A novel plasma proteinase potentiates {alpha}2-antiplasmin inhibition of fibrin digestion. *Blood*. 2004;103:3783-3788
7. Lee KN, Jackson KW, Christiansen VJ, Lee CS, Chun J-G, McKee PA. Antiplasmin-cleaving enzyme is a soluble form of fibroblast activation protein. *Blood*. 2006;107:1397-1404
8. Rettig WJ, Pilar G-C, Beresford HR, Oettgen HF, Melamed MR, Old LJ. Cell-surface glycoproteins of human sarcomas: Differential expression in normal and malignant tissues and cultured cells. *Proc. Natl. Acad. Sci. USA*. 1988;85:3110-3114
9. Dippold WG, Lloyd KO, Li Lucy TC, Ikeda H, Oettgen HF. Cell surface antigens of human malignant melanoma: Definition of six antigenic systems with mouse monoclonal antibodies. *Proc. Nati. Acad. Sci. USA*. 1980;77:6114-6118
10. Davì G, Patrono C. Platelet activation and atherothrombosis. *New England Journal of Medicine*. 2007;357:2482-2494
11. Folsom AR. Hemostatic risk factors for atherothrombotic disease: An epidemiologic view. *Thromb Haemost*. 2001;86:366-373
12. Haumer M, Amighi J, Exner M, Mlekusch W, Sabeti S, Schlager O, Schwarzinger I, Wagner O, Minar E, Schillinger M. Association of neutrophils and future cardiovascular events in patients with peripheral artery disease. *Journal of Vascular Surgery*. 2005;41:610-617
13. Leclercq A, Houard X, Philippe M, Ollivier V, Sebbag U, Meilhac O, Michel J-B. Involvement of intraplaque hemorrhage in atherothrombosis evolution via neutrophil protease enrichment. *Journal of Leukocyte Biology*. 2007;82:1420-1429
14. Massberg S, Grahl L, von Bruehl M-L, Manukyan D, Pfeiler S, Goosmann C, Brinkmann V, Lorenz M, Bidzhekov K, Khandagale AB, Konrad I, Kennerknecht E, Reges K, Holdenrieder S, Braun S,

Reinhardt C, Spannagl M, Preissner KT, Engelmann B. Reciprocal coupling of coagulation and innate immunity via neutrophil serine proteases. *Nat Med*. 2010;16:887-896

15. Szmitko PE, Wang C-H, Weisel RD, de Almeida JR, Anderson TJ, Verma S. New markers of inflammation and endothelial cell activation: Part i. *Circulation*. 2003;108:1917-1923
16. Rajavashisth TB, Xu X-P, Jovinge S, Meisel S, Xu X-O, Chai N-N, Fishbein MC, Kaul S, Cercek B, Sharifi B, Shah PK. Membrane type 1 matrix metalloproteinase expression in human atherosclerotic plaques. *Circulation*. 1999;99:3103-3109
17. Skinner MP, Raines EW, Ross R. Dynamic expression of alpha 1 beta 1 and alpha 2 beta 1 integrin receptors by human vascular smooth muscle cells. Alpha 2 beta 1 integrin is required for chemotaxis across type i collagen-coated membranes. *The American Journal of Pathology*. 1994:1070-1081
18. Sluijter JPG, Pulskens WPC, Schoneveld AH, Velema E, Strijder CF, Moll F, de Vries J-P, Verheijen J, Hanemaaijer R, de Kleijn DPV, Pasterkamp G. Matrix metalloproteinase 2 is associated with stable and matrix metalloproteinases 8 and 9 with vulnerable carotid atherosclerotic lesions: A study in human endarterectomy specimen pointing to a role for different extracellular matrix metalloproteinase inducer glycosylation forms. *Stroke*. 2006;37:235-239
19. Sukhova GK, Shi GP, Simon DI, Chapman HA, Libby P. Expression of the elastolytic cathepsins s and k in human atheroma and regulation of their production in smooth muscle cells. *The Journal of Clinical Investigation*. 1998;102:576-583
20. Lutgens SPM, Cleutjens KBJM, Daemen MJAP, Heeneman S. Cathepsin cysteine proteases in cardiovascular disease. *FASEB J.* 2007;21:3029-3041
21. Galis ZS, Khatri JJ. Matrix metalloproteinases in vascular remodeling and atherogenesis: The good, the bad, and the ugly. *Circ Res*. 2002;90:251-262
22. Burke AP, Farb A, Malcom GT, Liang Y-h, Smialek J, Virmani R. Coronary risk factors and plaque morphology in men with coronary disease who died suddenly. *New England Journal of Medicine*. 1997;336:1276-1282
23. Virmani R, Burke AP, Farb A, Kolodgie FD. Pathology of the vulnerable plaque. *Journal of the American College of Cardiology*. 2006;47:C13-C18
24. Shah P, Falk E, Badimon J, Fernandez-Ortiz A, Mailhac A, Villareal-Levy G, Fallon J, Regnstrom J, Fuster V. Human monocyte-derived macrophages induce collagen breakdown in fibrous caps of atherosclerotic plaques. Potential role of matrix-degrading metalloproteinases and implications for plaque rupture. *Circulation*. 1995;92:1565-1569
25. Brown DL, Hibbs MS, Kearney M, Loushin C, Isner JM. Identification of 92-kd gelatinase in human coronary atherosclerotic lesions : Association of active enzyme synthesis with unstable angina. *Circulation*. 1995;91:2125-2131
26. Aikawa M, Rabkin E, Sugiyama S, Voglic SJ, Fukumoto Y, Furukawa Y, Shiomi M, Schoen FJ, Libby P. An hmg-coa reductase inhibitor, cerivastatin, suppresses growth of macrophages expressing matrix metalloproteinases and tissue factor in vivo and in vitro. *Circulation*. 2001;103:276-283
27. Crisby M, Nordin-Fredriksson G, Shah PK, Yano J, Zhu J, Nilsson J. Pravastatin treatment increases collagen content and decreases lipid content, inflammation, metalloproteinases, and cell death in human carotid plaques : Implications for plaque stabilization. *Circulation*. 2001;103:926-933
28. Hansson GK. Inflammation, atherosclerosis, and coronary artery disease. *N Engl J Med*. 2005;352:1685-1695
29. Spagnoli LG, Bonanno E, Mauriello A, Palmieri G, Partenzi A, Sangiorgi G, Crea F. Multicentric inflammation in epicardial coronary arteries of patients dying of acute myocardial infarction. *J Am Coll Cardiol*. 2002;40:1579-1588

30. Kong Y-Z, Yu X, Tang J-J, Ouyang X, Huang X-R, Fingerle-Rowson G, Bacher M, Scher LA, Bucala R, Lan HY. Macrophage migration inhibitory factor induces mmp-9 expression: Implications for destabilization of human atherosclerotic plaques. *Atherosclerosis*. 2005;178:207-215

CHAPTER 5

GENERAL DISCUSSION

5.1 THE ROLE OF FAP IN INFLAMMATORY DISEASE

While atherosclerosis is a chronic disease that begins early in life, late-stage vulnerable plaques are the most clinically relevant. Indeed many individuals live long lives with significant plaque burden, and never experience symptoms. Conversely, other individuals with comparatively little plaque burden may succumb to cardiovascular events at a young age due to a single vulnerable plaque disruption. Therefore a mechanistic understanding of the factors involved in plaque vulnerability and atherothrombosis remain of high clinical importance.

Nature teaches us that atherosclerosis and vulnerable plaque rupture parallels the pathophysiology of other inflammatory diseases such as chronic liver disease and rheumatoid arthritis. Therefore, in formulating the hypotheses presented in this thesis, we closely observed similar pathways in other inflammatory diseases and often found the congruent mechanisms of action. Indeed the finding of macrophage-induced FAP expression is a key underpinning of these findings. Specifically we found that macrophage-derived TNF-α induced FAP expression in vascular smooth muscle cells. This is the first published mechanism of FAP expression in a mesenchymal cell population by inflammatory stimuli. Given FAP's collagenase and prothrombotic activities, these findings may be extrapolated to other FAP associated inflammatory diseases (i.e. rheumatoid arthritis, chronic liver disease, and tumor formation) and underline the therapeutic potential of anti-FAP therapies.

A common pathological mechanism of vulnerable plaque rupture, tumour formation, and atherothrombosis is angiogensis. In vulnerable plaques, angiogenesis leads to vasa vasorum formation, which in turn directs intraplaque hemorrhage and lesion complication.[1] Neovacularization in rheumatoid arthritis provides nutrients for pathological tissue formation which contributes to disease progression. FAP has been shown to work in concert with CD26 to promote angiogenesis, via invading endothelial cells. [2, 3] In our studies, we found that thin-cap human coronary atheromata endothelial cells also express FAP. This finding combined with the known role of FAP in neovascularization, may indicate a potential contributory role of FAP in vasa vasorum formation and highlight the potential of anti-FAP strategies in preventing pathogenic angiogenesis.

Hyperthrombogenic blood increases patient vulnerability to cardiovascular events including myocardial infarction, peripheral artery occlusive disease, and stroke.[4] We found enhanced FAP in rupture-prone atherosclerotic plaque and in occluding coronary thrombi, and also identified its causal role in accelerated blood coagulation. Given the know presence of FAP in other inflammatory diseases (i.e. rheumatoid arthritis and chronic inflammatory liver disease), it is plausible the FAP also spills-over into the blood and may play a role in accelerated blood coagulation of these diseases as well. Interestingly patients with rheumatoid arthritis are at an increased risk of atherothrombotic events.[5] Therefore, it is plausible that FAP may contribute to this link.

5.4 FUTURE STUDIES - OUTLOOK

While this work associated FAP expression to plaque progression and atherothrombosis, evidence as to the causal role of FAP *in-vivo* is still missing. Further *in-vitro* studies will also be needed to address the mechanism of FAP induction in endothelial cells and may also shed light on the role of FAP in other inflammatory diseases. To identify a clinical application of the work presented in this thesis, the potential of FAP as a diagnostic biomarker in patients with acute coronary syndromes should be addressed. Moreover the effect of FAP inhibiting agents on blood coagulation *ex-vivo* should be identified.

To identify the causal for of FAP in atherogenesis, we have performed preliminary studies in atherosclerotic Apolipoprotein E deficient mice ($ApoE^{-/-}$), to determine if this model is suitable for the

study of FAP in-vivo. It was found that the ApoE$^{-/-}$ mouse on a high cholesterol diet indeed express FAP in atherosclerotic plaque (**Figure 56**). Therefore, future experiments may seek to generate an ApoE$^{-/-}$FAP$^{-/-}$ mouse to determine the role of FAP on atherogenesis and thrombosis *in-vivo*.

To determine whether FAP can be used as a therapeutic target against atherothrombosis *in-vivo* remains to be seen. We intend to approach this question by first testing the effect of FAP-specific inhibiting agents on coagulation of blood from human patients *ex-vivo*. Specifically, blood will be drawn from patients with acute coronary syndromes and treated with FAP-inhibiting agents to assess their effect on blood coagulation.

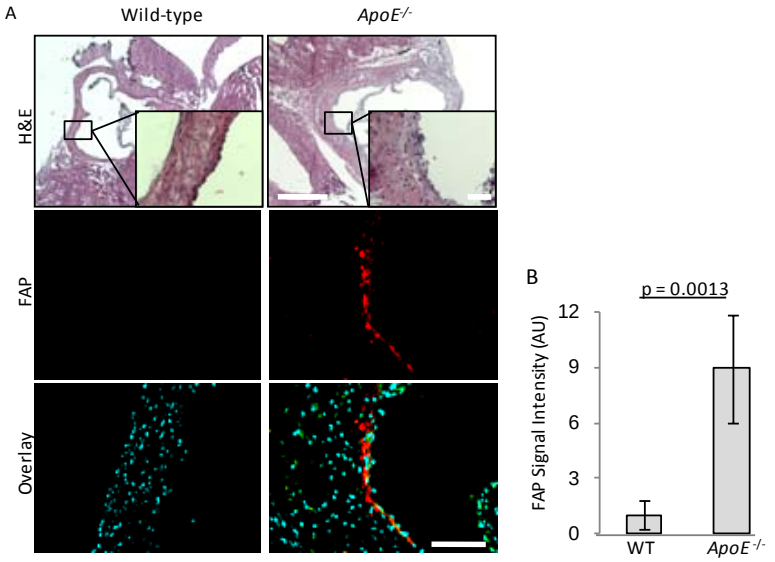

Figure 56. ApoE-/- mice on high cholesterol diet express FAP in atherosclerotic plaques. A. H&E staining shows aortic roots from healthy wildtype and atherosclerotic ApoE-/- mice (scale=300μm). Regions of interest indicated by the black boxes are shown at high magnification (inlays, scale=50μm). Adjacent staining reveal FAP expression (red) in ApoE-/- plaques, but not in healthy wild-type arteries. Sections are counterstained in DAPI (blue) **B.** FAP expression is quantitatively greater in ApoE-/- mice (n=5) compared to WT controls (n=4).

5.2 Potential of FAP as a Diagnostic Target

While we found that FAP associates with vulnerable plaque rupture and atherothrombosis, its potential as a target for clinical use has not been assessed. As FAP is expressed in the endothelium of thin-cap coronary fibroatheromata and neutrophils of occluding coronary thrombi, it is plausible that soluble forms of FAP may indeed spill over into the circulation. While circulating FAP has been detected in human blood (identified as Anti-plasmin cleaving enzyme) its value as a predictive marker of cardiovascular events has not been assessed on any level.[6] We found that FAP was specifically enhanced in the acute coronary thrombi, but not in chronic peripheral artery thrombi. Therefore, FAP levels may specifically associate to the risk of acute, but not slow-forming chronic events. Moreover, the direct causal role of FAP in accelerated blood coagulation supports the notion of its role in acute thrombus formation. However, it is important to note that FAP is not known to play a direct role in blood coagulation, but rather acts via the activation α2-antiplasmin which in turn inhibits plasmin mediated fibrinolysis. Therefore, antiplasmin may have yet better potential as a diagnostic biomarker than FAP.

Expression of FAP in the endothelium of thin-cap coronary fibroatheromata may attract interest in FAP directed molecular imaging. Currently there is an unmet clinical need to identify rupture prone atherosclerotic plaques. FAP-directed molecular imaging may theoretically employ a labeled FAP-specific agent which, when introduced into the blood, would bind FAP on the superficial surface of the plaque. In cases of atherothrombosis due to coronary fibrous cap rupture, it may be plausible that the imaging agent binds directly to the endothelium in the vulnerable fibrous cap. Even in cases of superficial intimal erosion, where an intact endothelium is not present, our data suggests that FAP is highly expressed in the intima. Therefore, it is plausible that FAP directed molecular imaging may hold

future potential in diagnostic strategies. However, the feasibility of this approach has not yet been verified on any level.

5.3 POTENTIAL OF FAP AS A THERAPEUTIC TARGET

Given the role FAP in fibrous cap collagen degradation presented in this thesis, inhibition of FAP activity may draw interest as a therapeutic strategy to prevent plaque rupture. Moreover, the contribution of FAP in accelerated blood coagulation may present future therapeutic options. Indeed FAP has been pursued in the past as a therapeutic target in tumor formation, via two different approaches.

First, in antibody based imaging studies, the FAP-specific antibody F19 was found to specifically bind tumors in patients. However, F19 does not inhibit FAP. While F19 was well tolerated, it showed no efficacy in a phase II trial for metastatic colorectal cancer.[7] However, more recently it has been reported that an F19 conjugated to maytansinoid, a cytotoxic drug, could inhibit tumor growth and was well tolerated.[8] Moreover, another group has reported that antibodies which inhibit the proteolytic activity of FAP slowed tumor growth in a xenograft model.[9] However, whether these approaches can be directed toward atherosclerosis remains to be seen.

Several groups have also attempted to inhibit FAP's enzymatic activity using inhibiting small chemical molecules. Val-boro-Pro (PT-100; Talabostat) demonstrates potential to attenuate tumor growth in a variety of tumor mouse models. While this drug was well tolerated and effective in preliminary trial, it failed to pass phase III clinical trials due to inefficacy in treating lung cancer. Moreover the use of Val-boro-Pro to inhibit FAP's enzymatic activity is not specific, as it also inhibits CD26 and DPP7, which may lead to undesired side effects and safety concerns.

Taken together, FAP does show early potential as a therapeutic target against tumor formation. However, the potential of FAP-inhibition in vulnerable coronary plaque rupture and atherothrombosis remains to be seen. Further pre-clinical trials in atherosclerotic animal models will be useful in identifying the therapeutic benefit of FAP-inhibition.

5.4 REFERENCES

1. Kolodgie FD, Gold HK, Burke AP, Fowler DR, Kruth HS, Weber DK, Farb A, Guerrero LJ, Hayase M, Kutys R, Narula J, Finn AV, Virmani R. Intraplaque hemorrhage and progression of coronary atheroma. *New England Journal of Medicine*. 2003;349:2316-2325
2. Chen H, Yang W-W, Wen Q-T, Xu L, Chen M. Tgf-[beta]-induced fibroblast activation protein expression, fibroblast activation protein expression increases the proliferation, adhesion, and migration of ho-8910pm. *Experimental and Molecular Pathology*. 2009;87:189-194
3. Chen WT. Dppiv and seprase in cancer invasion and angiogenesis. In: Back N, Cohen IR, Kritchevsky D, Lajtha A, Paoletti R, eds. *Dipeptidyl aminopeptidases in health and disease*. Springer US; 2004:197-203-203.
4. Ajjan R, Grant PJ. Coagulation and atherothrombotic disease. *Atherosclerosis*. 2006;186:240-259
5. Lindhardsen J, Ahlehoff O, Gislason GH, Madsen OR, Olesen JB, Torp-Pedersen C, Hansen PR. The risk of myocardial infarction in rheumatoid arthritis and diabetes mellitus: A danish nationwide cohort study. *Annals of the Rheumatic Diseases*. 2011
6. Lee KN, Jackson KW, Christiansen VJ, Lee CS, Chun J-G, McKee PA. Antiplasmin-cleaving enzyme is a soluble form of fibroblast activation protein. *Blood*. 2006;107:1397-1404
7. Santos AM, Jung J, Aziz N, Kissil JL, Puré E. Targeting fibroblast activation protein inhibits tumor stromagenesis and growth in mice. *The Journal of Clinical Investigation*. 2009;119:3613-3625
8. Ostermann E, Garin-Chesa P, Heider KH, Kalat M, Lamche H, Puri C, Kerjaschki D, Rettig WJ, Adolf GR. Effective immunoconjugate therapy in cancer models targeting a serine protease of tumor fibroblasts. *Clinical Cancer Research*. 2008;14:4584-4592
9. Cheng JD, Dunbrack RL, Valianou M, Rogatko A, Alpaugh RK, Weiner LM. Promotion of tumor growth by murine fibroblast activation protein, a serine protease, in an animal model. *Cancer Research*. 2002;62:4767-4772

CHAPTER 6

APPENDIX

6.1 IMAGE ANALYSIS SOFTWARE CODE – BACKGROUND SUBTRACTION

The below image analysis Matlab 7.10.0 code was used to perform isotype control and background signal subtraction, while calculating representative histograms.

```
clear
threshold = 0;
% Image input - Cy3 & Cy5 VAIRABLE ARE ESPECIALLY FOR Cy3 AND Cy5
% RESPECTIVELY (FOR PROPER COLOCALIZATION COEFFICIENT READOUT)

%Import Images

    % Sample Images
    Cy3 = imread('Sample_Image_Cy3.tif'); %import picture - green channel =
Cy3(:,:,2)%
    Cy5 = imread('Sample_Image_Cy5.tif'); %import picture - red channel =
Cy5(:,:,1)%

    % Isotype Images (image from the antibody isotype control)
    iCy3 = imread('Isotype_Image_Cy3.tif'); %import isotype control picture -
green channel = Cy3(:,:,2)%
    iCy5 = imread('Isotype_Image_Cy5.tif'); %import isotype control picture -
red channel = Cy5(:,:,1)%

    % Background Images (image from different plane - average is 200 microns
under the sample, in the glass slide)
    bCy3 = imread('Background_Image_Cy3.tif'); %import background picture -
green channel = Cy3(:,:,2)%
    bCy5 = imread('Background_Image_Cy5.tif'); %import background picture -
red channel = Cy5(:,:,1)%

%Background Thresholds

    % Thresholds for the isotype control images
    i_backlimit = .95;  % background Cy3 percent limit
    i_backlimitT = .05; % background Cy5 percent limit (percentage of the
pixels from the background image should be removed from the sample image)

    % Thresholds for the background image
    backlimit = .95;  % background Cy3 percent limit
    backlimitT = .05; % background Cy5 percent limit (percentage of the
pixels from the background image should be removed from the sample image)

% Create blank Scatter plot Matrix (255x255, all zeros)

SP = zeros(256,256,3);
NSP = zeros(256,256,3);

% Green Channel (standard is Cy3)

    % Sample Image
    X = size(Cy3);
    A = Cy3;
    A(:,:,1) = [];
```

```
    A(:,:,2) = [];
    Max3 = double(max(max(A))); % Maximum Cy3 value for the normalized
scattergram

    % Aimage for the unadjusted image output in the final figure
    Aimage = A;

    % Background Image
    bX = size(bCy3);
    bA = bCy3;
    bA(:,:,1) = [];
    bA(:,:,2) = [];

    % Isotype Image
    iX = size(iCy3);
    iA = iCy3;
    iA(:,:,1) = [];
    iA(:,:,2) = [];

    % Define variables for the first channel
    Ncol = X(2);
    col = 1;
    Nrow = X(1);
    row = 1;

    % Calculate average pixel for the FIRST Channel

    B = sum(A);
    C = sum(B);
    Cy3_Cumulative_Before = C
    AV_before = C /(Ncol*Nrow);
    Cy3_Average_Before = AV_before

% Red Channel (standard is Cy5)

    %Sample Image
    XT = size(Cy5);
    AT = Cy5;
    AT(:,:,2) = [];
    AT(:,:,2) = [];
    Max5 = double(max(max(AT))); % Maximum Cy5 value for the normalized
scattergram

    % ATimage for the unadjusted image output in the final figure
    ATimage = AT;

    % Background Image
    bXT = size(bCy5);
    bAT = bCy5;
    bAT(:,:,2) = [];
    bAT(:,:,2) = [];

    % Isotype Image
    iXT = size(iCy5);
    iAT = iCy5;
```

```
    iAT(:,:,2) = [];
    iAT(:,:,2) = [];

    %  Define variables for the SECOND channel

    NcolT = XT(2);
    colT = 1;
    NrowT = XT(1);
    rowT = 1;

     % Calculate the average for the SECOND Channel

     BT = sum(AT);
     CT = sum(BT);
     Cy5_Cumulative_before = CT;
     AV_beforeT = CT/(Ncol*Nrow);
     Cy5_Average_Before= AV_beforeT;

% Background calculation to identify threshold

     % Cy3 calculation

            % Background Image Subtraction
                bA = double(bA);
                n_vector = reshape(bA.',[],1);
                n_vector_d = double(n_vector);
                n_b_HIST = hist(n_vector_d, 255);
                Sum_shar = sum(n_b_HIST);  % sum of all pixels
                w = Sum_shar * backlimit; % number of pixels above backlimit
                rest = Sum_shar - w; % number of pixels below the 5%
threshold
                i = 1; % background loop index and threshold value (after the
loop is ran)
                y = 0; % cumulation of pixels below threshold
                while y < w;
                    y = y + n_b_HIST(i);
                    i=i+1;
                end
                threshold = i-1;

            % Isotype Control Image Subraction
                iA = double(iA);
                n_vector = reshape(iA.',[],1);
                n_vector_d = double(n_vector);
                n_b_HIST = hist(n_vector_d, 255);
                Sum_shar = sum(n_b_HIST);  % sum of all pixels
                w = Sum_shar * backlimit; % number of pixels above backlimit
                rest = Sum_shar - w; % number of pixels below the 5%
threshold
                i = 1; % background loop index and threshold value (after the
loop is ran)
                y = 0; % cumulation of pixels below threshold
                while y < w;
                    y = y + n_b_HIST(i);
                    i=i+1;
```

```
                end
                i_threshold = i-1;

    % Cy5 calculation

            % Background Control Image Threshold Calculation

                bAT = double(bAT);
                nT_vector = reshape(bAT.',[],1);
                nT_vector_d = double(nT_vector);
                Sum_nT_vector_d = sum(nT_vector_d); % Sum_nT_vector_d = Sum
of all pixel intensities
                Sum_nT_vector_d_limit = Sum_nT_vector_d * backlimitT; %
Sum_nT_vector_d_limit = value of pixels below threshold
                nT_b_HIST = hist(nT_vector_d, 255);
                Sum_nT_b_HIST = sum(nT_b_HIST);
                HIST_Limit = Sum_nT_b_HIST * backlimitT;
                iT = 1; % background loop index (and threshold value - after
the loop is ran)
                yT = 0; % accumulation of pixels below backlimit
                % find the intensity when the threshold exists
                while yT < HIST_Limit;
                    % yT = current value leading up to Sum_sharT (Sum_sharT =
the sum of pixels below the threshold), frequency = (nT_b_HIST(iT)),
intensity = (iT)
                    yT = yT + (nT_b_HIST(iT));
                    iT=iT+1;
                end

                thresholdT = iT-1;
                %Cy5_Background_Threshold = the intensity below which
                %sample pixel will be excluded.

                Cy5_Background_Threshold = thresholdT
                Cy5_Background_Threshold_bin = round(thresholdT/5);


            % Isotype Control Image Threshold Calculation

                iAT = double(iAT);
                nT_vector = reshape(iAT.',[],1);
                nT_vector_d = double(nT_vector);
                Sum_nT_vector_d = sum(nT_vector_d); % Sum_nT_vector_d = Sum
of all pixel intensities
                Sum_nT_vector_d_limit = Sum_nT_vector_d * i_backlimitT; %
Sum_nT_vector_d_limit = value of pixels below threshold
                nT_b_HIST = hist(nT_vector_d, 255);
                Sum_nT_b_HIST = sum(nT_b_HIST);
                HIST_Limit = Sum_nT_b_HIST * i_backlimitT;
                iT = 1; % background loop index (and threshold value - after
the loop is ran)
                yT = 0; % accumulation of pixels below backlimit
                % find the intensity when the threshold exists
                while yT < HIST_Limit;
```

```
                    % yT = current value leading up to Sum_sharT (Sum_sharT =
the sum of pixels below the threshold), frequency = (nT_b_HIST(iT)),
intensity = (iT)
                    HIST_Limit;
                    yT = yT + (nT_b_HIST(iT));
                    iT=iT+1;
                end


                i_thresholdT = iT-1;
                %Cy5_Isotype_Threshold = the intensity below which
                %sample pixel will be excluded.

                Cy5_Isotype_Threshold = i_thresholdT
                Cy5_Isotype_Threshold_bin = round(i_thresholdT/5);

                % define arbitrary variable values for the while loop

                p = 0;
                q = 0;
                tdif = 0;
                dif = 0;
                tavg = 0;
                tavgt = 0;
                tclc = 0;
                gel = 0;
                counted = 0;


                    % Validates that images are of the same dimensions

                    if (Ncol ~= NcolT);
                        error('images of different sizes')
                    end

                    if (Nrow ~= NrowT);
                        error('images of different sizes')
                    end


% Generate a histogram of intensities from the Cy5 image

%Sample Image
    Cy5_vector = reshape(AT.',[],1);
    Cy5_vector_d = double(Cy5_vector);
    Cy5_HIST = hist(Cy5_vector_d, 100);

%Background Image
    Cy5_b_vector = reshape(bAT.',[],1);
    Cy5_b_vector_d = double(Cy5_b_vector);
    Cy5_b_HIST = hist(Cy5_b_vector_d, 100);

%Isotype control Image
    Cy5_i_vector = reshape(iAT.',[],1);
```

```
    Cy5_i_vector_d = double(Cy5_i_vector);
    Cy5_i_HIST = hist(Cy5_i_vector_d, 100);

% Generate custom histograms of intensities from the Cy5 image for plotting
with the bar function

% Sample Image Histogram Calculations
    % Reshape the image into a vector
        Cy5_Image_vector = reshape(AT.',[],1);
        Cy5_Image_vector = double(Cy5_Image_vector);
    % Set the histogram vector to 255 zeros
        Cy5_Sample_Histogram_Vector = zeros([1 51]);
    % Bin the pixel intensity values into the histogram vector
        i=1;
        % Loop through the image vector
        while i <= length(Cy5_Image_vector)
            t=1;
            y=0;
            % Place the pixel values into the histogram vector
            while y < 1
                bins = 5*t;
                if Cy5_Image_vector(i) <= bins
                    Cy5_Sample_Histogram_Vector(t) =
Cy5_Sample_Histogram_Vector(t) + 1;
                    y = 2;
                end
            t=t+1;
            end

            i=i+1;
        end

        Cy5_Sample_Histogram_Vector_new = Cy5_Sample_Histogram_Vector;

% Background Image Histogram Calculations
    % Reshape the image into a vector
        Cy5_Background_vector = reshape(bAT.',[],1);
        Cy5_Background_vector = double(Cy5_Background_vector);
    % Set the histogram vector to 255 zeros
        Cy5_Background_Histogram_Vector = zeros([1 51]);
    % Bin the pixel intensity values into the histogram vector
        i=1;
        % Loop through the Background vector
        while i <= length(Cy5_Background_vector)
            t=1;
            y=0;
            % Place the pixel values into the histogram vector
            while y < 1
                bins = 5*t;
                if Cy5_Background_vector(i) <= bins
                    Cy5_Background_Histogram_Vector(t) =
Cy5_Background_Histogram_Vector(t) + 1;
                    y = 2;
                end
            t=t+1;
            end
```

```
            i=i+1;
        end

% Bin the background threshold into the original
        Cy5_Background_Threshold_bin = round(Cy5_Background_Threshold / 5) ;
        Cy5_Background_Histogram_Vector_new =
Cy5_Background_Histogram_Vector;

% In Cy5_S_minus_B, set all values below the Cy5_Background_Threshold equal
to zero.
        Cy5_S_minus_B = Cy5_Sample_Histogram_Vector;
        %Loop through Cy5_S_minus_B_before, setting everything below
Cy5_Background_Threshold equal to zero.
            i=1;
            Cy5_Background_Threshold_Bin = ((Cy5_Background_Threshold/5)-1);
            while i < Cy5_Background_Threshold_Bin
                    Cy5_S_minus_B(i) = 0;
                  i=i+1;
            end


% Isotype Image Histogram Calculations
    % Reshape the image into a vector
        Cy5_Isotype_vector = reshape(iAT.',[],1);
        Cy5_Isotype_vector = double(Cy5_Isotype_vector);
    % Set the histogram vector to 255 zeros
        Cy5_Isotype_Histogram_Vector = zeros([1 51]);
    % Bin the pixel intensity values into the histogram vector
        i=1;
        % Loop through the Isotype vector
        while i <= length(Cy5_Isotype_vector)
            t=1;
            y=0;
            % Place the pixel values into the histogram vector
            while y < 1
                bins = 5*t;
                if Cy5_Isotype_vector(i) <= bins
                    Cy5_Isotype_Histogram_Vector(t) =
Cy5_Isotype_Histogram_Vector(t) + 1;
                    y = 2;
                end
            t=t+1;
            end

            i=i+1;
        end

% Bin the Isotype threshold into the original
        Cy5_Isotype_Threshold_bin = round(Cy5_Isotype_Threshold / 5) ;
        Cy5_Isotype_Histogram_Vector_new = Cy5_Isotype_Histogram_Vector;



       % Cy5_Isotype_Threshold_bin = Cy5_Isotype_Threshold_bin + 3;
```

```
% In Cy5_S_minus_I, set all values below the Cy5_Isotype_Threshold equal to
zero.
        Cy5_S_minus_I = Cy5_S_minus_B;
        %Loop through Cy5_S_minus_I_before, setting everything below
Cy5_Isotype_Threshold equal to zero.
            i=1;
            %Cy5_Isotype_Threshold_Bin = Cy5_Isotype_Threshold_Bin-1;
            while i < Cy5_Isotype_Threshold_bin
                    Cy5_S_minus_I(i) = 0;
                    i=i+1;
            end



% BACKGROUND control sub-threshold pixel removal

col = 1;

    while col <  Ncol
       row = 1;
       while row < Nrow

    % Change every value that is below BACKGROUND threshold to zero

    % Cy3
        % Remove BACKGROUND AND ISOTYPE Control Image Threshold
            if A(row, col) < threshold
                A(row, col) = 0;
            end

    % Cy5
       % Remove BACKGROUND AND ISOTYPE Control Image Threshold
            if AT(row, col) < thresholdT
                AT(row, col) = 0;
            end

       row = row +1;
      end
       col = col +1;
    end

% Set the Sample - Background subtrated matix to report as an image

    %Cy3
        Cy3_S_min_B_grey = mat2gray(A);
    %Cy5
        Cy5_S_min_B_grey = mat2gray(AT);

% Calculate the Background subtracted images

    %Cy3
        Cy3_S_min_B = reshape(A.',[],1);
```

```
        Cy3_S_min_B = double(Cy3_S_min_B);
        Cy3_S_min_B_HIST = hist(Cy3_S_min_B, 255);
        %Remove the values from 1 to 3 intensity
        Cy3_S_min_B_HIST(1:3) = nan;

    %Cy5
        Cy5_S_min_B = reshape(AT.',[],1);
        Cy5_S_min_B = double(Cy5_S_min_B);
        Cy5_S_min_B_HIST = hist(Cy5_S_min_B, 255);
        %Remove the values from 1 to 3 intensity
        Cy5_S_min_B_HIST(1:3) = nan;

% ISOTYPE control sub-threshold pixel removal

i_thresholdT;

first_sum = reshape(AT.',[],1);
first_sum = sum(first_sum)

col = 1;
    while col <  Ncol
       row = 1;
       while row < Nrow

    % Change every value that is below ISOTYPE CONTROL threshold to zero

    % Cy3
        % Remove Isotype Control Image Threshold
            if A(row, col) < i_threshold
                A(row, col) = 0;
            end

    % Cy5
       % Remove Isotype Control Image Threshold
            if AT(row, col) < i_thresholdT
                AT(row, col) = 0;
            end

       row = row +1;
      end
       col = col +1;
    end

second_sum = reshape(AT.',[],1);
second_sum = sum(second_sum)


% Set the Sample - Isotype and Background subtrated matix to report as an
image

    %Cy3
        Cy3_S_min_BI_grey = mat2gray(A);
    %Cy5
        Cy5_S_min_BI_grey = mat2gray(AT);
```

```
% Calculate the Isotype and Background subtracted images

    %Cy3
        Cy3_S_min_BI = reshape(A.',[],1);
        Cy3_S_min_BI = double(Cy3_S_min_BI);
        Cy3_S_min_BI_HIST = hist(Cy3_S_min_BI, 255);
        %Remove the values from 1 to 3 intensity
        Cy3_S_min_BI_HIST(1:3) = nan;

    %Cy5
        Cy5_S_min_BI = reshape(AT.',[],1);
        Cy5_S_min_BI = double(Cy5_S_min_BI);
        Cy5_S_min_BI_HIST = hist(Cy5_S_min_BI, 255);
        %Remove the values from 1 to 3 intensity
        Cy5_S_min_BI_HIST(1:3) = nan;

% Report the values for the background and isotype control subtracted
% images

    B_n = sum(A);
    C_n = sum(B_n);
    Cy3_Cumulative_After = C_n;
    AV_after = C_n /(Ncol*Nrow);
    Cy3_Average_After = AV_after


    B_n = sum(AT);
    C_n = sum(B_n);
    Cy5_Cumulative_After = C_n;
    AV_after = C_n /(Ncol*Nrow);
    Cy5_Average_After = AV_after


 % Set grayscale images

     %Cy3
        Cy3_S = mat2gray(Aimage);
        Cy3_I = mat2gray(iA);
        Cy3_B = mat2gray(bA);

     %Cy 5
        Cy5_S = mat2gray(ATimage);
        Cy5_I = mat2gray(iAT);
        Cy5_B = mat2gray(bAT);

% DISPLAY IMAGES

    % First of Two Cy5 Histogram Images

    figure

    ax(1) = subplot(151);
```

```
    bar(Cy5_Sample_Histogram_Vector, 1, 'facecolor','green', 'EdgeColor',
'none')
    axis([0 51 0 150000])
    title 'Sample'

    ax(2) = subplot(152);
    mydata=Cy5_Background_Histogram_Vector_new;
    bar_h=bar(mydata, 1);
    bar_child=get(bar_h,'Children');
    set(bar_child,'CData',mydata);
    mycolor=[1 0 0;0 0 0;0 1 0];
    for iCount=1:length(mydata)
        if (iCount < Cy5_Background_Threshold_bin)
                index(iCount)=1;
            elseif (iCount == Cy5_Background_Threshold_bin)
                index(iCount)=2;
            elseif (iCount > Cy5_Background_Threshold_bin)
                index(iCount)=3;
        end
    end
    set(bar_child, 'CData',index);
    colormap(mycolor);
    set(bar_child, 'EdgeColor', 'none')
    axis([0 51 0 150000])
    title 'Background'

    ax(3) = subplot(153);
    mydata=Cy5_S_minus_B;
    bar_h=bar(mydata, 1);
    bar_child=get(bar_h,'Children');
    set(bar_child,'CData',mydata);
    mycolor=[1 0 0;0 0 0;0 1 0];
    for iCount=1:length(mydata)
        if (iCount < Cy5_Background_Threshold_bin)
                index(iCount)=1;
            elseif (iCount == Cy5_Background_Threshold_bin)
                index(iCount)=2;
            elseif (iCount > Cy5_Background_Threshold_bin)
                index(iCount)=3;
        end
    end
    set(bar_child, 'CData',index);
    colormap(mycolor);
    set(bar_child, 'EdgeColor', 'none')
    axis([0 51 0 150000])
    title 'Sample - Background'

    % Second of Two Cy5 Histogram Images

figure

    ax(4) = subplot(154);
    mydata=Cy5_Isotype_Histogram_Vector_new;
    bar_h=bar(mydata, 1);
    bar_child=get(bar_h,'Children');
    set(bar_child,'CData',mydata);
```

```
mycolor=[1 0 0;0 0 0;0 1 0];
for iCount=1:length(mydata)
    if (iCount < Cy5_Isotype_Threshold_bin)
            index(iCount)=1;
        elseif (iCount == Cy5_Isotype_Threshold_bin)
            index(iCount)=2;
        elseif (iCount > Cy5_Isotype_Threshold_bin)
            index(iCount)=3;
    end
end
set(bar_child, 'CData',index);
colormap(mycolor);
set(bar_child, 'EdgeColor', 'none')
axis([0 51 0 150000])
title 'Isotype'


ax(4) = subplot(155);
mydata = Cy5_S_minus_I;
bar_h=bar(mydata, 1);
bar_child=get(bar_h,'Children');
set(bar_child,'CData',mydata);
mycolor=[1 0 0;0 0 0;0 1 0];
for iCount=1:length(mydata)
    if (iCount < Cy5_Isotype_Threshold_bin)
            index(iCount)=1;
        elseif (iCount == Cy5_Isotype_Threshold_bin)
            index(iCount)=2;
        elseif (iCount > Cy5_Isotype_Threshold_bin)
            index(iCount)=3;
    end
end
set(bar_child, 'CData',index);
colormap(mycolor);
set(bar_child, 'EdgeColor', 'none')
axis([0 51 0 150000])
title 'Final Image'


%%%       Background subration images


    figure

    ax(1) = subplot(351);
    imshow(Cy5_S)
    colormap(jet(256))
    title('Cy5_S')

    ax(2) = subplot(352);
    imshow(Cy5_B)
    colormap(jet(256))
    title('Cy5_B')

    ax(3) = subplot(353);
```

```
imshow(Cy5_S_min_B_grey)
colormap(jet(256))
title('Cy5_S_-_B')

ax(4) = subplot(354);
imshow(Cy5_I)
colormap(jet(256))
title('Cy5_I')

ax(5) = subplot(355);
imshow(Cy5_S_min_BI_grey)
colormap(jet(256))
title('Cy5_S_-_B_-_I')

ax(6) = subplot(356);
imshow(Cy3_S)
colormap(jet(256))
title('Cy3_S')

ax(7) = subplot(357);
imshow(Cy3_B)
colormap(jet(256))
title('Cy3_B')

ax(8) = subplot(358);
imshow(Cy3_S_min_B_grey)
colormap(jet(256))
title('Cy3_S_-_I')

ax(9) = subplot(359);
imshow(Cy3_I)
colormap(jet(256))
title('Cy3_I')

ax(10) = subplot(3,5,10);
imshow(Cy3_S_min_BI_grey)
colormap(jet(256))
title('Cy3_S_-_B_-_I')
```

6.1 IMAGE ANALYSIS SOFTWARE CODE – POPULATION SPECIFIC QUANTIFICATION

The below image analysis Matlab 7.10.0 code was used to perform isotype control and background signal subtraction, while calculating representative histograms in specific cell populations.

```
clear
threshold = 0;
% Image input - Cy3 & Cy5 VAIRABLE ARE ESPECIALLY FOR Cy3 AND Cy5
% RESPECTIVELY (FOR PROPER COLOCALIZATION COEFFICIENT READOUT)

%Import Images


     % Sample Images
    Cy3 = imread('Sample_Image_Cy3.tif'); %import picture - green channel =
Cy3(:,:,2)%
    Cy5 = imread('Sample_Image_Cy5.tif'); %import picture - red channel =
Cy5(:,:,1)%

    % Isotype Images (image from the antibody isotype control)
    iCy3 = imread('Isotype_Image_Cy3.tif'); %import isotype control picture -
green channel = Cy3(:,:,2)%
    iCy5 = imread('Isotype_Image_Cy5.tif'); %import isotype control picture -
red channel = Cy5(:,:,1)%

    % Background Images (image from different plane - average is 200 microns
under the sample, in the glass slide)
    bCy3 = imread('Background_Image_Cy3.tif'); %import background picture -
green channel = Cy3(:,:,2)%
    bCy5 = imread('Background_Image_Cy5.tif'); %import background picture -
red channel = Cy5(:,:,1)%


%Background Thresholds

    % Thresholds for the isotype control images
    i_backlimit = .95;  % background Cy3 percent limit
    i_backlimitT = .05; % background Cy5 percent limit (percentage of the
pixels from the background image should be removed from the sample image)

    % Thresholds for the background image
    backlimit = .95;  % background Cy3 percent limit
    backlimitT = .05; % background Cy5 percent limit (percentage of the
pixels from the background image should be removed from the sample image)

% Create blank Scatter plot Matrix (255x255, all zeros)

SP = zeros(256,256);
NSP = zeros(256,256);

% Green Channel (standard is Cy3)

    % Sample Image
```

```
    X = size(Cy3);
    A = Cy3;
    A(:,:,1) = [];
    A(:,:,2) = [];
    Max3 = double(max(max(A))); % Maximum Cy3 value for the normalized
scattergram

    % Aimage for the unadjusted image output in the final figure
    Aimage = A;

    % Background Image
    bX = size(bCy3);
    bA = bCy3;
    bA(:,:,1) = [];
    bA(:,:,2) = [];

    % Isotype Image
    iX = size(iCy3);
    iA = iCy3;
    iA(:,:,1) = [];
    iA(:,:,2) = [];

    % Define variables for the first channel
    Ncol = X(2);
    col = 1;
    Nrow = X(1);
    row = 1;

    % Calculate average pixel for the FIRST Channel

    B = sum(A);
    C = sum(B);
    Cy3_Cumulative_Before = C
    AV_before = C /(Ncol*Nrow);
    Cy3_Average_Before = AV_before

% Red Channel (standard is Cy5)

    %Sample Image
    XT = size(Cy5);
    AT = Cy5;
    AT(:,:,2) = [];
    AT(:,:,2) = [];
    Max5 = double(max(max(AT))); % Maximum Cy5 value for the normalized
scattergram

    % ATimage for the unadjusted image output in the final figure
    ATimage = AT;

    % Background Image
    bXT = size(bCy5);
    bAT = bCy5;
    bAT(:,:,2) = [];
    bAT(:,:,2) = [];
```

```
    % Isotype Image
    iXT = size(iCy5);
    iAT = iCy5;
    iAT(:,:,2) = [];
    iAT(:,:,2) = [];

    %  Define variables for the SECOND channel

    NcolT = XT(2);
    colT = 1;
    NrowT = XT(1);
    rowT = 1;

     % Calculate the average for the SECOND Channel

     BT = sum(AT);
     CT = sum(BT);
     Cy5_Cumulative_before = CT;
     AV_beforeT = CT/(Ncol*Nrow);
     Cy5_Average_Before= AV_beforeT;

% Background calculation to identify threshold

     % Cy3 calculation

            % Background Image Subtraction
                bA = double(bA);
                n_vector = reshape(bA.',[],1);
                n_vector_d = double(n_vector);
                n_b_HIST = hist(n_vector_d, 255);
                Sum_shar = sum(n_b_HIST);  % sum of all pixels
                w = Sum_shar * backlimit; % number of pixels above backlimit
                rest = Sum_shar - w; % number of pixels below the 5%
threshold
                i = 1; % background loop index and threshold value (after the
loop is ran)
                y = 0; % cumulation of pixels below threshold
                while y < w;
                    y = y + n_b_HIST(i);
                    i=i+1;
                end


                threshold = i-1;

          threshold = 0;

            % Isotype Control Image Subraction
                iA = double(iA);
                n_vector = reshape(iA.',[],1);
                n_vector_d = double(n_vector);
                n_b_HIST = hist(n_vector_d, 255);
                Sum_shar = sum(n_b_HIST);  % sum of all pixels
                w = Sum_shar * backlimit; % number of pixels above backlimit
```

```
                rest = Sum_shar - w; % number of pixels below the 5%
threshold
                i = 1; % background loop index and threshold value (after the
loop is ran)
                y = 0; % cumulation of pixels below threshold
                while y < w;
                    y = y + n_b_HIST(i);
                    i=i+1;
                end
                i_threshold = i-1;

             i_threshold = 0;

     % Cy5 calculation

            % Background Control Image Threshold Calculation

                bAT = double(bAT);
                nT_vector = reshape(bAT.',[],1);
                nT_vector_d = double(nT_vector);
                Sum_nT_vector_d = sum(nT_vector_d); % Sum_nT_vector_d = Sum
of all pixel intensities
                Sum_nT_vector_d_limit = Sum_nT_vector_d * backlimitT; %
Sum_nT_vector_d_limit = value of pixels below threshold
                nT_b_HIST = hist(nT_vector_d, 255);
                Sum_nT_b_HIST = sum(nT_b_HIST);
                HIST_Limit = Sum_nT_b_HIST * backlimitT;
                iT = 1; % background loop index (and threshold value - after
the loop is ran)
                yT = 0; % accumulation of pixels below backlimit
                % find the intensity when the threshold exists
                while yT < HIST_Limit;
                    % yT = current value leading up to Sum_sharT (Sum_sharT =
the sum of pixels below the threshold), frequency = (nT_b_HIST(iT)),
intensity = (iT)
                    yT = yT + (nT_b_HIST(iT));
                    iT=iT+1;
                end

                thresholdT = iT-1;

            thresholdT = 0;

                %Cy5_Background_Threshold = the intensity below which
                %sample pixel will be excluded.

                Cy5_Background_Threshold = thresholdT;
                Cy5_Background_Threshold_bin = round(thresholdT/5);


            % Isotype Control Image Threshold Calculation

                iAT = double(iAT);
                nT_vector = reshape(iAT.',[],1);
                nT_vector_d = double(nT_vector);
```

```
                Sum_nT_vector_d = sum(nT_vector_d); % Sum_nT_vector_d = Sum
of all pixel intensities
                Sum_nT_vector_d_limit = Sum_nT_vector_d * i_backlimitT; %
Sum_nT_vector_d_limit = value of pixels below threshold
                nT_b_HIST = hist(nT_vector_d, 255);
                Sum_nT_b_HIST = sum(nT_b_HIST);
                HIST_Limit = Sum_nT_b_HIST * i_backlimitT;
                iT = 1; % background loop index (and threshold value - after
the loop is ran)
                yT = 0; % accumulation of pixels below backlimit
                % find the intensity when the threshold exists
                while yT < HIST_Limit;
                    % yT = current value leading up to Sum_sharT (Sum_sharT =
the sum of pixels below the threshold), frequency = (nT_b_HIST(iT)),
intensity = (iT)
                    HIST_Limit;
                    yT = yT + (nT_b_HIST(iT));
                    iT=iT+1;
                end


                i_thresholdT = iT-1;

            i_thresholdT = 0;


                %Cy5_Isotype_Threshold = the intensity below which
                %sample pixel will be excluded.

                Cy5_Isotype_Threshold = i_thresholdT;
                Cy5_Isotype_Threshold_bin = round(i_thresholdT/5);


                % define arbitrary variable values for the while loop

                p = 0;
                q = 0;
                tdif = 0;
                dif = 0;
                tavg = 0;
                tavgt = 0;
                tclc = 0;
                gel = 0;
                counted = 0;


                    % Validates that images are of the same dimensions

                    if (Ncol ~= NcolT);
                        error('images of different sizes')
                    end

                    if (Nrow ~= NrowT);
                        error('images of different sizes')
```

```
                    end


% Generate a histogram of intensities from the Cy5 image

%Sample Image
    Cy5_vector = reshape(AT.',[],1);
    Cy5_vector_d = double(Cy5_vector);
    Cy5_HIST = hist(Cy5_vector_d, 100);

%Background Image
    Cy5_b_vector = reshape(bAT.',[],1);
    Cy5_b_vector_d = double(Cy5_b_vector);
    Cy5_b_HIST = hist(Cy5_b_vector_d, 100);

%Isotype control Image
    Cy5_i_vector = reshape(iAT.',[],1);
    Cy5_i_vector_d = double(Cy5_i_vector);
    Cy5_i_HIST = hist(Cy5_i_vector_d, 100);

% Generate custom histograms of intensities from the Cy5 image for plotting
with the bar function

% Sample Image Histogram Calculations
    % Reshape the image into a vector
        Cy5_Image_vector = reshape(AT.',[],1);
        Cy5_Image_vector = double(Cy5_Image_vector);
    % Set the histogram vector to 255 zeros
        Cy5_Sample_Histogram_Vector = zeros([1 51]);
    % Bin the pixel intensity values into the histogram vector
        i=1;
        % Loop through the image vector
        while i <= length(Cy5_Image_vector)
            t=1;
            y=0;
            % Place the pixel values into the histogram vector
            while y < 1
                bins = 5*t;
                if Cy5_Image_vector(i) <= bins
                    Cy5_Sample_Histogram_Vector(t) =
Cy5_Sample_Histogram_Vector(t) + 1;
                    y = 2;
                end
            t=t+1;
            end

            i=i+1;
        end

        Cy5_Sample_Histogram_Vector_new = Cy5_Sample_Histogram_Vector;

% Background Image Histogram Calculations
    % Reshape the image into a vector
        Cy5_Background_vector = reshape(bAT.',[],1);
        Cy5_Background_vector = double(Cy5_Background_vector);
```

```
    % Set the histogram vector to 255 zeros
        Cy5_Background_Histogram_Vector = zeros([1 51]);
    % Bin the pixel intensity values into the histogram vector
        i=1;
        % Loop through the Background vector
        while i <= length(Cy5_Background_vector)
            t=1;
            y=0;
            % Place the pixel values into the histogram vector
            while y < 1
                bins = 5*t;
                if Cy5_Background_vector(i) <= bins
                    Cy5_Background_Histogram_Vector(t) =
Cy5_Background_Histogram_Vector(t) + 1;
                    y = 2;
                end
            t=t+1;
            end

            i=i+1;
        end

% Bin the background threshold into the original
        Cy5_Background_Threshold_bin = round(Cy5_Background_Threshold / 5) ;
        Cy5_Background_Histogram_Vector_new =
Cy5_Background_Histogram_Vector;

% In Cy5_S_minus_B, set all values below the Cy5_Background_Threshold equal
to zero.
        Cy5_S_minus_B = Cy5_Sample_Histogram_Vector;
        %Loop through Cy5_S_minus_B_before, setting everything below
Cy5_Background_Threshold equal to zero.
            i=1;
            Cy5_Background_Threshold_Bin = ((Cy5_Background_Threshold/5)-1);
            while i < Cy5_Background_Threshold_Bin
                    Cy5_S_minus_B(i) = 0;
                  i=i+1;
            end


% Isotype Image Histogram Calculations
    % Reshape the image into a vector
        Cy5_Isotype_vector = reshape(iAT.',[],1);
        Cy5_Isotype_vector = double(Cy5_Isotype_vector);
    % Set the histogram vector to 255 zeros
        Cy5_Isotype_Histogram_Vector = zeros([1 51]);
    % Bin the pixel intensity values into the histogram vector
        i=1;
        % Loop through the Isotype vector
        while i <= length(Cy5_Isotype_vector)
            t=1;
            y=0;
            % Place the pixel values into the histogram vector
            while y < 1
                bins = 5*t;
                if Cy5_Isotype_vector(i) <= bins
```

```
                    Cy5_Isotype_Histogram_Vector(t) =
Cy5_Isotype_Histogram_Vector(t) + 1;
                    y = 2;
                end
            t=t+1;
            end

            i=i+1;
        end

% Bin the Isotype threshold into the original
        Cy5_Isotype_Threshold_bin = round(Cy5_Isotype_Threshold / 5) ;
        Cy5_Isotype_Histogram_Vector_new = Cy5_Isotype_Histogram_Vector;



       % Cy5_Isotype_Threshold_bin = Cy5_Isotype_Threshold_bin + 3;


% In Cy5_S_minus_I, set all values below the Cy5_Isotype_Threshold equal to
zero.
        Cy5_S_minus_I = Cy5_S_minus_B;
        %Loop through Cy5_S_minus_I_before, setting everything below
Cy5_Isotype_Threshold equal to zero.
            i=1;
            %Cy5_Isotype_Threshold_Bin = Cy5_Isotype_Threshold_Bin-1;
            while i < Cy5_Isotype_Threshold_bin
                    Cy5_S_minus_I(i) = 0;
                    i=i+1;
            end



% BACKGROUND control sub-threshold pixel removal

col = 1;

    while col <  Ncol
       row = 1;
       while row < Nrow

    % Change every value that is below BACKGROUND threshold to zero

    % Cy3
        % Remove BACKGROUND AND ISOTYPE Control Image Threshold
            if A(row, col) < threshold
                A(row, col) = 0;
            end

    % Cy5
       % Remove BACKGROUND AND ISOTYPE Control Image Threshold
            if AT(row, col) < thresholdT
                AT(row, col) = 0;
            end
```

```
       row = row +1;
      end
       col = col +1;
    end

% Set the Sample - Background subtrated matix to report as an image

    %Cy3
        Cy3_S_min_B_grey = mat2gray(A);
    %Cy5
        Cy5_S_min_B_grey = mat2gray(AT);

% Calculate the Background subtracted images

    %Cy3
        Cy3_S_min_B = reshape(A.',[],1);
        Cy3_S_min_B = double(Cy3_S_min_B);
        Cy3_S_min_B_HIST = hist(Cy3_S_min_B, 255);
        %Remove the values from 1 to 3 intensity
        Cy3_S_min_B_HIST(1:3) = nan;

    %Cy5
        Cy5_S_min_B = reshape(AT.',[],1);
        Cy5_S_min_B = double(Cy5_S_min_B);
        Cy5_S_min_B_HIST = hist(Cy5_S_min_B, 255);
        %Remove the values from 1 to 3 intensity
        Cy5_S_min_B_HIST(1:3) = nan;

% ISOTYPE control sub-threshold pixel removal



i_thresholdT;

first_sum = reshape(AT.',[],1);
first_sum = sum(first_sum);




col = 1;
    while col <  Ncol
       row = 1;
       while row < Nrow

    % Change every value that is below ISOTYPE CONTROL threshold to zero

    % Cy3
        % Remove Isotype Control Image Threshold
            if A(row, col) < i_threshold
                A(row, col) = 0;
            end
```

```
    % Cy5
       % Remove Isotype Control Image Threshold
            if AT(row, col) < i_thresholdT
                AT(row, col) = 0;
            end

       row = row +1;
      end
       col = col +1;
    end

second_sum = reshape(AT.',[],1);
second_sum = sum(second_sum)


% Set the Sample - Isotype and Background subtrated matix to report as an
image

    %Cy3
        Cy3_S_min_BI_grey = mat2gray(A);
    %Cy5
        Cy5_S_min_BI_grey = mat2gray(AT);

% Report the values for the background and isotype control subtracted
% images

    B_n = sum(A);
    C_n = sum(B_n);
    Cy3_Cumulative_After = C_n;
    AV_after = C_n /(Ncol*Nrow);
    Cy3_Average_After = AV_after
    AV = Cy3_Average_After;

    B_n = sum(AT);
    C_n = sum(B_n);
    Cy5_Cumulative_After = C_n;
    AV_after = C_n /(Ncol*Nrow);
    Cy5_Average_After = AV_after
    AVT = Cy5_Average_After;

% redefine arbitrary variable values for the while loop

    p = 0;
    q = 0;
    tdif = 0;
    dif = 0;
    tavg = 0;
    tavgt = 0;
    tclc = 0;
    col = 1;

% Iterations to quantify individual pixels
```

```
while col <  Ncol
   row = 1;
   while row < Nrow

   % P / PT are the indexed pixel values
   P = double(A(row,col)); % Cy3 - green channel
   PT = double(AT(row,col)); % Cy5 - red channel

   % Generate Scattergram
   SP((P+1),(PT+1)) = SP((P+1),(PT+1))+50;

   % SUM 1
   dif = (P - AV) * (PT - AVT);
   tdif = dif + tdif;

   % SUM 2
   avg = (P - AV)^2;
   tavg = avg + tavg;

   % SUM 3
   avgt = (PT - AVT)^2;
   tavgt = tavgt + avgt;

    % Cy 3 channel

    % (t is a 'switch' for accumulating colocalization coefficient values,
    % if it is changes to '1', then the Cy3 has a positive pixel, and Cy5
    % will be checked for a positive pixel as well

    t = 0;
    if A(row,col) > i_threshold
        p = p+1;
        t = 1;
    end

    % Cy 5 channel
    if AT(row,col) > i_thresholdT
        q = q+1;
        if t > 0
            clc = 1;
            tclc = clc + tclc;
        end
    end

    row = row +1;
   end
   col = col +1;
end

col = 1;
Ncol = 256;
Nrow = 256;

while col <  Ncol
```

```
   row = 1;
   while row < Nrow

       if row == 1
            SP(row, col) = 0;
       end
       if col == 1
            SP(row, col) = 0;
       end
   row = row +1;
   end
   col = col +1;
end

% Pearson's Correlation Coefficient
pearson = tdif / sqrt (tavg * tavgt)

% Colocalization Coefficients
Cy3clc = tclc / p;   % Percentage of Cy3 pixels that colocalize to Cy5
Cy5clc = tclc / q   % Percentage of Cy5 pixels that colocalize to Cy3

% Signal Quantification
Cy3pix = p;
Cy5pix = q;
Cy5normCy3 = q/p;

% Image Scatter Gram
SPU = double(SP);
SPUgray = mat2gray(SPU);

% Amplify all values
col = 1;
Ncol = 256;
Nrow = 256;

while col <  Ncol
   row = 1;
   while row < Nrow
       if SPUgray(row, col) > 0
            SPUgray(row, col) = 255;
       end
       row = row +1;
   end
   col = col +1;
end

C_Scatter = zeros(256,256,3);

% Put values of SPU scattergram into C_Scatter matrix
col = 1;
Ncol = 256;
Nrow = 256;

while col <  Ncol
   row = 1;
```

```
   while row < Nrow
       if SPUgray(row, col) > 0
            C_Scatter(row,col,2) = SPUgray(row, col);
       end
       row = row +1;
   end
   col = col +1;
end

%Make a Scattergram from the double isotype control matrix
col = 1;
Ncol = 256;
Nrow = 256;

bSP = zeros(256,256);

while col <  Ncol
   row = 1;
   while row < Nrow

       % bP / bPT are the indexed pixel values
       bP = double(bA(row,col)); % Cy3 - green channel
       bPT = double(bAT(row,col)); % Cy5 - red channel

       % Generate Scattergram
       bSP((bP+1),(bPT+1)) = bSP((bP+1),(bPT+1))+50;

        row = row +1;
   end
   col = col +1;
end

%Put values of iSP into C_Scatter
col = 1;
Ncol = 256;
Nrow = 256;


while col <  Ncol
   row = 1;
   while row < Nrow
        if  bSP(row, col) > 0
            C_Scatter(row,col,2) = 0;
            C_Scatter(row,col,3) = 255;
        end
        row = row +1;
   end
   col = col +1;
end




%Make a Scattergram from the isotype matrix
```

```
col = 1;
Ncol = 256;
Nrow = 256;

iSP = zeros(256,256);

while col <  Ncol
   row = 1;
   while row < Nrow

       % iP / iPT are the indexed pixel values
       iP = double(iA(row,col)); % Cy3 - green channel
       iPT = double(iAT(row,col)); % Cy5 - red channel

       % Generate Scattergram
       iSP((iP+1),(iPT+1)) = iSP((iP+1),(iPT+1))+50;

        row = row +1;
   end
   col = col +1;
end

%Put values of iSP into C_Scatter
col = 1;
Ncol = 256;
Nrow = 256;


while col <  Ncol
   row = 1;
   while row < Nrow
        if  iSP(row, col) > 0
            C_Scatter(row,col,2) = 0;
            C_Scatter(row,col,1) = 255;
            C_Scatter(row,col,3) = 0;
        end
        row = row +1;
   end
   col = col +1;
end


% Plot both Normalized and Raw intensity scattergrams

    figure
    imshow(C_Scatter)

% Calculate the Isotype and Background subtracted images

    %Cy3
        Cy3_S_min_BI = reshape(A.',[],1);
        Cy3_S_min_BI = double(Cy3_S_min_BI);
        Cy3_S_min_BI_HIST = hist(Cy3_S_min_BI, 255);
        %Remove the values from 1 to 3 intensity
```

```
        Cy3_S_min_BI_HIST(1:3) = nan;

    %Cy5
        Cy5_S_min_BI = reshape(AT.',[],1);
        Cy5_S_min_BI = double(Cy5_S_min_BI);
        Cy5_S_min_BI_HIST = hist(Cy5_S_min_BI, 255);
        %Remove the values from 1 to 3 intensity
        Cy5_S_min_BI_HIST(1:3) = nan;



% Set grayscale images

    %Cy3
        Cy3_S = mat2gray(Aimage);
        Cy3_I = mat2gray(iA);
        Cy3_B = mat2gray(bA);

    %Cy 5
        Cy5_S = mat2gray(ATimage);
        Cy5_I = mat2gray(iAT);
        Cy5_B = mat2gray(bAT);
```

ACKNOWLEDGEMENTS

My thanks go to friends, family, and colleagues who contributed to this work.

First, I would like to thank Dr. Christian Matter at the University of Zurich and University Hospital Zurich for his most charming introduction to the field of cardiovascular research, and his imperative support throughout this work. I am indebted also to Professor François Verrey at the Institute of Physiology, University of Zurich, who directed my learning towards the important fundamentals of human physiology. My thanks also go to Dr. Elena Aikawa at the Harvard Institutes of Medicine, for her valuable input and challenging scientific questions.

Dr. Benedikt Weber at the Regenerative Medicine Group, also receives my appreciation for making long working hours a pleasure. I am indebted to my "big brother in the lab" Dr. Max Emmert, who consistently demonstrated the highest examples of diligence and composure. I also thank Dr. Johannes Nürnberg for his friendship and solidarity in conducting laboratory experiments over many sunny weekends. My thanks also go to each member of the Regenerate Medicine Program and Cardiovascular Research Group at the University of Zurich for their essential and friendly scientific collaborations.

My deepest appreciation goes to my chief and mentor Professor Simon Hoerstrup whose example of kindness, scientific excellence, and unshakeable optimism inspired me daily to achieve success.

I am indebted to Cornelia, Jolanda, and Dr. Michael Kreienbühl for inviting me into their house and making Switzerland my home. I also would like to thank my father for his sincere interest in my scientific endeavors, and his consistent moral support. This brings me to my mother, who in the most caring of ways, instilled in me the irreplaceable values of independence and tenacity.

Finally, my most devoted appreciation goes to the unmatched generosity and forthright character of Rod Morris; to which I owe everything.

CURRICULUM VITAE

Chad Brokopp was born in 1982 in Boise, Idaho, USA. After one year of exchange studies in Zurich, Switzerland from 1999-2000, he completed his undergraduate university studies in 2005 with a BSc in Biomedical Engineering and a BA in German at the University of Utah, Salt Lake City, USA. Under the guidance of Professor Patrick Tresco, he received his MSc in Biomedical Engineering with honors in 2006 also from the University of Utah. Following one year as a project engineer for biomedical startup ZARS pharmaceuticals, Chad returned to Zurich to pursue doctoral studies in cardiovascular integrative molecular medicine from 2007-2011 under the supervision of Prof. Simon P. Hoerstrup and Dr. Christian Matter at the University of Zurich.